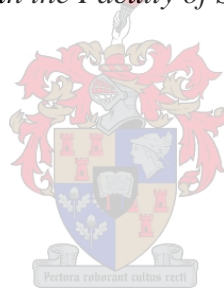


**MONITORING REHABILITATION SUCCESS USING REMOTELY SENSED
VEGETATION INDICES AT NAVACHAB GOLD MINE, NAMIBIA**

MARIA ALETTA BELL

BSc Agric, BSc Environmental Management, BSc Hons Environmental Monitoring &
Modelling

*Thesis presented in partial fulfilment of the requirements for the degree of Masters of Science in
Geography & Environmental Studies in the Faculty of Science at the Stellenbosch University.*



Supervisors: Prof A van Niekerk

Mr PJ Eloff

December 2015

DECLARATION

By submitting this report electronically, I declare that the entirety of the work contained therein is my own, original work, that I am the sole author thereof (save to the extent explicitly otherwise stated), that reproduction and publication thereof by Stellenbosch University will not infringe any third party rights and that I have not previously in its entirety or in part submitted it for obtaining any qualification.

Date:

.....

SUMMARY

Remote sensing and vegetation indices were evaluated for its usefulness to monitor the success of the rehabilitation programme of the decommissioned tailings storage facility (TSF1) of the Navachab Gold Mine, Karibib, Namibia. The study aimed to objectively illustrate the rehabilitation progression from tailings (baseline) to soil (capping) and vegetation (planted as well as natural). Baseline data sets of 2004 and 2005 were compared with imagery of 2009, 2010 and 2011. All the images were subjected to panchromatic sharpening using the subtractive resolution merge (SRM) method before georegistration. As no recent accurate topographical maps were available of the study area, the May 2010 image was used as a reference image. All other images were georegistered to this image. A number of vegetation indices (VIs) were evaluated.

The results showed that the normalised difference vegetation index (NDVI) and the transformed vegetation index (TVI) provided the most promising results. Although the difference vegetation index (DVI) and enhanced vegetation index (EVI) distinguished the vegetation, rock, and soil classes, it was not as successful as the other VIs in classifying the rain water pond.

TVI and NDVI were further evaluated for their efficacy in detecting changes. This was done by generating a series of change images and by qualitatively comparing them to false colour images of the same period. Both the NDVI and TVI delivered good results, but it was found that the TVI is more successful when water is present in the images. The research concludes that change analyses based on the TVI is an effective method for monitoring mine rehabilitation programmes.

KEYWORDS

Remote sensing, mining, rehabilitation, pansharpening, monitoring, change detection, vegetation indices

OPSOMMING

Afstandswaarneming en plantegroei-indekse is ge-evalueer vir die gebruikswaarde daarvan om sukses van die rehabilitasieprogram vir die geslote slykdam of *tailings storage facility* (TSF1) van die Navachab Goudmyn, Karibib, Namibië vas te stel. Die studie se doelwit was om die progressie in die rehabilitasie van slyk (basislyn) na grond (dekmateriaal) en plantegroei (aangeplant en natuurlik) te illustreer. Basislyndatastelle 2004 en 2005 is vergelyk met 2009, 2010, en 2011 beelde. Al die beelde is panchromaties verskerp deur die *subtractive resolution merge* (RSM) metode voor georegistrasie uit te voer. Aangesien geen onlangse, akkurate topografiese kaarte van die studiegebied beskikbaar was nie, is die beeld vir Mei 2010 as 'n verwysingsbeeld gebruik. Al die ander beelde is op die laasgenoemde beeld gegeoregistreer.

Die resultate het gewys dat die *normalised difference vegetation index* (NDVI) en die *transformed vegetation index* (TVI) die mees belowende resultate lewer. Al het die *difference vegetation index* (DVI) en *enhanced vegetation index* (EVI) goed onderskei tussen plantegroei-klasse en grond- en gesteentesklasse was dit nie so suksesvol met die klassifikasie van die reënwaterpoel nie.

TVI en NDVI is verder geëvalueer vir effektiwiteit om verandering waar te neem. Dit is gedoen deur 'n reeks van veranderingsbeelde te skep en dit dan kwalitatief met die vals-kleur-beelde vir dieselfde tydperk te vergelyk. Beide die NDVI en TVI het goeie resultate gelewer, maar die TVI was meer suksesvol om beelde met water te klassifiseer. Die navorsing lei tot die gevolgtrekking dat veranderingsanalises met die TVI 'n effektiewe metode vir die monitoring van rehabilitasie programme is.

TREFWOORDE

Afstandswaarneming, rehabilitasie, panchromatiese verskerping, monitering, veranderingswaarneming, plantegroei-indekse

ACKNOWLEDGEMENTS

I sincerely thank the following people and institutions for assisting me in some way or another during the course of doing this research:

- The administrative staff of the Department of Geography and Environmental Studies, Stellenbosch University, for helping with all registrations and queries - Marianne Cronje and Catherine Liederman deserve special mention;
- Prof Adriaan van Niekerk and Mr Piet Eloff for technical guidance and encouragement;
- Jaurez Dorfling, Hanna Mazus and Dillon Panizzolo from Geo Data Design for endless hours spent on the telephone explaining technicalities on the data provided and ERDAS software;
- INTERGRAPH for kindly supplying a student's license of ERDAS Imagine software for four years running;
- Malcolm Sutton and Kobus Reynecke for assisting me with ArcGIS at short notice, and special thanks to Kobus for the crash course in ArcGIS;
- Dr Pieter de Necker for invaluable assistance editing this document; and
- My husband, Graham, and our two daughters, Sunél and Marlise, for believing in me and supporting me throughout.

CONTENTS

DECLARATION.....	ii
SUMMARY.....	iii
OPSOMMING.....	iv
ACKNOWLEDGEMENTS.....	v
CONTENTS.....	vi
TABLES.....	viii
FIGURES.....	x
ACRONYMS AND ABBREVIATIONS.....	xii
CHAPTER 1 INTRODUCTION	1
1.1 REMOTE SENSING TOOLS FOR MINE REHABILITATION ASSESSMENT ..	1
1.1.1 Mine rehabilitation.....	2
1.1.2 Rehabilitation monitoring options using remote sensing	3
1.2 NAVACHAB GOLD MINE AS A MODEL FOR STUDY	6
1.3 RESEARCH PROBLEM	9
1.4 AIM AND OBJECTIVES	9
1.5 STUDY SITE	10
1.6 RESEARCH METHODOLOGY AND RESEARCH DESIGN	11
CHAPTER 2 LITERATURE REVIEW	14
2.1 RESOLUTION	14
2.1.1 Spectral resolution.....	14
2.1.2 Radiometric resolution	18
2.1.3 Spatial resolution.....	19
2.1.4 Temporal resolution	21
2.2 SPECTRAL CHARACTERISTICS OF LAND COVERS.....	21
2.2.1 Water	22
2.2.2 Vegetation characteristics.....	23
2.2.3 Rock and soil.....	24
2.3 SENSORS AND SENSOR CHARACTERISTICS	25
2.4 PROCESSING OF SATELLITE IMAGES	27
2.4.1 Image classification	27
2.4.2 Image pre-processing	31

2.4.3	Pansharpening	34
2.4.4	Accuracy assessment	39
2.5	TRUE AND FALSE COLOUR IMAGES	41
2.6	VEGETATION INDICES	41
2.6.1	Simple ratio index.....	43
2.6.2	Difference vegetation index	43
2.6.3	Normalised difference vegetation index	43
2.6.4	Transformed vegetation index	44
2.6.5	Square root simple ratio index.....	44
2.6.6	Enhanced vegetation index.....	45
2.6.7	Soil-adjusted vegetation index.....	46
2.6.8	Atmospherically resistant vegetation index	46
2.6.9	Transformed soil-adjusted vegetation index.....	47
2.7	CHANGE DETECTION	47
2.7.1	Transformational techniques	48
2.7.2	Change classification techniques.....	49
2.8	SUMMARY	50
CHAPTER 3 DATA COLLECTION AND MANIPULATION		53
3.1	DATA ACQUISITION	54
3.1.1	Data matching time-frame.....	54
3.1.2	Moisture condition and seasonal classification of images.....	55
3.2	IMAGE PREPROCESSING.....	58
3.2.1	Pansharpening	59
3.2.2	Georegistration of the images.....	61
3.3	SUMMARY	63
CHAPTER 4 VEGETATION INDICES AND CHANGE DETECTION		64
4.1	SPECTRAL PROPERTIES OF LAND COVER CLASSES IN TSF1	64
4.1.1	TSF1 rainwater pond	65
4.1.2	TSF1 soil and rock classes	67
4.1.3	TSF1 vegetation classes.....	69
4.2	VEGETATION INDEX SELECTION	70
4.3	CHANGE DETECTION RESULTS	72
4.3.1	Changes from wet and dry baselines to Image 3 (2009 wet season image)	72
4.3.2	Changes from baselines to Image 4 (2009 dry season image)	76

4.3.3	Changes from baselines to Image 5 (2010 wet season image)	77
4.3.4	Changes from baselines to Image 6 (2010 dry season image)	77
4.3.5	Changes from baselines to Image 7 (2011 wet season image)	78
4.3.6	Changes from baselines to Image 8 (2011 dry season image)	78
4.4	SUMMARY	79
CHAPTER 5 CONCLUSIONS AND RECOMMENDATIONS		80
5.1	EVALUATION OF SATELLITE REMOTE SENSING FOR MINE REHABILITATION MONITORING.....	80
5.2	PROBLEMS ENCOUNTERED AND SUGGESTIONS FOR FURTHER STUDY	81
5.3	RECOMMENDATIONS.....	82
5.4	PRACTICAL IMPLICATIONS FOR NAVACHAB GOLD MINE	84
REFERENCES		86
Appendix A	NAVACHAB RAINFALL	98
Appendix B	CHANGE DETECTION RESULTS	101

TABLES

Table 2.1	Comparison of various high-resolution (<5m) sensors	26
Table 3.1	High-resolution satellite images inventory for Navachab Gold Mine	54
Table 3.2	Classification of images according to season.....	57
Table 3.3	Mean opinion score grades.....	59
Table 3.4	Mean opinion score for eight pansharpening methods tested	61
Table 3.5	GPS reference points surveyed on TSF1	62
Table 4.1	Normalised vegetation index values calculated from Image 5	70

FIGURES

Figure 1.1	Location of the Navachab Gold Mine in Namibia.....	7
Figure 1.2	Main mining areas at Navachab Gold Mine	8
Figure 1.3	Picture taken of TSF1 during capping process	10
Figure 1.4	Comparison of the top of the first tailings storage facility (TSF1) (a) directly after capping in January 2005 and (b) in March 2009 following a few years of rehabilitation. Source: author	11
Figure 1.5	Research design for evaluating remote sensing in monitoring the success of the rehabilitation programme at Navachab Gold Mine	12
Figure 2.1	The electromagnetic spectrum	15
Figure 2.2	Spectra for Prima cotton, Royal cotton and road surface area using an imaging spectrometer	17
Figure 2.3	Reflection spectrum of a deciduous leaf.....	17
Figure 2.4	Angular instantaneous field of view (IFOV), α , showing the projection X-Y on the ground where X-Y is the diameter of a circle.	19
Figure 2.5	Instantaneous field of view (IFOV) defined by the amplitude of the point spread function (PSF).	20
Figure 2.6	Spectral signature for water, soil and vegetation in the visible, NIR and intermediate IR regions	22
Figure 2.7	Change in spectral curves with different vegetation moisture levels	23
Figure 2.9	Complete coverage of Germany in five days by RapidEye satellites.....	27
Figure 2.10	New York and New Jersey land cover derived from Landsat TM data	30
Figure 2.11	Residuals and root mean square error per point	40
Figure 2.12	Tolerance of root mean square error.....	40
Figure 3.1	Satellite image processing flow diagram	53
Figure 3.2	Navachab rainfall over the 10 years preceding the end of the study period.....	57
Figure 3.3	Comparison of (a) unsharpened multispectral image, (b) panchromatic image and (c) Ehlers fusion, (d) high pass filter, (e) modified intensity hue saturation, (f) Brovey transform, (g) multiplicative, (h) principle components analysis, (i) SRM and (h) wavelet pansharpening methods.....	60
Figure 4.2	Rainwater pond on old TSF	66
Figure 4.3	Close-up of water in pond.....	66
Figure 4.4	Spectral response pattern from the rain water pond as extracted from Image 5.....	67

Figure 4.5	Spectral profiles of (a) rock and (b) soil as extracted from Image 5	67
Figure 4.6	View of top of TSF during the 2010 rainy season indicating presence of pioneering ground cover species	68
Figure 4.7	Spectral profiles of vegetation classes (a) trees and (b) shrub.....	69
Figure 4.8	Normalised vegetation index values calculated from reflectance readings	71
Figure 4.9	Increases and reductions in vegetation cover between Image 1 and Image 3 according to (a) NDVI and (b) TVI.....	73
Figure 4.10	False colour images of (a) Image 1 (Quickbird January 2004) and (b) Image 3 (GeoEye-1 March 2009).....	74
Figure 4.11	Increases and reductions in vegetation cover between Image 2 and Image 3 according to (a) NDVI and (b) TVI.....	75
Figure 4.12	False colour images of (a) Image 2 (July 2005) and (b) Image 3 (March 2009).....	76

ACRONYMS AND ABBREVIATIONS

AN16	Anomaly 16
APAR	Absorbed photosynthetically active radiation
ARVI	Atmospherically resistant vegetation index
ASTER	Advanced Spaceborne Thermal Emission & Reflection Radiometer
DEM	Digital elevation model
DVI	Difference vegetation index
EFA	Ecological function analysis
EIA	Environmental impact assessment
EM	Electromagnetic
EMS	Environmental management system
EPB	Eastern pushback
ERE	Effective resolution element
ETM+	Enhanced thematic mapper plus
EVI	Enhanced vegetation index
FFT	Fast Fourier transform
GCP	Ground control point
GIS	Geographical information system
GPS	Global positioning system
GLm	German legal meter
HPF	High pass filter
HRV	High-resolution visible
HRVIR	High-resolution visible and infrared
IFOV	Instantaneous field of view
HIS	Intensity hue saturation
IR	Infrared
LAI	Leaf area index
LFA	Landscape function analysis
LOM	Life of mine
LPF	Low pass filter
LPS	ERDAS Imagine Photogrammetric Production Tools
Mid-IR	Mid-infrared
MOS	Mean opinion score

NDVI	Normalised difference vegetation index
NIR	Near-infrared
NSR	Nominal spatial resolution
PCA	Principal component analysis
PMSE	Perceptual mean square error
PSF	Point spread function
RATIO	Simple ratio vegetation index
RGB	Red green blue
RMSE	Root mean square error
SAVI	Soil-adjusted vegetation index
SD	Standard deviation
SEA	Strategic environmental assessment
SI _m	Système International d'Unités meter
SMA	Spectral mixture analysis
SNR	Signal-to-noise ratio
SRM	Subtractive resolution merge
SRP	Spectral response pattern
SSRI	Squared simple ratio index
SWIR	Short-wave infrared
T1	Time 1
T2	Time 2
TM	Thematic mapper
TSAVI	Transformed soil-adjusted vegetation index
TSF1	First tailings storage facility
TSF2	Second tailings storage facility
TVI	Transformed vegetation index
USA	United States of America
UTM	Universal transverse Mercator
UV	Ultraviolet
VHR	Very high resolution
VI	Vegetation index
WGS	World geodetic system
WRD	Waste rock dump

CHAPTER 1 INTRODUCTION

Environmental legislation is becoming stricter and more comprehensive by the year and, concomitantly, the need for mining companies to prove compliance with government regulations and requirements. One of these requirements from governments around the world is that of mine closure. In the Namibian environmental impact assessment regulations, under the Environmental Management Act 7 of 2007 (Namibia 2012: 12), it is stated that already in the scoping phase an Environmental Impact Assessment (EIA) should include “information on any proposed management, mitigation, protection or remedial measures to be undertaken to address the effects on the environment that have been identified including objectives in respect of the rehabilitation of the environment and closure.”

Because detailed Namibian guidelines for rehabilitation are not available, the AngloGold Ashanti (2009: 7) closure and rehabilitation standard document calls for the development of a rehabilitation programme to “assess the extent of impacts on land and to develop, implement, monitor, assess and refine rehabilitation methodologies in line with agreed closure objectives and/or environmental permit conditions.” This standard refers to one of the leading documents on mine closure and rehabilitation by the Australian Government Department of Resources, Energy and Tourism (Australia 2006: 1-2) where rehabilitation is described as “the process used to repair the impacts of mining on the environment” and one of the objectives of rehabilitation as “establishing appropriate sustainable ecosystems.”

Recent improvements in remote sensing sensors and software offer new possibilities for ecosystem change monitoring in mining areas. Instead of relying on ground-level studies of flora, satellite imagery combined with vegetation classification, vegetation indices and change detection can be used to assess the success of rehabilitation programmes.

The various remote sensing assessment and rehabilitation monitoring tools available are overviewed in the next section.

1.1 REMOTE SENSING TOOLS FOR MINE REHABILITATION ASSESSMENT

A basic understanding of mine rehabilitation is needed before monitoring options are discussed. The aims of monitoring mine rehabilitation progress are similar to other types of ecosystem change or succession monitoring.

The following sections describe mine rehabilitation procedures and remote sensing techniques that can be used to monitor progress.

1.1.1 Mine rehabilitation

Rehabilitation resembles a form of primary succession (Glenn-Lewin, Peet & Veblen 1992) where a disturbed and barren area like a waste rock dump (WRD) or tailings storage facility (TSF) is covered in soil and vegetated over time to a point where a stable ecosystem is established (Wiegleb & Felinks 2001). Succession is the orderly development of plant communities through a series of seral stages where a seral stage refers to an intermediate stage in ecosystem development (Clements, Weaver & Hanson 1929; Gibbons & Freudenberger 2006).

Walker & Del Moral (2003) describe primary succession as the process of ecosystem development of surfaces stripped of biological activity and includes the development of complex ecological systems from simple biotic and abiotic (non-biological) components that is initiated when plants, animals and microbes colonize the disturbed surfaces. Thompson & Thompson (2004) reported that even in Western Australia there were no mandated standards for assessing rehabilitation success for the mining industry. They argue that the primary objective for rehabilitation programmes should focus on the creation of near-natural, self-sustaining, functional ecosystems that can be assessed by monitoring flora and fauna. None of the existing mines used the same monitoring strategy and across the board the monitoring was outsourced.

Ecological function analysis (EFA) (Tongway & Hindley 2003; Randall 2004) is an effective but labour-intensive and time-consuming method to assess rehabilitation success by incorporating landscape organisation indices and soil surface indices. The core component of EFA is landscape function analysis (LFA), vegetation and structure composition and habitat complexity. Tongway & Hindley (2005:11) describes the LFA process as a “monitoring procedure that uses rapidly acquired field-assessed indicators to assess the biogeochemical functioning of landscapes at the hillslope scale.” This method is useful to standardise rehabilitation monitoring methods but it remains labour-intensive and needs to be done on the site. Gibbons & Freudenberger (2006) state that there are numerous other approaches also employed for rapid, in-situ assessments of vegetation condition. These methods only look at vegetation factors and not the associated changes in soil conditions. Remote sensing offers a distinct advantage in this regard as soil can be distinguished from tailings due to their spectral differences.

The question therefore arises on how to prove that a sustainable ecosystem has been established in an industry such as mining that is not focussed on employing full time ecologists?

In the next section some existing studies are overviewed.

1.1.2 Rehabilitation monitoring options using remote sensing

Various processing tools are available to convert remotely sensed images to thematic maps. Straker et al. (2004) demonstrated the potential of supervised classification of Quickbird images combined with an existing ground-based vegetation sampling programme for use in rehabilitation assessment and as documented proof of fulfilment of regulatory objectives. In a very recent study Al-Ruzouq & Al Rawashdeh (2014) used remote sensing and supervised classification to highlight landscape characterization needed for mine rehabilitation.

Change detection using remotely sensed images is a way to quantify the success of rehabilitation efforts. Several studies have monitored changes in vegetation status using various broadband multispectral satellite images. For example, Li et al. (2004) investigated change from barren land to grassland and cropland in the Yulin prefecture of China using Landsat Thematic Mapper (TM) data, whereas Röder et al. (2008) analysed a time series of remote sensing data spanning 1984 to 2000 for a retrospective assessment of rangeland processes¹ in a test area of northern Greece using Landsat-5 TM and Landsat-7 enhanced thematic mapper plus (ETM+) imagery. They then interpreted the data in the light of land-use practices and previous management interventions. Another example is Zhang & Guo (2008) who used SPOT-4 high-resolution visible and infrared (HRVIR) and Landsat-5 TM imagery to evaluate vegetation health.

Mehner et al. (2004) examined the improvement of vegetation classification from low-resolution imagery (Landsat TM and SPOT HRV) to high-resolution imagery (Ikonos) by applying traditional remote sensing classification techniques. Basic radiometric corrections were carried out and the data was geometrically corrected and referenced to the British National Grid by using ground control points (GCPs). They needed a ground resolution of 10m or better and multispectral imagery with coverage in the near-infrared (NIR) wavelengths to maximise spectral discrimination between vegetation types and this was obtained through Ikonos data with 4m spatial resolution

¹ Rangeland processes here refers to the local grazing regime and the factors driving it.

and a NIR band (Band 4). Unfortunately, the short-wave infrared (SWIR) information, which would have been provided by Landsat TM Band 5, was not available from the Ikonos data. They also found that winter and summer images maximised the discrimination between vegetation types as some plants are spectrally more distinct in winter. The normalised difference vegetation index (NDVI) was calculated to enhance discrimination between different vegetation types and to aid vegetation classification. Shadows were mainly a result of the steep relief of the study area. Switching from a hard or rigid to a soft classification approach improved the identification of mixed vegetation types. Problems related to snow and shaded areas on the winter image were experienced.

Turner et al. (2003) and Walsh et al. (2008) concluded that imagery with high spatial resolutions, such as those provided by Ikonos and Quickbird, show great potential for the identification of vegetation types up to species level. Species differences in phenology (onset of greenness, fruiting and senescence) allow accurate identification of species type but require sensors with high temporal resolution. However, costs escalate when an area has to be scanned repeatedly (Gross, Goetz & Cihlar 2009). Therefore, instead of having to perform actual species-level flora identification, vegetation indices offer a measure to evaluate the state of vegetation. Data continuity can also be ensured by a multisensor detection procedure (Wulder, Butson & White 2007).

Vegetation indices are dimensionless, radiometric measures that indicate relative abundance and activity of green vegetation (Jensen 2007). Various indices have been developed for vegetation monitoring, NDVI being the most commonly used example. Leblon (1997) maintains that an ideal vegetation index should be sensitive to the vegetation and not the underlying soil. This author further explains that most ratio-based vegetation indices use the red and near-infrared (NIR) bands which contain the most information on vegetation characteristics and where the contrast between vegetation and soil is maximal. Shank (2008) showed that revegetation of mine sites can be successfully evaluated using NDVI and high-resolution Quickbird MS imagery while Zhang & Guo (2008) compared 13 different vegetation indices calculated from SPOT-4 and Landsat-5 TM imagery for evaluating the prairie ecosystem characterised by an abundance of dead material along with soil and green vegetation classes.

NDVI's limitations relate to saturation effects for dense vegetation canopies and a negative influence on soil background, especially for bright soils and sparse vegetation canopies. In their

study, Röder et al. (2008) introduced laboratory measurements of weathered gneiss rock and developed cambisol soil to represent potential background materials and minimise the effect of the soil. Considering the problems encountered with the NDVI, they opted for linear spectral mixture analysis to infer quantitative estimates of proportional green vegetation on a per-pixel basis. They used Landsat imagery but introduced a digital elevation model (DEM) to register a master image onto the Greek universal transverse Mercator (UTM)-based reGENCY system. All other images were subsequently referenced to the master image with vast numbers of GCPs identified in cross-correlation search windows.

These cited studies were done over relatively large areas, but given that satellite sensor technology is becoming more advanced and higher-resolution imagery from Ikonos (Menher et al. 2004) and Quickbird (Shank 2008; Wulder et al. 2008; Hester et al. 2011) show promising results, more accurate change detection over smaller areas like mine sites has become feasible. Furthermore, image fusion or pansharpening can be implemented to increase the spatial resolution of MS data but care needs to be taken to employ the methods that preserve spectral fidelity (Švab & Oštir 2006).

Short-term assessment of change detection was done by Jarlan et al. (2007), Antwi, Krawczynski & Wiegleb (2008) and Koruyan et al. (2012) whereas Wulder et al. (2008) studied multitemporal cross-sensor change detection with medium-resolution images from Landsat, ASTER and SPOT and also highlighted the importance of data continuity for long-term monitoring programmes.

A long-term reclamation assessment of mine rehabilitation using NDVI derived from red and NIR bands of multitemporal airborne MS imagery has been done for the period 2001 to 2011 for the Highland Valley Copper Mine reclamation project (Richards, Martínez & Borstad 2003; Richards, Borstad & Martínez 2004; Brown et al. 2006; Borstad et al. 2009; Martínez et al. 2012). This assessment was one of the first published, long-term remote monitoring programmes of mine rehabilitation.

Repeatability of image scans is crucial to ensure continuous monitoring. Pre-ordered collections of higher-resolution images is possible but sensor characteristics still need to correspond to historical collections regarding spectral band response function, solar zenith angle as well as sun-object sensor orientation to ensure accurate assessments. The timing of the imagery acquisition is very important to eliminate any effects caused by changes in soil moisture changes (Shank 2008) and precipitation patterns must be studied before placing orders.

Validation of classes can be done either by comparing the spectral classes to an extensive available database of spectral reflectance measurements of typical soils, rocks and plant types (Röder et al. 2008) or by visually identifying features from the images and obtaining their spectral curves (Zhang & Guo 2008). Object-based image analysis is often the preferred and more accurate method for classification of medium to high spatial resolution images in land-use and land cover studies (Walsh et al. 2008; Castillejo-González et al. 2009; Myint et al. 2011; Whiteside, Boggs & Maier 2011; Agarwal et al. 2013).

Imaging spectroscopy and hyperspectral data also play important roles in accurately describing mine rehabilitation regarding the unique, pH levels related to acid mine drainage¹ (AMD) as well as land-use and land cover changes (Paniagua et al. 2009).

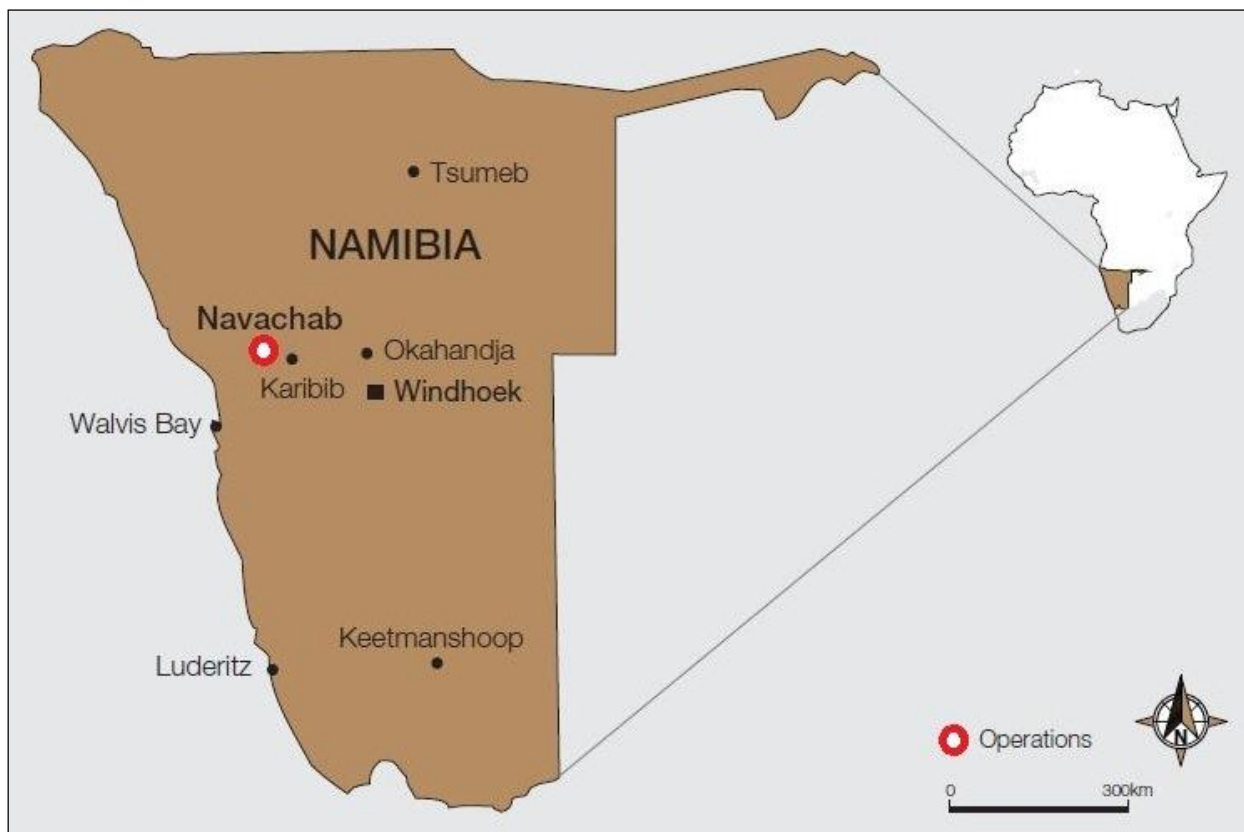
In summary, several areas of investigation relevant to the study of a small-scale rehabilitation project have been highlighted, namely the characteristics of satellite imagery, the availability of satellite imagery, vegetation characteristics, the calculation of vegetation indices and methods of change detection. These areas of investigation will be pursued in a study of rehabilitation monitoring at the Navachab Gold Mine in Namibia. The rest of the chapter is devoted to describing the research problem, aim and objectives, the study site, the research methodology followed and methods applied, as well as the design of the research.

1.2 NAVACHAB GOLD MINE AS A MODEL FOR STUDY

The Navachab Gold Mine is situated about 150km north-north-west from the Namibian capital of Windhoek. The mine is located on Navachab Farm 10km west of Karibib. The farm is roughly 6000ha in size of which about 500ha is now under some form of mining activity. Figure 1.1 shows the location of the Navachab mine in Namibia as indicated by the AngloGold Ashanti Namibia Country Report (AngloGold Ashanti 2008). During the initial study period, Navachab was the only gold mine in Namibia and belonged to AngloGold Ashanti. The mine was sold to QKR Namibia during 2014.

¹ Acid mine drainage, or also called acid rock drainage, is the term used in the mining industry when sulphide-containing rock is exposed to air through the mining process. The natural oxidation process can acidify water which in turn has increased capacity to leach elements from the rock.

Exploration work on the farm started in 1984 and mining activities commenced in 1989. By 1990 the opencast gold mine was in full production. The processing plant uses a cyanide process to remove the gold from the ores and because a fraction of the cyanide remains in the waste product or tailings, all tailings have to be covered under capping material. The first tailings storage facility, TSF1, was commissioned in 1998 for the disposal of tailings. Waste rock is deposited on various waste rock dumps (WRDs) while ore-containing rock is stored in stockpiles until processed. TSF1 was decommissioned in 2003 and TSF2 was commissioned in 2004.



Source: Adapted from AngloGold Ashanti (2008: 7)

Figure 1.1 Location of the Navachab Gold Mine in Namibia

Mining activities at Grid A commenced in 2005 with the bulldozing of roads for exploration drilling. Excavation work started on the eastern pushback (EPB) of the main pit to widen the pit before it could be deepened. To cope with the additional volume of waste rock generated by the EPB, dumping of waste rock material also began at the East WRD in 2006 (Badenhorst 2009, Pers com).

Rehabilitation mainly comprises three phases: a sloping phase during which areas are shaped by bulldozing; a capping phase during which a suitable growth medium (soil) is first dumped on the

area to be rehabilitated and then levelled by bulldozing; and a planting phase. The sloping and capping activities at TSF1 were completed in 2007 to finalise decommissioning while rehabilitation planting activities commenced soon thereafter. Rehabilitation is a process of stabilising disturbed areas and is considered successful when sufficient vegetation cover is established.

In 2010, mining at Grid A ceased and rehabilitation bulldozing was done on the Grid A WRD in May 2010. Sloping and capping activities were completed in 2010 and rehabilitation planting was done in the rainy seasons of 2010, 2011 and 2012. The various mining areas are illustrated in Figure 1.2 below.

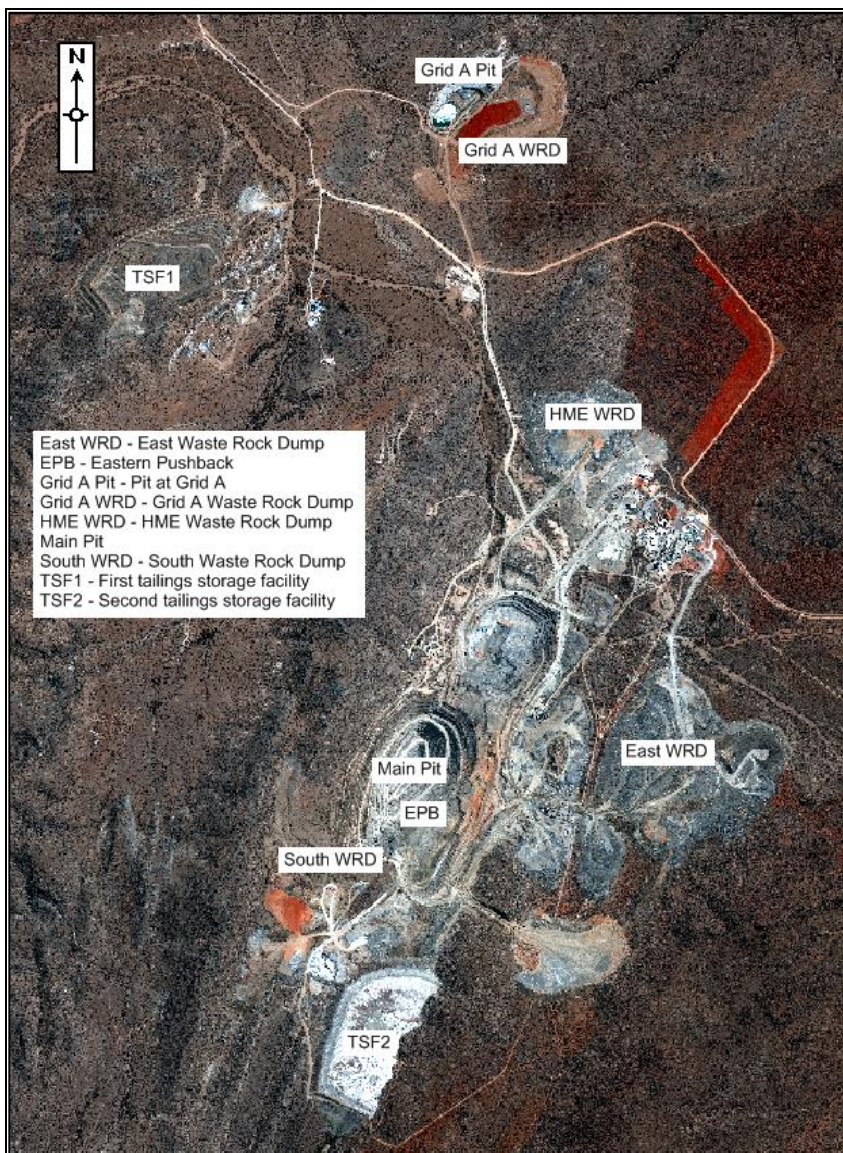


Figure 1.2 Main mining areas at Navachab Gold Mine

The research problem is outlined in the next section.

1.3 RESEARCH PROBLEM

According to the Navachab Gold Mine's procedure for rehabilitation and closure, all decommissioned WRDs and TSFs are sloped down by bulldozing to a maximum gradient of 18° and then covered with a suitable capping material. During the following rainy season, the Navachab Environmental Department starts with rehabilitation planting activities which involve the planting of indigenous trees and shrubs grown at the mine's own nursery.

The shortcoming of the rehabilitation and closure programme is that *no documented method exists to objectively monitor and quantify the programme's success or failure*. Gauged by the year-on-year improvement in vegetation cover, visually the programme appears to be successful, but a quantitative method that delivers a measured spatial output of the success or failure of the rehabilitation programme is absent. This constitutes the real world problem.

It has been shown that very high resolution (VHR) remotely sensed imagery holds much potential for vegetation monitoring. However, very little research has been done on using VHR imagery for monitoring mine rehabilitation progress. The techniques that have been applied are complex and require advanced remote sensing skills. There is consequently a need for a simple change detection method can be routinely applied by environmental managers with limited or no remote sensing background to quantify the effectiveness of the rehabilitation programmes.

The hypothesis is that remotely sensed vegetation indices and simple techniques such as image-to-image change detection can effectively be used for monitoring mine rehabilitation success.

1.4 AIM AND OBJECTIVES

The aim of this research is to determine whether synthesised high-resolution change detection maps will qualitatively illustrate the success or failure of the rehabilitation programme for TSF1 of the Navachab Gold Mine in Namibia. The following five objectives were set:

1. Review the literature on the available satellite sensors and image characteristics, and the various image-processing methods related to vegetation indices and change detection.
2. Collect information on Navachab Gold Mine's operational history and acquire climatic data and satellite imagery for the study period (2004 to 2011).
3. Preprocess the satellite imagery to improve image comparability.

4. Evaluate the most suitable method(s) of vegetation indexing and change detection for rehabilitation monitoring as evidenced by the experiments conducted.
5. Produce change detection maps and evaluate whether the procedure is suitable for quantifying the success of the rehabilitation programme.

The study requires the identification of an area that has been decommissioned and rehabilitated over an extensive period. Such areas are discussed in the next section.

1.5 STUDY SITE

The most suitable study area within the Navachab mine for evaluating the tools offered by remotely sensed images (satellite images) and remote sensing software is one that allows for study over a few consecutive years during which no modification occurs apart from rehabilitation plantings. Only two areas, namely TSF1 and the South WRD (Figure 1.2) have been fully decommissioned and rehabilitated to date but the possibility exists that the latter will be re-opened under a new mining plan. The most appropriate area for this investigation is consequently the decommissioned TSF1, which is 16ha in size. Since decommissioning in 2003, TSF1 has been capped with soil and some areas, where the slopes were very steep and eroding, were re-covered with waste rock (Figure 1.3).

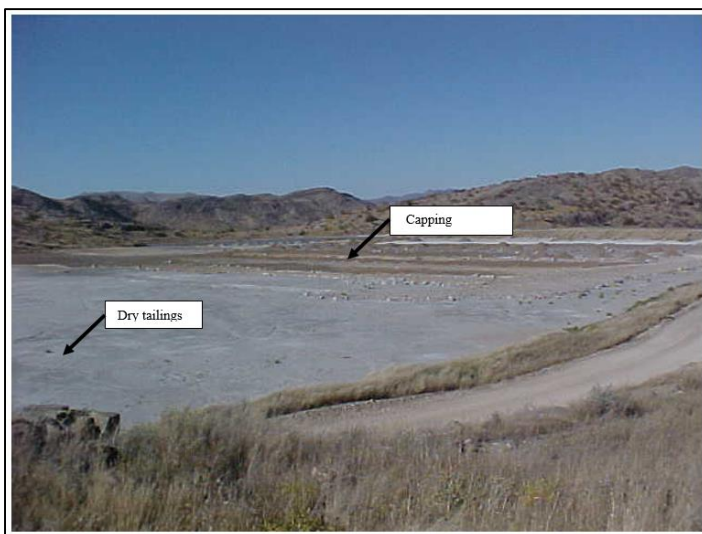


Figure 1.3 Picture taken of TSF1 during capping process

Tailings and capping material (soil) are clearly distinguishable in Figure 1.3. These features will be discussed in the later reporting on the georeferencing process.

Figure 1.4 illustrates the change in the top or upper surface area of TSF1 directly after capping (a), and after completion of several rehabilitation planting sessions (b). Rehabilitation started with sloping and capping in 2004 and the last rehabilitation planting was done in 2011. This time frame will be the period of this study.



Figure 1.4 Comparison of the top of the first tailings storage facility (TSF1) (a) directly after capping in January 2005 and (b) in March 2009 following a few years of rehabilitation. Source: author

The research methodology on how to reach the aim and objectives is described in Section 1.6.

1.6 RESEARCH METHODOLOGY AND RESEARCH DESIGN

According to Mouton (2001:158) implementation (process) evaluation aims “...to answer the question of whether an intervention (programme...) has been properly implemented..., whether the target group has been adequately covered and whether the intervention was implemented as designed.”

This study was empirical in nature and used a hybrid data approach involving analysis of primary data (images) and secondary data. Data collection involved acquisition of satellite images for historical baseline information, while other images were ordered for new collection. The data is both numeric and textual and a medium degree of control was exercised in the research design (Figure 1.5).

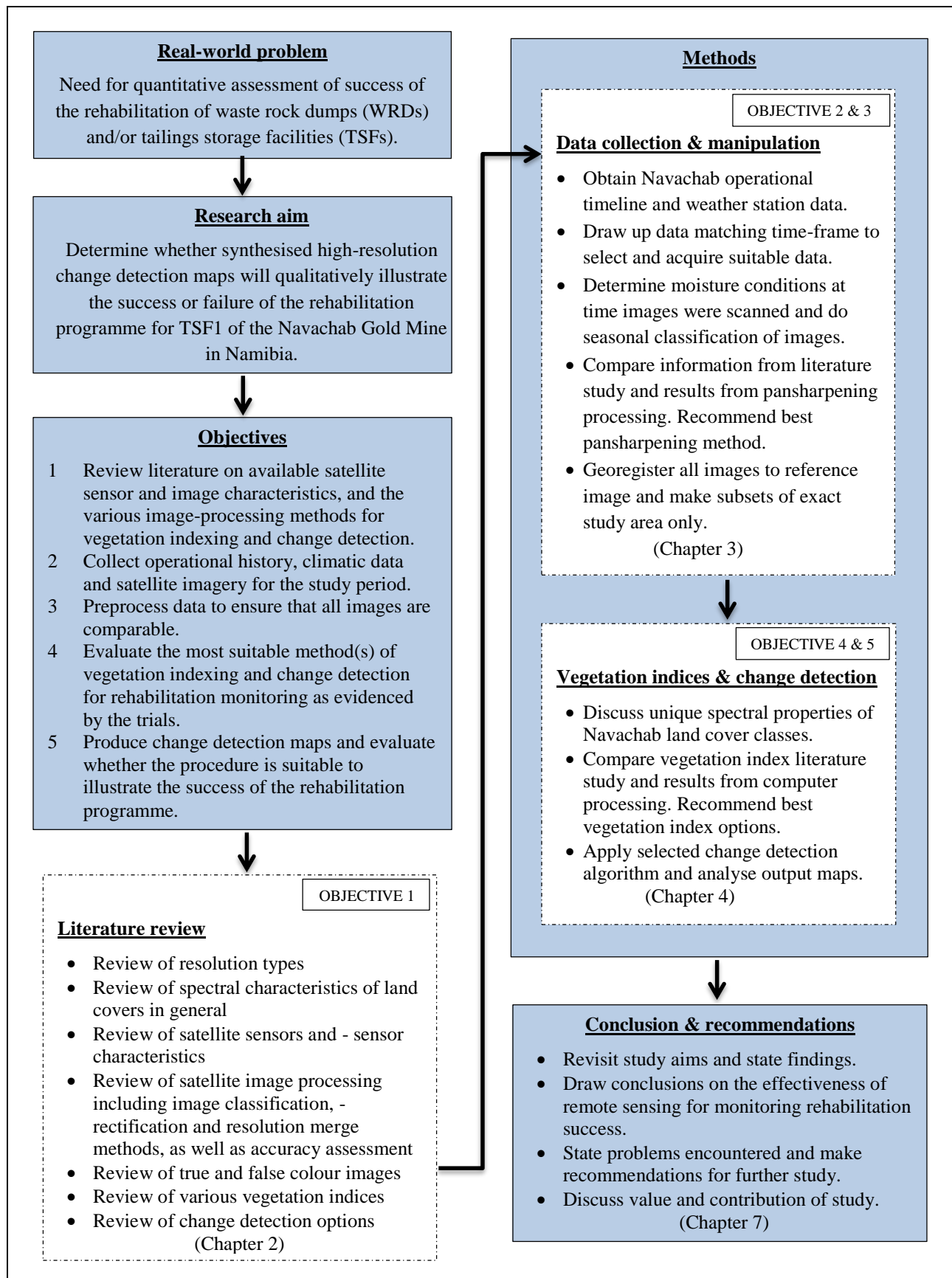


Figure 1.5 Research design for evaluating remote sensing in monitoring the success of the rehabilitation programme at Navachab Gold Mine

To assist interpretation of the images, a history of the mining process at Navachab was acquired for the mine which has been operational for more than 20 years. The life-of-mine (LOM) at commencement of this study was 2027 but this prediction changed many times during the research period. The research period started with the decommissioning of a specific area (baseline) and followed the progress in rehabilitation.

This chapter has outlined the background and purpose of the study. Chapter 2 focuses on the resolution and spectral characteristics of land covers as well as various earth observation sensors and the fundamentals of remote sensing and its applications. In Chapter 3 data collection and -manipulation procedures are detailed while the results of the various pansharpener and geometrical correction processing options are presented and discussed. It also contains a review of the spectral properties of the land cover classes in the study area. Vegetation index selection is discussed in Chapter 4 and change detection results are also presented and discussed. The thesis concludes with Chapter 5 in which the effectiveness of remotely sensed vegetation indices and change detection methods to monitor the success of rehabilitation programmes are evaluated.

The next chapter gives an account of types of resolution, properties of various satellite sensors and their images characteristics as well as the influence of vegetation factors on the appearance of satellite images.

CHAPTER 2 LITERATURE REVIEW

It is important to understand the technical details and options offered by remote sensing scanners and software to enable one to determine the implications of the choices one makes concerning the processing of remotely sensed data. This chapter focuses on fundamental remote sensing concepts. The review can guide rehabilitation managers in choosing the correct processing options for the tasks at hand or assist them to communicate with the remote sensing consultants.

A major factor in using satellite imagery is the cost of acquiring and processing the data. Although MODIS and Landsat images are free and consequently cheaper to obtain than Quickbird, Ikonos and GeoEye-1 images, the resolution of MODIS and Landsat images are not necessarily suitable for small areas. Moreover, processing software is expensive. Turner et al. (2003) noted that even more challenging than cost related to software and imagery, is the technical expertise required for processing imagery. The learning of these skills is not always part of the training of the personnel responsible for doing rehabilitation work at mines.

The literature review is initiated with a discussion of various sensor resolutions namely spectral resolution, spatial resolution, radiometric resolution and temporal resolution (Section 2.1). These resolutions describe how much data is captured in which bandwidths and how regularly. This is followed with a description of the spectral characteristics of land cover types relevant to the study area (Section 2.2). Details of satellites and sensor characteristics are given (Section 2.3), followed by considerations on the processing of satellite images (Section 2.4) and true and false colour images (Section 2.5). Lastly, the chapter is concluded with pertinent discussions on various vegetation indices (Chapter 2.6) and methods of change detection (Chapter 2.7).

2.1 RESOLUTION

To better understand what is meant by resolution and how it affects the data needs and research outcomes of this study, a short overview of spectral, radiometric, spatial and temporal resolution follows.

2.1.1 Spectral resolution

According to Mather (2006) the spectral resolution of an image relates to the width, number and position (in the electromagnetic spectrum) of the spectral bands. These factors determine the degree to which individual targets can be discriminated on the multispectral imagery. Two types

of images, namely panchromatic images and multispectral images, are relevant for this investigation. These images can be likened to black-and-white and colour photos respectively. For instance, the GeoEye-1 multispectral sensor records four bands namely blue (0.450–0.800 μm), green (0.510–0.580 μm), red (0.655–0.690 μm) and near-infrared (NIR) (0.780–0.920 μm), while its panchromatic scanner captures reflectance over a much wider range of wavelengths (0.450–0.900 μm) (see Figure 2.1). Multispectral imagery has a higher degree of discriminating power than panchromatic images. The underlying issues relating to spectral resolution are examined next.

2.1.1.1 Electromagnetic radiation and its properties

Bands are selected specifically for the type of features to be investigated. The electromagnetic (EM) spectrum, as illustrated by Figure 2.1, consists of various ranges of EM energy. All these ranges differ only by the wavelengths.

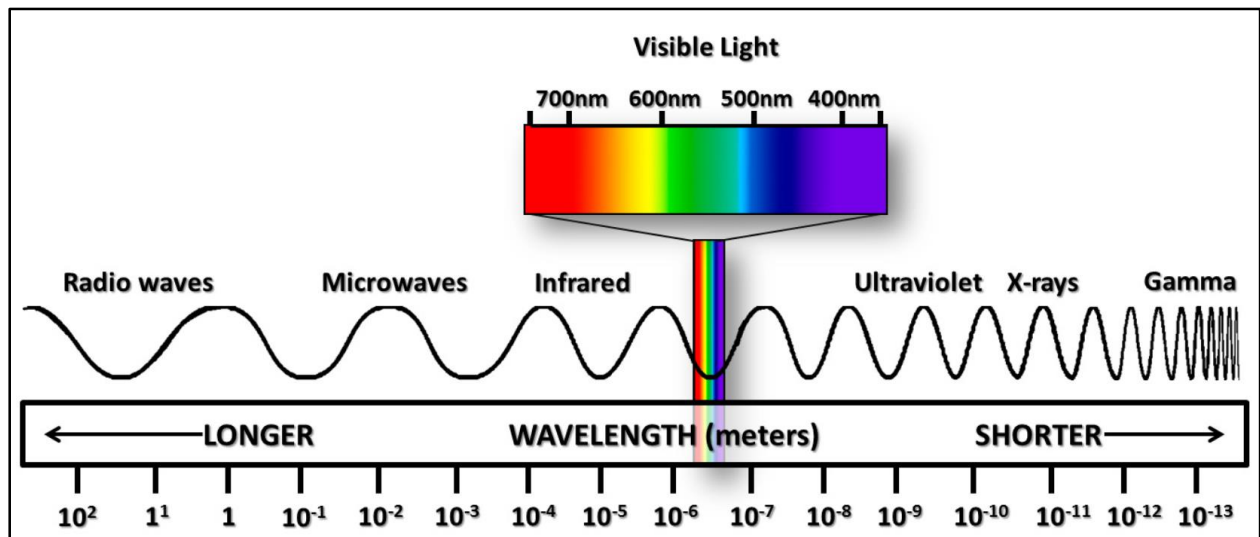


Figure 2.1 The electromagnetic spectrum

Source: NASA (2015)

The most well-known range of EM waves is that of visible light which consists of the portion of the EM spectrum that can be detected by the human eye. The colours range from violet (shortest visible wavelength) to red (longest visible wavelength). Visible light is divided into the three primary colours namely blue (0.4–0.5 μm), green (0.5–0.6 μm) and red (0.6–0.7 μm). Just shorter than the blue wavelength, is ultraviolet (UV). Progressively shorter, there are X-rays, γ -rays and cosmic rays (Lillesand, Kiefer & Chipman 2008).

At the end of the visible spectrum, just longer than visible red waves, are infrared (IR) waves, microwaves and radio waves. X-rays, γ -rays, cosmic rays, microwaves and radio waves are of little importance for multispectral remote sensing purposes. However, the IR region plays a major role and warrants more detailed examination. IR waves are divided into three categories, namely near-infrared (NIR), mid-infrared (mid-IR) and thermal infrared. The wavelengths of NIR ranges between $0.7\mu\text{m}$ and $1.3\mu\text{m}$, mid infrared between $1.3\mu\text{m}$ and $3.0\mu\text{m}$, and thermal infrared from $3.0\mu\text{m}$ to $14.0\mu\text{m}$. The IR bandwidths of waves have important applications in remote sensing of vegetation due to their unique and specific bandwidths of absorption or reflection by green plants (Ustin et al. 2004).

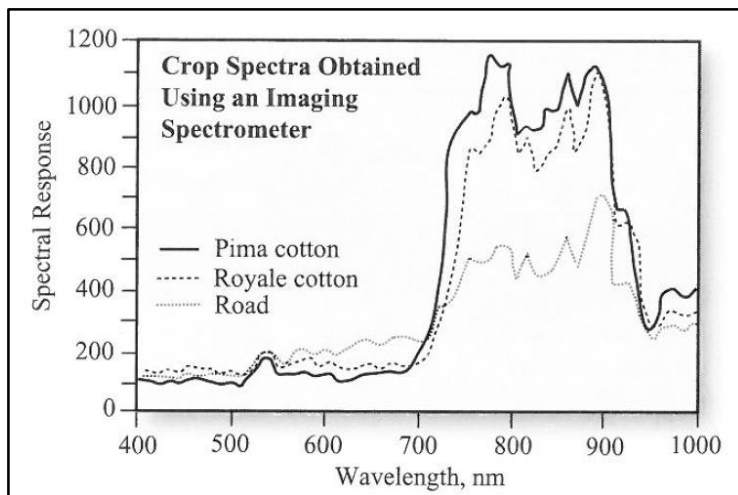
2.1.1.2 Choice of band width

The spectral resolution of an image sensor is partly defined by the width of the bands, measured in micrometres or nanometres, in which it records. Some sensors are designed to measure specific bandwidths. For example some sensors scan a single bandwidth or all visible bands (panchromatic) while others capture several bands (multispectral), hundreds of bands (hyperspectral) or many hundreds of bands (ultraspectral). A multispectral scanner produces sets of monochrome images in a small number of wide bands (Fonseca et al. 2011) with only one measurement being made in each band. The closer these bands are to the spectral reflective curve of the target, the better the target can be identified from the remotely sensed image (Jensen 2005) and consequently multispectral scanners are said to under sample the spectral characteristics of many land cover features.

In short, good contrast between the object of interest and its background provides the best discrimination. Careful selection of the bandwidth will give the best spectral contrast because the smaller the bandwidth, the better features such as rock type or vegetation species will be differentiated.

Hyperspectral and ultraspectral sensors scan at close intervals over a great number of spectral bands, often recording data in hundreds of narrow bands, whereas ultraspectral sensors record in many hundreds and even thousands of bands. To be able to use the information, special processing software is required to reduce the dimensionality (number of bands) to a manageable degree.

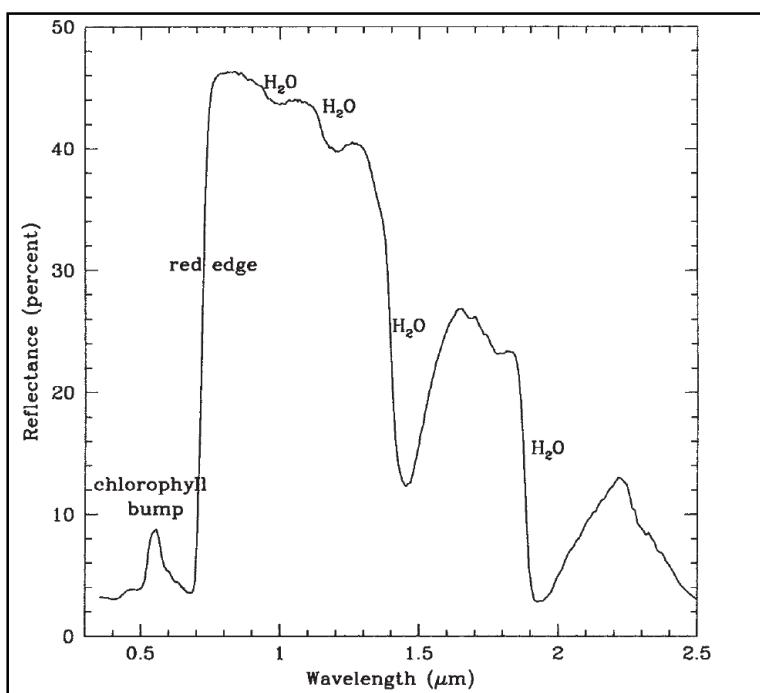
Figure 2.2 shows the spectra for two different types of cotton and a road surface using an imaging spectrometer.



Source: Jensen (2005: 91)

Figure 2.2 Spectra for Prima cotton, Royal cotton and road surface area using an imaging spectrometer

Jensen (2007: 240) points out that “...it is usually necessary to use algorithms that 1) analyse spectra to determine its constituent materials, and 2) compare the spectra with a library of spectra obtained using handheld spectra-radiometers... .” The purpose of a sensor therefore determines the type of optical imaging system. To determine the state of vegetation, bandwidths are selected within the blue, red, green and NIR spectral ranges. Red, green and blue wavelengths are mostly absorbed by photosynthesising vegetation whereas green light is reflected in a narrow band between $0.5\mu\text{m}$ and $0.6\mu\text{m}$ (Figure 2.3).



Source: Seager et al. (2005: 373)
reproduced from Clarke et al. 1993

Figure 2.3 Reflection spectrum of a deciduous leaf

Thus, non-photosynthetic (stressed) vegetation will lack the so-called ‘green peak’ or chlorophyll bump. Chlorophyll has a very specific absorption in the 0.64 – 0.69 μm range but healthy vegetation reflects about 50% of NIR waves and as a result appears bright above 0.7 μm . The steep increase in reflection from 0.75 μm is called the ‘red edge point’ (Horler, Dockray & Barber 1982; Seager et al. 2005) and this information is used extensively in vegetation change detection.

Blue bands distinguish water bodies from vegetation and green reflectance indicates the difference between aquatic plants and sediment (Mather 2006). The spectral characteristics of various land cover type features are discussed in greater detail in Section 2.2.

Unfortunately, bandwidths cannot be narrowed down indiscriminately. Determination of band width is a function of the signal-to-noise ratio (SNR) which is a measure of the purity of a signal. The higher the spectral resolution (narrower the bandwidth), the more noise it will contain. SNR can be influenced by the type of sensor. A pushbroom sensor with a linear array of sensors has a better SNR than a mechanical scanner with one detector. A pushbroom sensor gives more accurate measurements as there is no moving mirror and the linear array detectors will ‘look’ longer at a specific portion of the terrain (Fricker & Rohrbach 2005; Mather 2006). The next section explains how the signals that are captured by the detectors are converted to digital numbers.

2.1.2 Radiometric resolution

Radiometric resolution refers to the sensitivity of a sensor to incoming reflectance. The magnitude of electromagnetic energy is related to the number of divisions of bit-depth. A digital image can consist of two levels where 0 = black and 1 = white for a 1-bit quantization, 256 levels of grey for an 8-bit quantization (Liew 2001), or it can consist of up to 65 536 levels for 16-bit data (Khorram 2012).

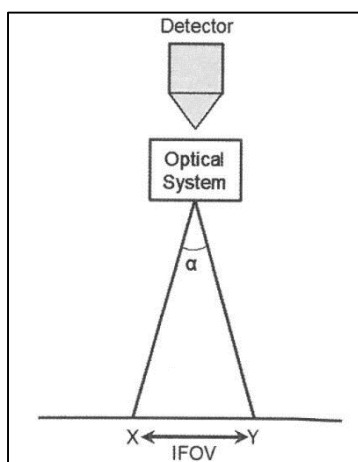
An older form of remote sensing is aerial photography with analogue cameras. These analogue images must be digitized to be processed by computer. Analogue images are scanned and the scanner divides the photograph into many small sections and assigns a number to each small section (pixel) related to the level of light reflected from that section (Mather 2006). As this number directly determines the amount of storage memory needed, the quantization level required should be based on the actual improvement in detail when higher levels are used. Tucker (1979), as cited by Mather (2006), found only a 2-3% improvement in classification accuracy was achieved when grey levels were increased from 64 to 256.

2.1.3 Spatial resolution

Spatial resolution relates to the amount of detail represented by an image and is expressed as the area on the ground captured by one pixel (Amro et al. 2011). Images consist of a matrix of pixels and the area covered by a pixel is a function of the spatial resolution of the sensor. Panchromatic images usually have a better spatial resolution than their corresponding multispectral images. For instance, GeoEye-1 panchromatic images have a resolution of 0.5m x 0.5m, that is each pixel represents an area of 0.5m x 0.5m (0.25m²) on the ground while the multispectral images have a spatial resolution of only 1.65m x 1.65m (2.72 m²) (GeoEye 2008).

Multispectral images often cover a wide range of wavelengths (spectral resolution) but usually at a lower spatial resolution, while panchromatic images normally have higher spatial resolution but with limited spectral resolution (Fonseca et al. 2011). Spatial resolution is influenced by a number of factors inherent to the sensor, namely the instantaneous field of view, point spread function, effective resolution element, nominal spatial resolution and look angle.

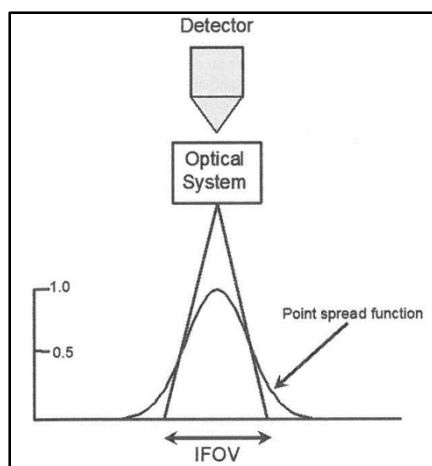
Instantaneous field of view (IFOV) is the measurement most often used in remote sensing to describe the spatial resolution of a sensor (Figure 2.4). IFOV can be measured as an angle (α) or as a circular area on the ground with the distance between two points being the diameter of the circle. The real IFOV is calculated by taking factors like a satellite's actual height above the surface of the earth into account. A smaller IFOV will deliver more detail and will produce an image with a higher spatial resolution (Amro et al. 2011).



Source: Mather (2006: 28)

Figure 2.4 Angular instantaneous field of view (IFOV), α , showing the projection X-Y on the ground where X-Y is the diameter of a circle.

Highly reflective point sources do not produce a single sharp image but rather resembles that of a three-dimensional bell curve and is called the point spread function. The shape of this curve is determined by the design of the optical system. The distribution of this curve is called the point spread function (PSF) and can be used as an alternate measure of spatial resolution. The presence of bright or dark objects within the IFOV of the sensor will increase or decrease the amplitude of the PSV curve which in turn will make the observed radiance either higher or lower than that of the surrounding areas. The difference between IFOV and PSF is shown in Figure 4.



Source: Mather (2006: 29)

Figure 2.5 Instantaneous field of view (IFOV) defined by the amplitude of the point spread function (PSF).

The better the contrast of the imagery, the sharper the image will be. Rivers and canals are often clearly visible in Landsat ETM+ images even though their width is less than the 30m spatial resolution of the sensor. However, some targets with dimensions larger than the 30m spatial resolution are blurry and not discernible in the same type of images. Atmospheric scattering and absorption may also cause a loss in contrast and further contribute to loss of clarity in the image (Otterman & Fraser 1979).

IFOV is a geometrical definition which considers the spectral properties of the target. Effective resolution element (ERE) not only records radiation but considers the way the radiation is generated. Mather (2006: 29) quotes the definition of ERE by Colvocoresses (cited by Simonett 1983) as “the size of an area for which a single radiance value can be assigned with reasonable assurance that the response is within 5 per cent of the value representing the actual relative radiance.”

Nominal spatial resolution (NSR) is the dimensions of the ground-projected IFOV in metres. Jensen (2005) advises that a greater spatial resolving power will be attained by a smaller the

nominal spatial resolution. For the collection of urban data, a high NSR of around 1m x 1m is needed. Imagery with an NSR lower than 10m x 10m is not of much use for urban analysis. For continental-scale analysis a lower NSR (e.g. 79m x 79m of the historical Landsat multispectral data) is appropriate for the analysis at global scale, and even resolutions of 700m x 700m (e.g. GOES) or 1100m x 1100m (e.g. AVHRR) are often suitable (Jensen 2005).

Images can be scanned at right angles to the earth's surface (vertical viewing or nadir) or at an angle (oblique viewing or off-nadir). Off-nadir images scanned from opposite, but equal, angles can be combined to enable stereoscopic imaging. A sensor that can scan off-nadir images is called 'pointable'. For analysis of change detection, the influence of sun-angle on the imaged surface needs to be minimised and scans should be taken as close to nadir as possible. Images acquired off-nadir will record reflection from the side of plants and other objects. The main advantage of off-nadir viewing capabilities is its ability to increase the temporal resolution of a sensor.

2.1.4 Temporal resolution

The revisit time or temporal resolution of a satellite is the time between subsequent passes over a certain area or object (Kerr & Ostrovsky 2003). Revisiting times range from 16 days for Landsat down to three to four days for GeoEye-1 (Jensen 2007; GeoEye 2008). Revisiting times of the various satellites will be discussed in more detail in Section 2.3. Temporal resolution is especially important in situations where a certain area or object has to be scanned very regularly or in areas where a high incidence of cloud cover prevents a full scan of the area on a specific day. Temporal resolution is also influenced by the sun-angle. Scans should ideally be repeated at approximately the same time of the day and preferably on the same day of the year in order to minimise the influence of seasonal sun-angle variations (Mather 2006) although corrections can be done to multi-seasonal images to eliminate these differences (Qi et al. 1995; Lillesand, Kiefer & Chipman 2008). Related to sun-angle are the phenological differences in plants due to variation in seasonal cycles and precipitation (Jenerette, Scott & Huete 2010). Because plants in different growth phases impact negatively on change detection studies, vegetation characteristics are treated in detail in the next section.

2.2 SPECTRAL CHARACTERISTICS OF LAND COVERS

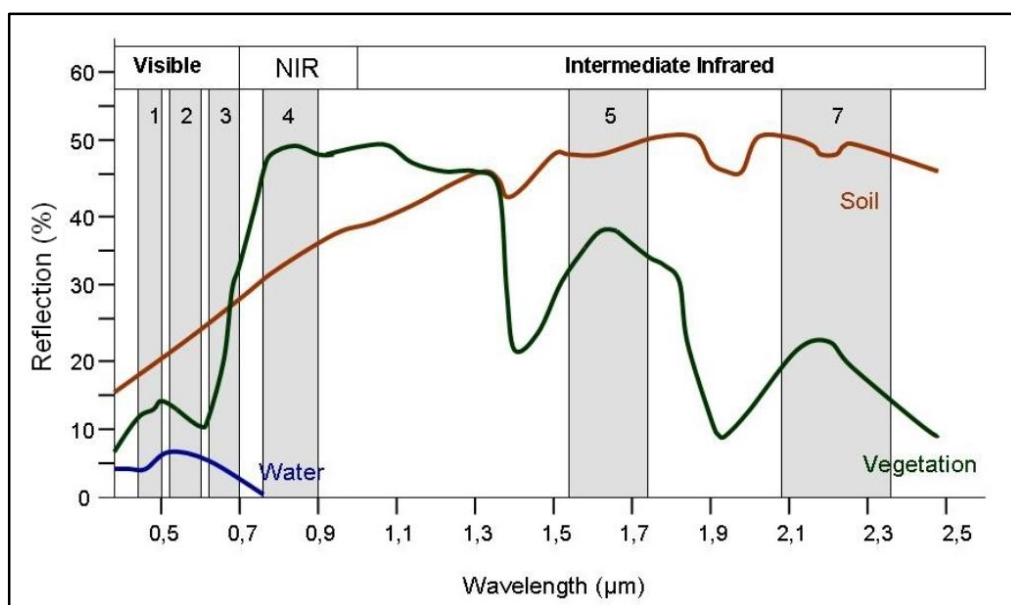
Spectral signatures (Kiefer & Chipman 2008) are spectral measurements taken of pure samples of substances with a spectrometer in laboratory conditions (Clark et al. 1993; Clark et al. 2007;

Lillesand; Matiwane 2009a; Matiwane 2009b). These spectral signatures contain unique patterns of absorption and reflection at specific wavelengths which can be used to identify certain land covers and to distinguish land cover types from each other (Singh 1989). Spectral measurements obtained from satellite images or similar platforms are less exact as the pixels often contain more than one land cover type and are therefore called spectral response patterns instead (DiBiase 2014). The characteristics of land cover classes water, bare (rock and soil), and vegetation (shrubs and trees) are important in this study. These land cover types are discussed in the following subsections.

2.2.1 Water

Clear water moderately reflects the blue, green and red wavelengths but the unique and identifying feature is the strong absorption in the near-infrared (NIR) and longer wavelengths. These wavelengths are absorbed by any type of moisture whether it is a lake or dam, or moisture contained within plants or even in wet soil (Hunt & Rock 1989; Sims & Gamon 2003).

The spectral reflectance of water is affected by the depth (Lyzena 1978) and clarity (Li & Li 2004) of the water body. Deep, clear water will have virtually no reflectance in the NIR region (Mather 2006). Figure 2.6 shows the reflective properties of vegetation, soil and water in the visible, NIR and intermediate IR regions (SEOS Project website 2014).



Source: SEOS Project website (2014)

Figure 2.6 Spectral signature for water, soil and vegetation in the visible, NIR and intermediate IR regions

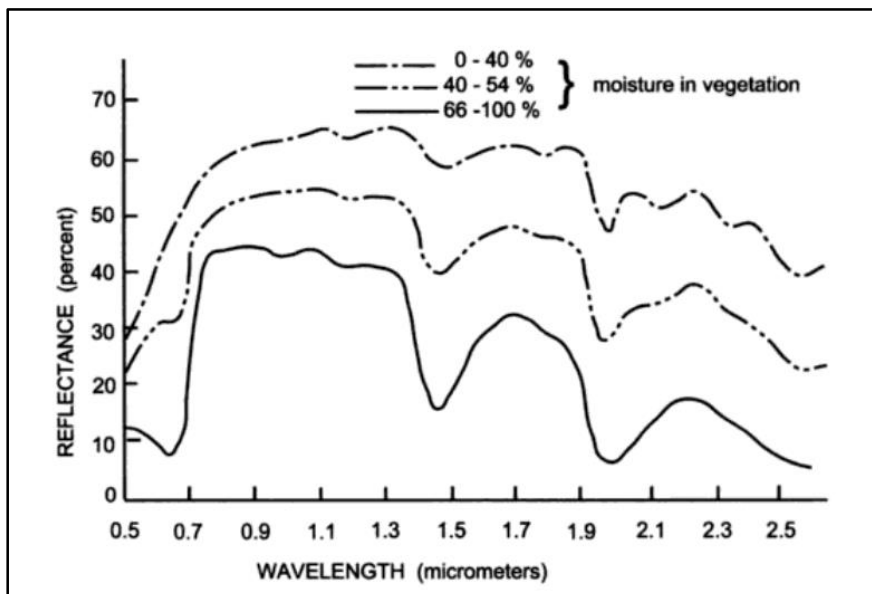
On the other hand an increase in chlorophyll due to aquatic plants will increase absorption and therefore decrease the reflectance in blue wavelengths and increase reflectance in the green and NIR wavelengths (Lillesand, Kiefer & Chipman 2008).

2.2.2 Vegetation characteristics

A good understanding of the interactions between energy and plants helps one to interpret remotely sensed data. McCoy (2005) lists some important interactions of energy with leaf pigments, leaf cell structure and plant moisture content. A short account follows.

2.2.2.1 Leaf pigments

Pigments in leaves consist mainly of chlorophyll (green), carotene (yellows), xanthophyll (browns) and anthocyanin (reds). In actively photosynthesising green leaves, reflection in the green wavelengths dominates with a strong absorption in the blue and red wavelengths (Buschman, Langsdorf & Lichtenthaler 2000; Nishio 2000). However, as leaf colour changes, either through dehydration or senescence, less reflection is observable in the green wavelengths and increased reflection in the blue and red wavelengths. Reduced moisture generally results in an overall increase in reflectance over all visible bands (Figure 2.7).



Source: Hoffer & Johannsen (1968) as cited by McCoy (2005: 73)

Figure 2.7 Change in spectral curves with different vegetation moisture levels

2.2.2.2 Leaf cell structure

The overall reflectance from plant leaves quadruples between wavelengths of 0.7 μ m and 1.2 μ m and absorption decreases to a minimum while a very strong reflectance is observed in certain NIR

wavelength regions (Thenkabail, Smith & De Pauw 2000). These increases in the NIR wavelengths are unique to plants and are caused by the cell structure rather than by pigments. A specific narrow band 0.9-0.94 μm called the ‘red-edge point’ provides an accurate distinction from other surface materials, especially soil and water (Leblon 1997). Variation in reflectance among plant species is also greater in the NIR wavelengths due to differences in the internal structures, mainly mesophilic tissues, and allows discrimination between various species (Prithvish & Kudrat 1998). Notably, some plants may be indistinguishable in the visible spectrum but show clear differences in the infrared wavelengths. Moreover, spectral responses also change with cover density. As plant cover decreases and more soil is detected through the vegetation, the spectral curve changes to a typical soil spectral curve. This provides the basis for estimations of cover density from image data (Huete, Jackson & Post 1985).

2.2.2.3 Energy transmission through leaves

In the NIR wavelengths, more incident energy reaches leaves that are not exposed to an overhead view. Lower-level leaves also reflect some of the incident energy so that there is an increase of reflected energy at the top of a plant – more than what the outer leaves reflect on their own – thereby presenting a useful method to determine the mass of a plant instead of just the crown diameter (Ollinger 2010).

2.2.2.4 Plant moisture content

Three major water absorption bands exist at 1.4 μm , 1.9 μm and 2.7 μm respectively. The values in these bands are directly related to the amount of moisture in a plant. A plant that is losing moisture shows an increased overall reflectance but the reflectance in the water-absorption bands decreases concomitantly. This information is used extensively in plant stress investigations using satellite imagery (Lillesand, Kiefer & Chipman 2008).

2.2.3 Rock and soil

Areas absent of water, vegetation or built-up objects are considered bare and are characterised by the spectral properties of soils and exposed rock. The spectral properties of most soil and rock types were documented by Baldrige et al. (2009) and can be used as a reference to identify various substrate. Soil and rock reflectance curves are related in that each soil will show reflectance characteristics that are similar to that of the parent rock material (Leblon 1997).

In the visible bands absorption is affected by the presence of organic matter, the presence of moisture and the presence of ferric iron (Stoner & Baumgardner 1981). In general dry rock and soil classes show a consistent rise in reflectivity as wavelength increases in the visible and NIR portions of the spectrum (Jensen 2007). Soil reflectance patterns are compared with those of water and vegetation in Figure 2.6. Organic material increases absorption and therefore reduces the reflectance of the soil in the visible wavelengths. Above levels higher than 2% organic matter content will dominate the soil colour but below this percentage other soil constituents will determine the colour of the soil (The presence of photosynthetically active plant material will result in a very sharp increase in the NIR region (Section 2.2.2).

Increasing soil moisture will show a strong reduction in reflectance in all wavelengths (Streck, Rundquist & Connot 2003), also the NIR region (Jensen 2007). This is due to the layer of water in the soil surface absorbing much of the incident radiation and therefore lowering the overall reflectivity (Section 2.2.1). Wet soils and rocks often appear visibly darker than dry soils and rocks (Jensen 2007). Texture also influences the reflectivity of soils. Finer soils are usually clayish in nature with poorer drainage and are consequently associated with higher soil moisture compared to soils with larger grains and better drainage (Baumgardner et al. 1985).

The presence of iron oxide significantly reddens the soil and therefore increases absorption of wavelengths shorter and longer than those in the red spectrum (Mather 2006).

How satellite images capture the spectral properties of soils and other land cover types is determined by their spectral, radiometric and spatial resolution as discussed in Section 2.1. For this study medium or lower spatial resolution imagery was not considered as it would not be suitable for monitoring rehabilitation progress in the study area. The next section provides an overview of the various very high spatial resolution imagery that are available.

2.3 SENSORS AND SENSOR CHARACTERISTICS

IKONOS, OrbView-3 and Quickbird scanners have the same bandwidths (Table 2.1) and all three satellites are sun-synchronous with an equatorial crossing between 10:00 and 11:00. The spatial resolutions are 1m x 1m panchromatic resolution and 4m x 4m multispectral resolution for IKONOS and OrbView (Kohm 2004). Improved 0.61m x 0.61m panchromatic and 2.44m x 2.44m multispectral resolutions for Quickbird have been introduced. GeoEye-1 collects data at 0.41m panchromatic and 1.65m multispectral resolution.

GeoEye-1, launched in September 2008, is also a sun-synchronous, polar-orbiting satellite, which orbits the earth 15 times per day at an altitude of 681km and its pass time at the equator is about 10:30 each day. The spatial accuracy is predicted to be within 3 metres. In accordance with USA legislation, any sub half-meter imagery is resampled to 0.5m before it is supplied to commercial customers (GeoEye 2008; DigitalGlobe 2013). The GeoEye-1 sensor can turn and swivel very quickly in orbit and the sensor can point directly below (nadir) or off-nadir. Off-nadir viewing can be up to 60° side-to-side or front-to-back giving the satellite exceptional temporal resolution and revisiting period (GeoEye 2008).

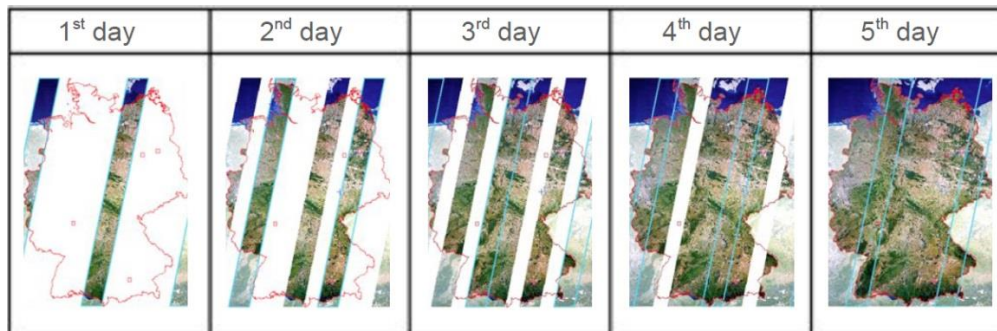
In Table 2.1 the properties of five very high spatial resolution sensors are compared.

Table 2.1 Comparison of various high-resolution (<5m) sensors

Description	Space Imaging Inc. IKONOS	Orbimage Inc. OrbView-3	DigitalGlobe Inc. Quickbird	GeoEye GeoEye-1	RapidEye
Blue band (µm)	0.45 – 0.52	0.45 – 0.52	0.45 – 0.52	0.450 – 0.800	0.440 – 0.510
Green band (µm)	0.52 – 0.60	0.52 – 0.60	0.52 – 0.60	0.510 – 0.580	0.520 – 0.590
Red band (µm)	0.63 – 0.69	0.63 – 0.69	0.63 – 0.69	0.655 – 0.690	0.630 – 0.685
Red edge band (µm)	N/A	N/A	N/A	N/A	0.690 – 0.730
Near Infrared band (µm)	0.76 – 0.90	0.76 – 0.90	0.76 – 0.90	0.780 – 0.920	0.760 – 0.850
Panchromatic band (µm)	0.45 – 0.90	0.45 – 0.90	0.45 – 0.90	0.450 – 0.900	N/A
Sensor type	Linear array pushbroom, Along and cross-track viewing Off-nadir up to 26°	Linear array pushbroom, Off-nadir up to 45°	Linear array pushbroom Along and cross-track viewing Off-nadir up to 25°	Linear array pushbroom Along and cross-track viewing Off-nadir up to 60° in any direction	Linear array pushbroom
Spatial resolution	1m x 1m (pan) 4m x 4m (multispectral)	1m x 1m (pan) 4m x 4m (multispectral)	0.61m x 0.61m (pan) 2.44m x 2.44m (multispectral)	0.41m x 0.41m (pan) 1.65m x 1.65m (multispectral)	6.5m x 6.5m (multispectral)
Swath width	11km	8km	20km – 40 km	15.2km	77km
Radiometric resolution	11 bits	11 bits	11 bits	11 bits	Up to 12 bit
Revisit time	< 3 days	< 3 days	1 to 5 days	3 days or less	Daily (off-nadir) & 5.5 days (at nadir)
Orbit	681km, 98.1° Sun-synchronous Equatorial crossing 10:00 – 11:00	470km Sun-synchronous Equatorial crossing 10:30	600km, 66° Not sun-synchronous Equatorial crossing varies	681km Sun-synchronous Equatorial crossing 10:30	630km Sun-synchronous Equatorial crossing 11:00
Launch date	24 September 1999	26 June 2003	18 October 2001	6 September 2008	29 August 2008

Source: Adapted from Jensen (2005: 88), GeoEye-1 fact sheet (2008) and RapidEye satellite sensor (2013)

The RapidEye constellation consists of five satellites with identical sensors that are also located in the same orbital plane. Revisit time is unsurpassed as each of the four actively scanning satellites does 15 orbits per day (Figure 2.8). The fifth satellite in the constellation is kept on standby (Lösel 2009). This rapid orbiting by the various RapidEye satellites allows for full coverage in five days.



Source: Lösel (2009)

Figure 2.8 Complete coverage of Germany in five days by RapidEye satellites

The processing of satellite image is discussed in the next section.

2.4 PROCESSING OF SATELLITE IMAGES

This section briefly introduces various classification methods and points out the decisions that need to be made when executing such processing. Attention is also given to the rectification of images and the nature of true and false colour images.

2.4.1 Image classification

Classification of remotely sensed images is the process of analysing an image to obtain thematic information. As explained in Section 2.2, materials respond to electromagnetic energy in specific ways and may reflect and/or absorb and/or transmit the energy. The pattern of interaction also differs between the different wavelengths so that a distinctive spectral response pattern (SRP) can be identified for each material. Each pixel of spectral data needs to be evaluated and assigned to the class of spatial data it belongs to. During this process data is changed into useful information. The process consists of two basic steps: The first is the recognition of categories or real-world objects, and the second is the labelling of the entities (often pixels) to be classified (Mather 2006).

Various methods, and combinations of methods, exist to do multispectral classification. Among these are (Jensen 2005; Mather 2006):

- Parametric and nonparametric statistics, and non-metric methods;
- Supervised or unsupervised classification logic;
- Hard or soft (fuzzy) classification logic;
- Per-pixel or object-based classification logic; and
- Hybrid approaches.

A short description of each of these methods follows.

2.4.1.1 Parametric, non-parametric and non-metric methods

The terms parametric and non-parametric are classifications of statistical procedures. Parametric methods make certain assumptions about the data or parameters involved while non-parametric data is regarded as ‘assumption free’ (Hoskin n.d.). An exact understanding of the meaning of the terms is not necessary but the following distinction given by Sheskin (2004: 97) will suffice:

“As a general rule, inferential statistical tests which evaluated categorical/nominal data and ordinal/rank-order data are categorized as nonparametric tests, while those tests that evaluated interval data or ratio data are categorized as parametric tests.”

Amongst the parametric methods are maximum likelihood classification and unsupervised clustering. Both assume normally distributed remotely sensed data and knowledge about the forms of the underlying class-density functions. Non-parametric methods such as nearest neighbour classifiers, fuzzy classifiers and neural networks are applicable to remotely sensed data that is not normally distributed and without the assumption that the forms of the underlying densities are known. Non-metric methods such as rule-based decision tree classifiers can operate on nominal, ordinal, interval or ratio data (Jensen 2005).

2.4.1.2 Supervised and unsupervised classifications

During supervised classification, a priori knowledge of the land cover types is used to identify specific sites that represent homogeneous examples of land cover types. Information about the area may be obtained from fieldwork, air photo analysis or appropriate maps (Mather 2006). These sites are referred to as training sites. Subsequently, the spectral characteristics of the training sites are used to train the classification algorithm for land cover mapping of the rest of the data. Every pixel within and outside the training site is evaluated and assigned to the class of which it has the

highest likelihood of belonging or being a member. Additional non-remotely-sensed data is more easily incorporated into a supervised classification using non-parametric methods (Mather 2006).

On the other hand, in unsupervised classification the identities of the land cover type are generally not known a priori because either there is a lack of ground-reference information or the surface features are not well defined. Hence, the software groups pixels with similar spectral characteristics into clusters or spectral classes while the analyst relabels and combines the spectral clusters into information classes (Lillesand, Kiefer & Chipman 2008), hence Mather (2006) suggests that the term ‘exploratory’ might better describe this process.

Change detection is a form of unsupervised classification of multitemporal data sets and the process is based on the principle of comparing the spectral qualities of pixels at different points in time. The spectral values of images sensed in different years or seasons are compared (Kennedy et al. 2009).

2.4.1.3 Hard and soft classification logic

Supervised and unsupervised classification algorithms that make use of hard classification logic, produce maps that consist of hard, discrete (unequivocal) categories and, consequently each pixel can only belong to one class (Straker et al. 2004). Conversely, soft (fuzzy) classification logic takes the heterogeneous and imprecise nature of the real world into account as pixels do not always just contain one class of object (Mehner et al. 2004; Jensen 2005; Nichol & Wong 2007).

Fuzzy classification is based on the sensors’ recording of reflected or emitted radiant flux from a mixture of materials and each pixel being described more extensively in terms of the various land cover types. Pixels are graded by membership to the classes they resemble and therefore can, and most probably will, belong to more than one class (Mather 2006; Musande et al. 2012).

An alternative method to deal with mixed pixels is to compare the spectral value of the pixel to reference values obtained by measuring a known object in a laboratory or even on a satellite image (Nichol & Wong 2007; Lillesand, Kiefer & Chipman 2008; Paniagua et al. 2009).

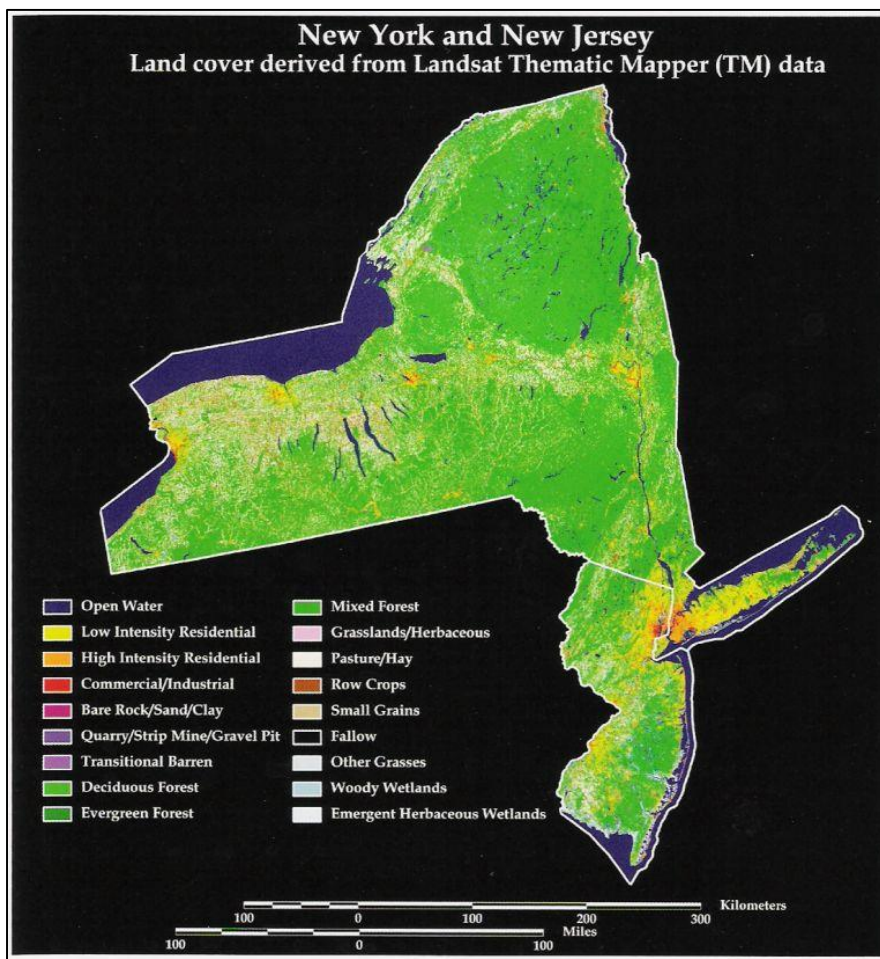
2.4.1.4 Per-pixel and object-based classifications

Per-pixel classification refers to processing the entire image pixel by pixel, while object-based classification allows the analyst to group the image into homogeneous patches or segments using

a multi-resolution image segmentation process (Jensen 2005). Consequently, the classes of interest dictate whether to use hard or fuzzy classification and whether per-pixel or object-orientated classification logic should be used. Walsh et al. (2008) found that the object-orientated classification performed better than the per-pixel method in their data analysis of invasive plant species.

2.4.1.5 Typical land-use and land cover classifications

Spectral signatures of topographical features provide a convenient method for identifying different substances or classes of substances into land-use and/or land cover classes without having to physically visit an area. Once a substance or class has been identified, all areas showing similar characteristics will be recognised similarly. An example of such a land cover map from Lillesand, Kiefer & Chipman (2008) is given as Figure 2.9.



Source: Lillesand, Kiefer & Chipman (2008)

Figure 2.9 New York and New Jersey land cover derived from Landsat TM data

Pure spectral signatures can only be obtained from laboratory tests where the spectral sensor is placed very close to the target object. When the sensor is very high above the target, the 'pureness' of the signature will depend on the spatial resolution of the sensor. Therefore, the greater the spatial resolution of a specific sensor is, the purer the spectral signature and the better the resulting classification.

When the spatial resolution of the spectral sensor is low, the sensor will cover a fairly large area at one time and a large number of classes of objects may be all detected at the same time. This gives rise to mixed pixels which in turn are subjected to hard or soft classification (Mather 2006).

Before any processing can be done on satellite images certain rectification or correction procedures have to be done (Van Niekerk 2009, Pers com). The various rectifications needed are described in the next section.

2.4.2 Image pre-processing

Digital satellite images play important roles in mapping and in the acquisition and visualization of data in a geographic information system (GIS). Such images help put some spatial concepts into perspective and are very useful for gathering spatial information. Errors from various sources are introduced during the remote sensing process. These include data acquisition errors, data processing errors and final product presentation errors (Lunetta et al. 1991).

To use images for accurately measuring distances, angles, positions and areas one must first remove distortions from the images through a process of correction (Ford & Zanelli 1985). The various correction or rectification activities include the following: Atmospheric and radiometric correction, geometric correction and topographic correction. A short description of each event is provided next.

2.4.2.1 Atmospheric and radiometric correction

Atmospheric and radiometric correction compensates for effects of scattering and absorption of EM waves by the atmosphere and the conversion of digital numbers (DN) (values stored in the images) to reflectance. Such corrections are particularly important whenever estimates of the ground-leaving radiances or reflectance are required (rather than relative values), for change-over-time studies or when the part of the signal that is of interest is smaller in magnitude than the atmospheric component.

DN can be transformed into percentage reflectance in a two-step mathematical calculation. First the spectral radiance (L_λ) is calculated (Equation 2.1) and then this radiance value is used in a successive formula (Equation 2.2) to calculate the reflectance (ρ_p) (Podger, Colwell & Taylor 2011).

$$L_\lambda = \text{Gain}_\lambda \times \text{DN}_\lambda + \text{Offset}_\lambda \quad \text{Equation 2.1}$$

where λ refers to the specific spectral band of the image (blue, green, red or NIR);
 L_λ is the spectral radiance for band λ at the sensor's aperture in $\text{mW}/\text{cm}^2/\mu\text{m}/\text{str}$;
 Gain_λ is the radiometric calibration gain in $\text{mW}/\text{cm}^2/\mu\text{m}/\text{str}$ for band λ ;
 DN_λ is the digital number value of band λ ; and
 Offset_λ is the radiometric calibration offset ($\text{mW}/\text{cm}^2/\mu\text{m}/\text{str}$) for band λ from image metadata.

The gain_λ and offset_λ values are supplied in the metadata text files received from the suppliers along with the earth-sun distance. The mean solar exo-atmospheric spectral irradiance ($E_{\text{Sun}\lambda}$) values in $\text{mW}/\text{cm}^2/\mu\text{m}/\text{str}$ are obtainable from an online solar position calculator (University of Oregon Solar Radiation Monitoring Laboratory 2013) for the respective image scan dates.

$$\rho_p = \frac{\pi \times L_\lambda \times d^2}{E_{\text{Sun}\lambda} \times \cos\theta_s} \times 100 \quad \text{Equation 2.2}$$

Where ρ_p is unitless planetary reflectance;
 π is the value 3.14159;
 L_λ is the calculated spectral radiance for band λ at the sensor's aperture in $\text{mW}/\text{cm}^2/\mu\text{m}/\text{str}$;
 d is the Earth-Sun distance in astronomical units;
 $E_{\text{Sun}\lambda}$ is the mean solar exo-atmospheric spectral irradiance in $\text{mW}/\text{cm}^2/\mu\text{m}/\text{str}$ at one astronomical unit Earth-Sun distance; and
 $\cos\theta_s$ is the solar zenith angle.

The solar zenith angle is calculated from the solar elevation angle by Equation 2.3 (Podger, Colwell & Taylor 2011). The solar elevation angle is usually supplied in the image metadata files.

$\theta_s=90^\circ$ - Solar Elevation Angle

Equation 2.3

When radiometric and atmospheric correction is done for the purpose of change detection, the same algorithm should be applied to all the images in the set (Jensen 2005).

2.4.2.2 Geometric correction

Lillesand, Kiefer & Chipman (2008) explains that raw digital images usually contain geometric distortions which have to be rectified before the image can be used as a map. These distortions originate from factors such as altitude, attitude and velocity of sensor platform as well as panoramic distortions, distortions due to earth curvature and relief displacement. The processing of data to conform to map coordinates is called geometric correction.

Georeferencing, is the transformation of a remotely-sensed image to have the scale and projection properties of a given map. Georegistration is a similar technique where an image is fitted to the coordinate system of a second image of the same area. Very accurate registration is needed when images will be used for change detection (Mather 2006). The goal is to keep each pixel in exactly the same location on the ground in consecutive images.

Jensen (2005) describes two types of geometric correction: The first type is image-to-map rectification where an image is processed to conform to map coordinates by selecting ground control point image pixel coordinates and aligning these with the map coordinates. The second form of geometric correction involves image-to-image registration where images are aligned with a reference image. This correction is done where temporal changes between two images need to be identified without a need for points to be assigned unique x and y coordinates in a map projection. This process is referred to as georegistration in this study. The transform should be over-defined, meaning that more than the minimum number of tie points are required to reduce the RMSE to the sub-pixel level needed for the required accuracy. Evaluation of the X- and Y-residual values along with the RMSE values will indicate the accuracy levels. More tie-points and a refined placing of tie-points might be required before an acceptable accuracy is obtained.

Orthorectification is an advanced method of terrain correction (Dial et al. 2003; Satellite Imaging Corporation 2013) that involves fitting a satellite image to a digital elevation model (DEM). By using a DEM the effects of relief displacement can be reduced (Dorfling 2013, Pers com).

Orthorectified images are planimetrically true images that represent ground objects as close as possible to their real world position.

2.4.2.3 Topographic correction

Topographic slope and aspect may introduce radiometric distortion of the recorded signal. Removing topographic effects, especially in mountainous regions, can enhance the usefulness of satellite images, for example when an area of interest is in complete shadow. Shadows and differences in radiation are removed, or at least reduced, in order to make the data more useful. Most of the research in this field is specifically directed at Landsat and SPOT digital multispectral data (Jensen 2005).

2.4.3 Pansharpening

Pansharpening combines the high spatial resolution of one image with the lower spatial resolution of another image. The process is also called resolution merge or image fusion. There are various pansharpening methods from which to choose. Švab & Oštir (2006) divide these methods into two broad groups. The first class consists of the colour related techniques including tri-stimulus colour composition in red green and blue (RGB) colour space and intensity hue and saturation (IHS) transformation. The second class consists of statistical and numerical techniques. Statistical methods include principle components analysis (PCA), regression and filters while the numerical methods follow arithmetic operations such as image addition, division, multiplication and subtraction. Wavelet pansharpening is a sophisticated and highly successful numerical approach.

Before pansharpening can be done, both images must be exactly the same size and precisely coregistered (Van Niekerk 2010, Pers com). If coregistration is not inherent in the data set, the two images have to be coregistered before the merge is attempted. The transform should be over-defined, meaning that more than the minimum number of tie points are required to reduce the RMSE to the sub-pixel level needed for the required accuracy. Evaluation of the X- and Y-residual values along with the RMSE values will indicate the accuracy levels. More tie-points and a refined placing of tie-points might be required before an acceptable accuracy is obtained.

Remote sensing software offer many different pansharpening techniques. Some of the most prominent techniques are subtractive pansharpening (SRM), high pass filter (HPF) pansharpening, modified IHS pansharpening, wavelet pansharpening, Ehlers fusion and three algorithm

pansharpener options, namely multiplicative, principle components analysis (PCA) and the Brovey transform. A short discussion of each of the pansharpener methods follows.

2.4.3.1 Modified intensity hue saturation pansharpener

Human colour perception is associated with the cone-shaped photoreceptors in the retina of the eye. The cones enable photopic vision that makes a distinction between colours (or hues) and degrees of saturation and levels of intensity. Three kinds of cones exist, each responding to one of the three primary colours of light (red, green or blue). Each colour of light is therefore made up of varying combinations of the primary colours and this is known as the tristimulus theory of colour vision (Mather 2006).

The IHS model explains colour perception in terms of hues (colours), saturation and intensity. Hue is the dominant wavelength of perceived colour while saturation refers to the purity of the colour and intensity to the brightness of the colour (Lillesand, Kiefer & Chipman 2008). IHS processing is usually limited to processing only three bands at a time. The transformation separates spatial (intensity) and spectral (hue and saturation) information from an RGB image. During the fusion phase the RGB image is converted into IHS components with the intensity component being substituted with a high spatial resolution panchromatic image. In a last step the process is reversed and the IHS is converted into RGB colours of the synthetic multispectral bands (Švab & Oštir 2006; Fonseca et al. 2011).

The modified IHS method allows for more than three bands to be merged by running multiple passes of the algorithm and merging the resulting layers. The method can be used for different layers and/or different sensors. The better the overlap of the wavelengths, the better the outcome will be but colour distortion can be significant. To overcome the problem of colour distortion the panchromatic image is matched to the intensity component before the reverse transform is applied (Jensen 2005; Fonseca et al. 2011). The IHS technique aims to increase processing speed and is therefore expensive due to large output files as well as the temporary files created during processing.

As the panchromatic values are changed through the histogram stretching, Chavez, Sites & Anderson (1991) warns that IHS methods distort the spectral characteristics and should be used with caution where radiometric analysis will be performed on the resultant images. IHS methods are therefore not the best method to use on images intended for quantitative analysis but they are

very useful in visual image interpretation as the colour composite is improved (Lillesand, Kiefer & Chipman 2008).

2.4.3.2 High pass filter pansharpening

High pass filter (HPF) pansharpening starts by calculating the ratio between the panchromatic and the multispectral images. A high pass convolution filter kernel is created and passed over the high-resolution image. This process involves adding an HPF image, weighted relative to global standard deviation, to each of the multispectral bands (Klonus & Ehlers 2009). The low-resolution multispectral image is then resampled to the pixel size of the high-resolution image using bilinear interpolation. In the last step of the procedure a linear stretch is performed which rescales the mean and standard deviation of the output to match the mean and standard deviation of the input multispectral image (ERDAS Imagine 2013a). The final output image therefore has the same radiometric resolution, usually unsigned 8-bit or unsigned 16-bit, as the input image. The output image contains the detail and pixel size of the panchromatic image and a realistic representation of original multispectral data but some spectral distortion is expected (Amro et al. 2011).

2.4.3.3 Ehlers fusion

The Ehlers fusion method is based on the IHS transform combined with Fourier domain filtering (Klonus & Ehlers 2009). This technique can cope with more than three bands by running successive IHS transforms until all the bands chosen have been processed. A fast Fourier transform (FFT) of the panchromatic image and the intensity component is performed after which a low pass filter (LPF) is used to filter the intensity spectrum while an inverse HPF is used to filter the panchromatic spectrum. Once the filtering process is completed, the images are transformed back into spatial domain with an inverse FFT and added together to form a fused intensity component with the low-frequency information from the low resolution multispectral image and the high-frequency information from the high resolution panchromatic image. This new intensity component is then combined with the original hue and saturation components of the multispectral image to form the new IHS image. The final step involves an inverse IHS transformation to produce a fused RGB image. This process is repeated with successive 3-band combinations until all bands are fused with the panchromatic image.

Ehlers fusion shows excellent spectral preservation but has very high computation times. To retain data integrity no additional filtering is applied and Ehlers, Klonus & Åstrand (2008) reported that

Ehlers fusion delivers pansharpened images with almost no spectral change even when multi-date and multi-sensor data are fused. The Ehlers fusion technique is consequently highly suitable for quantitative image analyses.

2.4.3.4 Wavelet pansharpening

Wavelet pansharpening can also be used to merge two grayscale images and is suitable for merging other types of imagery. Images that are to be merged should be spectrally identical. Corresponding bands, like SPOT panchromatic, can therefore be merged with Landsat TM Bands 1 to 4 but not with TM Band 6 (thermal).

Vijayaraj (2004) found that the spectral quality of wavelet-sharpened images are very good but that the spatial quality varies. The reason is that in the wavelet based sharpening method, spatial information is derived from the panchromatic image while spectral information is derived from the multispectral image. The spatial accuracy is therefore dependent on firstly, a high accuracy of co-registration between the multispectral and panchromatic image and secondly, on the resampling technique used to produce these images. It is therefore not always a good method for quantitative analysis.

2.4.3.5 Multiplicative

This is the simplest and fastest of the pansharpening methods and has with the least system-resource requirements. Any number of input bands can be used and the method is less sensitive to discrepancies between spectral bands than other methods (Švab & Oštir 2006). The cost of the fast computation is that the radiometric fidelity of the input multispectral image is not retained and special attention must be paid to colour preservation. Intensity is increased which makes it a good technique for highlighting urban features.

2.4.3.6 Principal components analysis

Jensen (2005: 296) describes PCA as “a technique that transforms the original remotely sensed dataset into a substantially smaller and easier to interpret set of uncorrelated variables that represents most of the information present in the original dataset.” The details of this statistical method is complex and beyond the scope of this thesis but in short, PCA generates uncorrelated images (PC1, PC2, ..., PC n , where n is number of input multispectral bands) and the first principle component (PC1) is then replaced with the panchromatic image. The method is useful because a

large data set of strongly correlated data can be transformed into a smaller data set of uncorrelated variables that are easier to interpret (Fonseca et al. 2011).

When the colour components of a digital image are represented in a scattergram, a strong positive correlation can be seen between the various visible bands. This means that if a pixel has a high value in one band, there is a strong possibility that the pixel will also have a high value in the other bands. The implication is that the various bands add little information to the image and therefore the image could be effectively interpreted using only the information provided by a single band (Mather 2006).

The most useful feature of PCA is that spatial information common to all bands is concentrated in the first component (Amro et al. 2011). PCA is therefore especially valuable for examining multispectral and hyperspectral remotely sensed data. Pansharpening by PCA is best used in applications that require retention of the radiometric fidelity or colour balance of the input multispectral image. The drawback is that the method has a high computational overhead and the fusion quality depends highly on the spectral overlap between the multispectral and panchromatic bands (Zang 2012).

2.4.3.7 Subtractive resolution merge

Zhang (2004) explains that traditional fusion techniques like IHS, PCA and wavelet pansharpening work very well with lower resolution images, for instance those from SPOT and Landsat, but rarely deliver adequate results with the high-resolution imagery. Subtractive resolution merge (SRM) is a fairly new method that uses a subtractive algorithm to pansharpen multi-spectral images. It was designed for high resolution images like Quickbird, Ikonos and Formosat which have the following common properties:

- both images must have the same radiometric resolution (8-bit or 16-bit unsigned);
- pixel values should be unaltered;
- images must overlap fully;
- panchromatic and multispectral images must have been scanned simultaneously;
- multispectral images should have four bands and the panchromatic image only a single band;
- a maximum pixel-size ratio of 4:1 exist between panchromatic and multispectral images; and

- both images must be georeferenced to a map coordinate system.

SRM produces a low resolution synthetic panchromatic image from the weighted sums of the multispectral bands which is then resampled to the same pixel size of the high resolution panchromatic image and then subtracted from the high resolution panchromatic image. A combination of high- and low pass filters are applied. Choosing the most suitable weights is crucial to retain both spectral - and spatial accuracy. Due to the spectral distortion introduced in the process, SRM is not ideal for quantitative analyses (Witharana & Civco 2012; Zhang & Mishra 2012).

2.4.3.8 Brovey transform

The Brovey transform is a relatively simple arithmetical method (Fonseca et al. 2011) that employs division and multiplication to fuse multispectral and panchromatic images. Švab & Oštir (2006) explain that the Brovey transform normalises multispectral bands used for RGB display by dividing each multispectral band by the panchromatic image. The resultant image is multiplied by the original panchromatic image to add a brightness component to the image. As it was developed to produce RGB images, only three bands at a time can be processed. The Brovey transform was developed to highlight the contrast in the low and high ends of the image's histogram and this so-called histogram stretching makes the Brovey transform an outstanding method for providing contrast between shadows, water and urban areas, all of which usually have a high reflectance. Brovey-transformed images are visually appealing but the method should not be used when it is necessary to retain radiometric and spectral fidelity (Vijayaraj 2004; Jensen 2005; Klonus & Ehlers 2009).

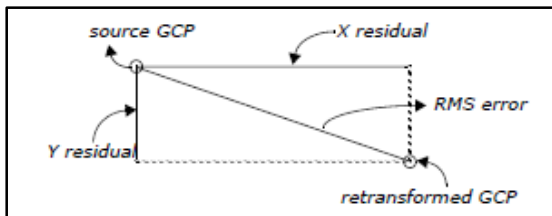
2.4.4 Accuracy assessment

Coppin et al. (2004:1589) states: "Precise registration of multi-date imagery is a critical prerequisite of accurate change detection". They use the term 'temporal trajectory analysis' to describe the monitoring change of a certain area over a long period of time. To ensure that the images were registered very accurately, accuracy assessment was undertaken. Below is a short discussion on the theory behind positional accuracy and root means square error (RMSE) analysis.

2.4.4.1 Positional accuracy

ERDAS Imagine (2013a:285) describes RMSE as “...the distance between the input (source) location of a GCP and the retransformed location for the same GCP.” In other words, it is the difference between the desired output coordinate for a GCP and the actual output coordinate for the same point, when the point is transformed with the geometric transformation.

Figure 2.10 below illustrates the relationship between the two GCPs and the RMSE.



Source: ERDAS Imagine (2013a: 285)

Figure 2.10 Residuals and root mean square error per point

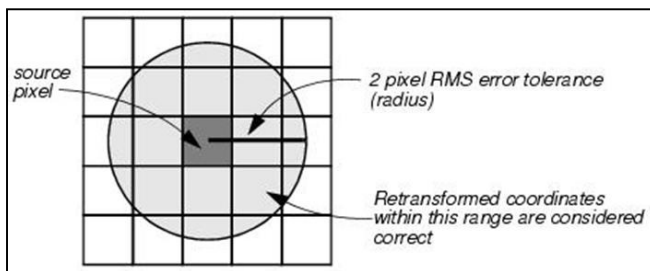
RMSE is calculated with a distance equation (Equation 2.14) by measuring the differences in the source coordinate system and is expressed in pixel widths.

$$RMSE = \sqrt{(x_r - x_i)^2 + (y_r - y_i)^2} \tag{Equation 2.4}$$

where x_i and y_i are input source coordinates; and

x_r and y_r are retransformed coordinates.

An RMSE of 2 implies that the reference pixel is 2 pixels away, in any direction, from the retransformed pixel (Figure 2.11). The acceptable RMSE value for an accurate registration is 0.5 (Congalton & Green 2009).



Source: ERDAS Field Guide (2013a:363)

Figure 2.11 Tolerance of root mean square error

RMSE is calculated and displayed in two ways. An evaluation is given for each GCP as well as an average RMSE calculation for all points involved. This allows single GCPs to be evaluated and corrected.

2.4.4.2 Thematic accuracy assessment

Thematic accuracy is a measure of how accurately a mapped land cover category compares with the actual land cover on the ground at the time of the survey. One way of representing classification accuracy of site-specific accuracy assessments is in the form of an error matrix. The matrix columns usually contain the reference data while matrix rows contain the classification data (Congalton 2005).

In this study false colour images will be used to assess the accuracy of the change detection maps in Section 5.4. The value of false colour images in comparison to the true images are discussed next.

2.5 TRUE AND FALSE COLOUR IMAGES

The bands of a satellite image can be combined in various ways to deliver very different portrayals. True colour images combine the blue, green and red bands (e.g. GeoEye-1 bands 1, 2 and 3 respectively), to deliver images similar in appearance to a colour photograph of an area under investigation (ERDAS Imagine 2013a). Other combinations of bands produce so-called ‘false colour’ images (Mather 2006). These images appear strange to the untrained eye but provide invaluable information that sometimes cannot be obtained from true colour images. By combining the bands in different ways, features can be represented in different colours of the visible spectrum and represented in a useful and informative format.

Images can also be altered mathematically to deliver specific outcomes. A vegetation index is one such type of reworking that delivers maps that shows change in vegetation. A number of vegetation indices are discussed in the next section.

2.6 VEGETATION INDICES

Jensen (2005:312) describes vegetation indices as “...dimensionless, radiometric measures that indicate relative abundance and activity of green vegetation, including leaf-area-index (LAI),

percent green cover, chlorophyll content, green biomass, and absorbed photosynthetically active radiation (APAR).”

Various indices are available to measure the differences between two or more radiometric bands of satellite imagery. A common application of indices is to highlight the difference between vegetation and other materials. Vegetation indices are also useful for monitoring and understanding environmental and climatic phenomena such as deforestation, desertification and drought (Gibbons & Freudenberger 2006). They are also helpful in classifying different types of vegetation (Nichol & Wong 2007).

Chlorophyll strongly absorbs visible light ($0.35\mu\text{m}$ – $0.7\mu\text{m}$) for photosynthesis but the cell structure of the leaves strongly reflects near-infrared light ($0.7\mu\text{m}$ – $1.2\mu\text{m}$) (Jensen 2007). Consequently, the more leaves the plant has, the greater the extent of absorption or reflection of these wavelengths. If there is more reflected radiation in NIR wavelengths than in visible wavelengths, the vegetation in a specific pixel is likely to be dense and indicative of some type of forest. The less the difference in the intensity of visible and NIR wavelengths reflected, the sparser the vegetation and greater the indication of grassland, tundra or desert (NASA 2008). Refer to Section 2.3 for details about the bandwidths of satellite sensors such as GeoEye-1.

Silleos et al. (2006) reviewed the nature and usefulness of various vegetation indices which they group into three categories: (1) slope-based, (2) distance-based or perpendicular, and (3) orthogonal transformation vegetation indices. Six sloped-based indices were considered namely the simple ratio index, normalised difference vegetation index, transformed vegetation index, squared simple ratio index and enhanced vegetation index. In addition, five distance-based indices are examined, namely the difference vegetation index, the soil-adjusted vegetation index, the transformed soil adjusted vegetation index, the atmospherically resistant vegetation index and transformed soil-adjusted vegetation index. Orthogonal transformation vegetation indices make use of statistical measures (e.g. PCA) and are as such sensitive to the spectral variation of the images being analysed. They are consequently not suitable for change analyses and were not considered in this study. The advantages and disadvantages of each of the ten vegetation indices considered are summarised in following subsections.

2.6.1 Simple ratio index

The simple ratio index (RATIO) described by Birth & McVey (Jensen 2007) is easy to use and effective for a wide range of conditions. The index expresses the contrast between the red and NIR bands for vegetated pixels (Silleos et al. 2006) and minimises problems introduced by topography. The RATIO index gives high values (>20) for dense vegetation and values close to 1 for soil, ice and water. This index is therefore very valuable to provide information about biomass or LAI (Stenberg et al. 2004; Jensen 2007).

The formula for RATIO is given in Equation 2.5.

$$\text{RATIO} = \frac{\text{NIR}}{\text{RED}} \quad \text{Equation 2.5}$$

where NIR is the reflectance value of the IR band; and
 RED is the reflectance value of the red band.

Due to the simplicity of the formula, errors such as division by zero may occur and therefore the resulting measurement scale is not linear.

2.6.2 Difference vegetation index

The difference vegetation index (DVI) is a very simple vegetation index as shown in Equation 2.6. It calculates the difference between the NIR and red bands and is a direct estimation of the amount of green vegetation present in the image.

$$\text{DVI} = \text{NIR} - \text{RED} \quad \text{Equation 2.6}$$

where NIR is the value of the NIR band; and
 RED is the value of the red band.

2.6.3 Normalised difference vegetation index

The normalised difference vegetation index (NDVI) was developed by Rouse et al. (1974) as quoted by Jensen (2007). NDVI is a widely used and is calculated from the difference between the reflection in NIR and red bands normalised by the sum of the same values (Silleos et al. 2006). NDVI was also the preferred VI used by Koruyan et al. (2012) in their paper on the use of remote sensing in monitoring mine rehabilitation.

The mathematical formula is shown in Equation 2.7.

$$\text{NDVI} = \frac{\text{NIR} - \text{RED}}{\text{NIR} + \text{RED}}$$

Equation 2.7

where NIR is the value of the NIR band; and
 RED is the value of the red band.

NDVI values range between -1 (clouds and snow) and +1 (vegetation). The RATIO and NDVI are quite similar to each other but RATIO performs better than NDVI in areas with dense vegetation when the LAI is high (Stenberg et al. 2004) opposed to NDVI which gives better results at low values for LAI.

2.6.4 Transformed vegetation index

Deering et al. (1975), as quoted by Silleos et al. (2006), developed the transformed vegetation index (TVI) as a more complex form of NDVI. The TVI formula was created by adding a constant of 0.5 to the NDVI before taking the square root of the sum. This stabilises variance and reduces problems related to negative numbers (Silleos et al. 2006).

The TVI formula is shown in Equation 2.8.

$$\text{TVI} = \sqrt{\frac{\text{NIR} - \text{RED}}{\text{NIR} + \text{RED}} + 0.5}$$

Equation 2.8

where NIR is the value of the IR band; and
 RED is the value of the red band.

Deering et al. (1975) found that the TVI (called TNDVI in their report) has a better signal-to-noise ratio in drylands than the NDVI and is therefore expected to perform better than NDVI with the satellite images of Navachab mine.

2.6.5 Square root simple ratio index

An additional index offered by some remote sensing software packages is the square simple ratio index (SSRI). The formulation improves RATIO by calculating the square root of RATIO (Equation 2.9).

$$\text{SSRI} = \sqrt{\frac{\text{NIR}}{\text{RED}}} \quad \text{Equation 2.9}$$

where NIR is the value of the IR band; and
 RED is the value of the red band.

This index is not expected to perform better than RATIO for this study as there is no change to the mathematical separation of the values.

2.6.6 Enhanced vegetation index

The enhanced vegetation index (EVI) shown as Equation 2.10, was developed by the MODIS Land Discipline Group (Jensen 2007).

$$\text{EVI} = G \left(\frac{\text{NIR} - \text{RED}}{(\text{NIR} + (\text{C1} * \text{RED}) - (\text{C2} * \text{BLUE}) + \text{L})} \right) \quad \text{Equation 2.10}$$

Where NIR is the value of the IR band;
 RED is the value of the red band;
 BLUE is the value of the blue band;
 G is a soil-adjustment factor with a value of 2.5;
 C1 is an empirically determined coefficient with a value of 6.0;
 C2 is an empirically determined coefficient with a value of 7.5; and
 L is an empirically determined coefficient with a value of 1.0.

The purpose of the development of EVI was to address some of the limitations of NDVI by incorporating the blue band (Band 1) to correct for soil background signals and to reduce atmospheric influences (Silleos et al. 2006). NDVI and EVI performs equally well in Mesic¹ grassland sites (Huete et al. 2002). EVI is more useful than NDVI in high-biomass regions with high levels of aerosols from burning and other sources of pollution. On the other hand NDVI gives a wider range of values in semi-arid regions (Jensen 2005).

¹ Mesic refers to habitats containing a moderate amount of moisture.

2.6.7 Soil-adjusted vegetation index

Huete (1988) developed the soil-adjusted vegetation index (SAVI) as a hybrid of a ratio-based index and a perpendicular index. It introduces an adjustment factor L for different levels of vegetation cover (Equation 2.11).

$$\text{SAVI} = \left(\frac{\text{NIR} - \text{RED}}{\text{NIR} + \text{RED} + L} \right) \times (1+L) \quad \text{Equation 2.11}$$

where NIR is the value of the IR band;
 RED is the value of the red band; and
 L is an adjustment factor.

The value of L will vary according to the level of vegetation cover with L = 0.25 for high vegetation cover, L = 0.5 for intermediate cover and L = 1.0 for low cover. Where L = 0, SAVI results are equal to those of NDVI (Silleos et al. 2006).

2.6.8 Atmospherically resistant vegetation index

Equation 2.12 below expresses the atmospherically resistant vegetation index (ARVI) which is an improvement of NDVI and SAVI. ARVI includes reflectance values in the blue band to correct atmospheric scattering of the red band. It is useful in areas with high atmospheric aerosol content and allows for prior correction for molecular scattering and ozone absorption of the blue, red and infrared data (Jensen 2007).

$$\text{ARVI} = \frac{\text{NIR} - (2 \text{ RED} - \text{BLUE})}{\text{NIR} + (2 \text{ RED} - \text{BLUE})} \quad \text{Equation 2.12}$$

where NIR is the value of the NIR band;
 RED is the value of the red band; and
 BLUE is the value of the blue band.

Huete & Liu (1994) tested the NDVI against the various improved variants, including ARVI, and came to the following conclusions:

- all variants of NDVI outperformed the original NDVI;
- the atmospherically resistant variants minimised atmospheric noise but increased soil noise;

- the soil-adjusted variants (e.g. SAVI) minimised soil noise but were sensitive to atmospheric influences; and
- where no atmospheric corrections are included, the NDVI and ARVI performed the worst with highest noise.

2.6.9 Transformed soil-adjusted vegetation index

Baret, Guyot & Major (1989) described the transformed soil-adjusted vegetation index (TSAVI) to improve high sensitivity to soil brightness suffered by other VIs like SAVI which are based on combinations of red and NIR bands (Baret & Guyot 1991). TSAVI was specifically developed for semi-arid regions which corresponds well to the Karibib region where the Navachab Gold Mine is located.

The formula for TSAVI is expressed in Equation 2.13 below.

$$\text{TSAVI} = \frac{a(\text{NIR} - a) (\text{RED} - b)}{\text{RED} + (a*\text{NIR}) - (a*b)} \quad \text{Equation 2.13}$$

where NIR is the value of the NIR band;
 RED is the value of the red band;
 a is the slope of the soil line; and
 b is the soil line intercept.

Vegetation indices need to be put through change detection analysis to determine the amount of change that occurred in the time-frame. Some of the change detection methodologies are discussed in the next section.

2.7 CHANGE DETECTION

Change detection requires information regarding land-use and land cover changes at local, regional and global scale to be extracted from remotely sensed images. Multitemporal images are run through algorithms that determine the amount of change in each pixel from one image to the next. Change detection algorithms can be broadly divided into two main categories namely transformational techniques and change classification techniques (Coppin & Bauer 1996). These techniques are described in the subsections to follow.

2.7.1 Transformational techniques

Transformational techniques require the analyst to establish a change threshold below which change is regarded to be due to natural causes and above which change is reported as real change (Green, Kempka & Lackey 1994; Lu, Mausel & Brondizio 2004; Radke et al. 2005; ERDAS Imagine 2013b). Several variations of transformation techniques are discussed here.

2.7.1.1 Relative difference

The simplest form of transformational change detection involves subtracting each image pixel from the later image (T2) from the corresponding pixel in the earlier image (T1). In this instance the pixels that increased in brightness will have negative values and the pixels for which brightness decreased will have positive values. The percentage change is then calculated by subtracting T1 from T2 and dividing by the pixels' value at T1 and T2 respectively. The two values are then added together and multiplied by 100 to deliver the percentage change (Equation 2.13).

$$\text{Relative difference} = \left(\frac{T2-T1}{|T1|} + \frac{T2-T1}{|T2|} \right) \times 100 \quad \text{Equation 2.13}$$

where T1 is the brightness value of the earlier image; and

T2 is the brightness value of the later image.

All changes identified in this manner are not necessarily the result of actual change in the scene but could also be the result of natural spectral variability of objects in the image. A change threshold therefore needs to be established and this is done by selecting a percentage change below which change is regarded as due to natural factors and above which change is regarded as actual change and which is then displayed in the change detection map.

2.7.1.2 Magnitude difference

Magnitude difference involves calculating the brightness magnitude for each pixel across all bands in the image. Each pixels' magnitude at T1 is then subtracted from its value at T2 (Jensen 2005) and transformed to a positive value.

For 8 bit data the resultant values from the differencing process can vary between -255 and 255 and the constant (c) is a value which needs to be added to all the values in order to make the resulting pixel values positive.

The magnitude difference is computed by the following formula (Equation 2.14):

$$\Delta BV_{ijk} = BV_{ijk}(1) - BV_{ijk}(2) + c \quad \text{Equation 2.14}$$

where ΔBV_{ijk} is the change in pixel value;
 $BV_{ijk}(1)$ is the brightness value on date 1;
 $BV_{ijk}(2)$ is the brightness value on date 2;
 c is a constant (to make all values positive);
 i is the line number;
 j is the column number; and
 k is the band number.

This method works best for phenomena that leads to a change in pixel value across all the bands in the image including situations where an object is present in one image but absent in the next image (Vakalopoulou & Argialas 2012; ERDAS Imagine 2013b).

2.7.1.3 Tasseled Cap differences

The Tasseled Cap transformation is very useful for vegetation studies. It involves weighting bands of suitable multispectral imagery using transformation coefficients specific to the sensor. Linear transformation equations are applied to the original data sets to deliver a new transformed image that corresponds to soil brightness and greenness respectively. These components are then differenced to deliver a change image that shows positive or negative changes in soil brightness and greenness (Kauth & Thomas 1976; Crist & Cicone 1984; Collins & Woodcock 1996; Lobser & Cohen 2007; Sheng, Huang & Tang 2011).

2.7.2 Change classification techniques

In the change classification technique all changed pixels are detected directly and mapped as change.

2.7.2.1 Primary colour differences

The primary colour difference algorithm highlights changes in objects based on one primary colour. Pixels are allocated a threshold value in T1 and T2 based on how blue, green or red they

appear. Elaborate calculations are then carried out to determine if there is significant colour change. The limitation of this method is that the entire pixel needs to be of one colour and therefore it is not very suitable for medium resolution imagery where a pixel can cover an area of 30 x 30m and larger (Vakalopoulou & Argialas 2012).

2.7.2.2 Single-band differences

The single-band difference method is useful when most change occurs in one band or where there is only one band of imagery available. The process is simple but can also lead to excessive reporting of changes that are insignificant. This method is best suited for panchromatic imagery (Ehlers et al. 2012).

2.7.2.3 Band-slope difference

Band-slope difference values are calculated by computing pixel values for T1 and T2 for each of the bands in the band-slope algorithm. The difference values are then calculated by the relative difference formula (Equation 2.13). The band-slope value is specified for the lower band therefore slope 1 refers to the band slope between Bands 1 and 2 (Vakalopoulou & Argialas 2012).

As discussed above, most of the change detection techniques can be applied on single or multiple image bands of two images. Another approach is to apply the change detection technique on a transformation of the two images. For instance T1 and T2 in Equation 2.13 can represent the NDVI values of each image.

The output of change detection techniques are often illustrated in a change detection map. Individual pixels are often assigned to one of three classes, namely no-change, reduced and increased. The three classes in the resulting change detection map are normally symbolised using black, red and green respectively. Consequently, a black coloured pixel on the change detection map indicates that the land cover remained the same, while green or red coloured pixels indicate that there was either a positive or negative change in the land cover respectively (ERDAS Imagine 2013a).

2.8 SUMMARY

Absorption and reflection characteristics differ between various plants and also between plants in various growth stages, therefore an understanding of the vegetation characteristics is essential to

interpret the results of change detection. Leaf pigment, moisture content and reflection by leaf cell structure all contribute to unique reflective patterns used in image interpretation.

Spectral resolution describes the colour detail contained in an image while spatial resolution indicates the area covered by one pixel of the image. The smaller the surface area contained in one pixel, the higher the spatial resolution. Multispectral scanners are designed to capture more detail in their smaller bandwidths and preserve the image SNR in a high spectral resolution image. On the other hand, panchromatic scanners capture less detail but in a wider range of bandwidths and therefore panchromatic images often have higher spatial resolutions compared to multispectral images. Radiometric resolution describes the amount of digital detail (bits) contained in the images and temporal resolution is the revisit time of the scanner. Revisit frequency can be increased by sensors that are pointable but such off-nadir images are not ideal for change detection purposes.

The sensor characteristics of various satellites also determine their usefulness for specific purposes. Ikonos, Quickbird, Orbview-3, GeoEye-1 and RapidEye are all sun-synchronous, polar-orbiting satellites suitable for regular monitoring of relative small areas. The RapidEye constellation has the best temporal resolution but GeoEye-1 is superior in spatial resolution. Although the GeoEye-1 sensor is highly pointable, the best manifestations of change detection will be obtained from images taken at nadir or as close to nadir as possible.

The spatial resolution of multispectral images can be improved by making use of pansharpening (resolution merge) techniques. Zhou, Civco & Silander (2010) found that, compared to IHS, PCA and Brovey transform, the wavelet transform delivered simultaneous best spectral and spatial quality and therefore outperformed these methods. Ashraf, Brabyn & Hicks (2012) tested the performance of SRM against the Brovey transform, PCA and HPF on Quickbird imagery and concluded that SRM outperformed the other methods qualitatively and quantitatively. Quickbird, Ikonos and Formosat images work well with this algorithm as will images from any other sensor (like GeoEye-1) with the same spectral qualities.

Accuracy assessments are needed to determine how well images have been georegistered. For this purpose the RMSE and SD values should be calculated. The SAVI and TSAVI vegetation indices usually perform better in semi-arid regions. SAVI can be corrected for semi-arid regions with low vegetation cover, while the formula for ARVI also incorporates the blue band to correct for atmospheric scattering.

Spectral signatures and false-colour images give an indication of the correctness of a classification or change detection result. Spectral signatures can also be used to determine the likelihood of a specific vegetation index giving a superior or less accurate assessment of vegetation change. False colour images are useful to assess the accuracy of the change detection process. By combining Bands 4, 3 and 2 (NIR, red, green) healthy vegetation will manifest as bright red.

The data collection and steps taken to prepare the images for change detection at the Navachab mine is discussed in the next chapter.

CHAPTER 3 DATA COLLECTION AND MANIPULATION

Change detection is based on comparing the spectral values of a given pixel over time. Kennedy et al. (2009) defines the stages in a remote sensing change detection study as: 1) data acquisition, 2) preprocessing and/or enhancement, 3) analysis and 4) evaluation. The process followed in this study is shown in Figure 3.1. This chapter reports on the data acquisition and preprocessing steps which includes pansharpening and georegistration. The vegetation index generation and change detection steps are covered in Chapter 4.

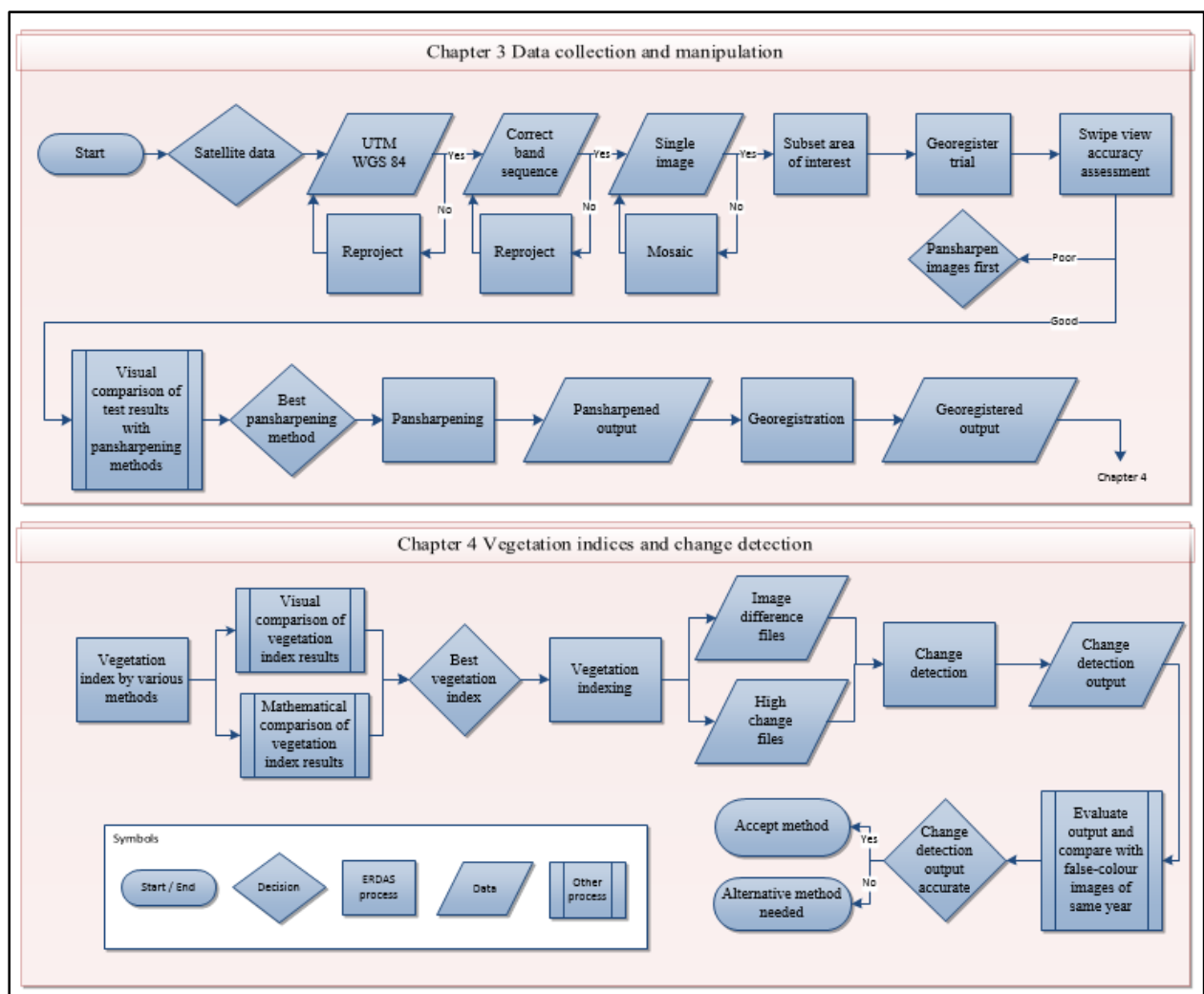


Figure 3.1 Satellite image processing flow diagram

The main challenges relating to data acquisition was to decide on suitable imagery and to determine the appropriate timing of the image scans (Section 3.1). This was followed by data manipulation procedures to ensure that all images had exactly the same coordinate system and band sequence (Section 3.2). Once completed, an initial evaluation of the georegistration process

was done to assess accuracy of the georegistration process with the unsharpened images. These steps are explained in more detail in the following sub-sections.

3.1 DATA ACQUISITION

Given the remoteness of the study area, very few historical high spatial resolution satellite images were available of the Navachab mine on the databases of satellite image suppliers. The selection of baseline images was consequently dependent on the availability of recorded (archived) images. An image on which the tailings are visible was needed as a baseline for the change analyses, which meant that the acquisition date of this image had to have been prior to the onset of rehabilitation. The period of interest consequently starts in 2004 when TSF1 was decommissioned and ends in 2011. Images for monitoring the rehabilitation progress were also needed. The process of obtaining suitable images is referred to here as the data matching time-frame.

3.1.1 Data matching time-frame

The inventory of all available satellite data with very high resolution included Ikonos, Quickbird and GeoEye-1 images (Table 3.1). Quickbird and SPOT5 were the only satellites that provided historical images suitable to be used as a baseline. Quickbird images were available from DigitalGlobe for the years 2004, 2005 and 2008, while SPOT 5 images were available for 2006 and 2008. New Ikonos, Quickbird and GeoEye-1 acquisitions could also be ordered (Carr-Hyde 2009, Pers com) but only from 2009 when the study was initialized.

Table 3.1 High-resolution satellite images inventory for Navachab Gold Mine

Sensor	Resolution	Bands	Minimum order size	Archived image dates	New collect
Ikonos	80cm multispectral	3 multispectral + 1 panchromatic	100km ²	-	Yes
Quickbird Archive	60cm panchromatic; 2.4m multispectral	3 multispectral + 1 panchromatic	25km ²	2004; 2005; 2008	Yes
SPOT 5	2.5m panchromatic 10m multispectral	3 multispectral + 1 panchromatic	Per scene 60km scene or ¼ scene (15km)	2006; 2008	Yes
GeoEye-1	50cm panchromatic; 1.65m multispectral	3 multispectral + 1 panchromatic	100km ²	-	Yes

Source: (Carr-Hyde 2009, Pers com)

Quickbird images were considered more suitable than SPOT 5 images due to their superior spatial resolution. The Quickbird images of July 2004 and January 2005 were consequently ideal for

providing prerehabilitation baselines. New orders of Quickbird, Ikonos and GeoEye-1 images were considered for the duration of the study period.

Tailings, soil and natural rock may appear differently under wet and dry conditions (Section 2.2.3) and this can have a significant effect on change analyses. To accommodate these changes a distinction was made between images acquired under wet and dry conditions. The appearance of vegetation also changes considerably from being brown and non-photosynthetic in the dry season, to growing vigorously during the rainy season. It is consequently important to compare images scanned during the same season to get an accurate estimation of the true improvement in vegetation from one year to the next. The moisture conditions and seasonal classifications of the available images are discussed next.

3.1.2 Moisture condition and seasonal classification of images

Imagery of the study area is not scanned regularly by imaging companies and only two Quickbird images, one from 2004 and one from 2005, covering the TSF1 were available from DigitalGlobe. In addition, scan dates of newly collected images depended on whether local conditions (cloud cover) were conducive to a successful image scan. Moisture conditions at the time the images were scanned was therefore researched in retrospect, after confirmation of image scan date. Image acquisition dates are listed in Table 3.2.

Table 3.2 Classification of images according to season

Image number	Satellite	Scan date	Tailing conditions	Season
1	Quickbird	28 January 2004	Wet	Wet (baseline)
2	Quickbird	29 July 2005	Dry	Dry (baseline)
3	GeoEye-1	12 March 2009	Dry	Wet
4	GeoEye-1	12 October 2009	Dry	Dry
5	GeoEye-1	22 May 2010	Dry	Wet
6	GeoEye-1	1 October 2010	Dry	Dry
7	GeoEye-1	22 April 2011	Wet	Wet
8	GeoEye-1	31 October 2011	Dry	Dry

Because the Karibib area usually receives rain between October and May, with peak rainfall between January and March, the images acquired before the onset of the rainy season were

classified as dry season images and those images scanned during the rainy season as wet season images.

The 2003-4 rainy season was relatively dry with a total rainfall of only 124mm. Most of the rain in 2004 was recorded in January. Unfortunately, daily rainfall figures for Navachab were not available for this period so that precise comparison of the rainfall with the timing of the available images was not possible. Even so, TSF1 was operational at the time and the tailings on the top of the TSF were still wet, regardless of the rainfall. A Quickbird image of 28 January 2004 (Image 1) was considered suitable as a baseline for wet tailing conditions.

A similar trend is seen for the 2005-6 rainy season. During June 2005, when Image 2 was scanned, no rain fell and the two preceding months had minimal rain. TSF1 had already been decommissioned and the tailings had dried out sufficiently for capping activities to commence. Image 2 is thus suitable for use as a dry baseline image. The January 2004 and July 2005 images were consequently selected as wet and dry baseline images for change detection respectively.

Owing to their higher spatial resolution, GeoEye-1 was chosen in favour of Ikonos for the rehabilitation monitoring. Although the study area is relatively small (16ha), high-resolution imagery such as GeoEye-1 can only be ordered in units of 100km² or larger, which makes the cost of acquiring a large number of images very high. The acquisition of images was consequently restricted to one image per season. Nadir images were preferred but were not always available due to cloud cover. Cloud cover was especially problematic during the rainy season. In such cases consecutive passes of the satellite were required for off-nadir scanning.

Image 3 (GeoEye-1 image) was scanned on 12 March 2009. The preceding month had an exceptionally high rainfall of 232mm and another 61mm fell in March to give a total rainfall of 430mm for the 2008-9 rainy season. Most of the precipitation occurred during the first five days of March 2009 followed by a hot, dry week before the image was scanned. This image was selected as a suitable dry (wet-season) image.

A GeoEye-1 image for October 2009 (Image 4) was scanned on 12 October 2009. Virtually no rain had fallen from the beginning of the 2009-10 rainy season up to the scan date so the tailing conditions were dry. The rest of the 2009-10 rainy season remained very dry with rainfall totalling only 115mm for the period between October 2009 and March 2010. Yet the rain was well distributed over the entire period and despite the total rainfall being low, an improvement in

vegetation growth was expected to be visible on the GeoEye-1 image scanned on 22 May 2010 (Image 5). Three dry weeks preceded the scan date so the tailing conditions were dry.

The scan dates of the imagery were related, where possible, to the rainfall figures of Navachab (Figure 3.2) below.

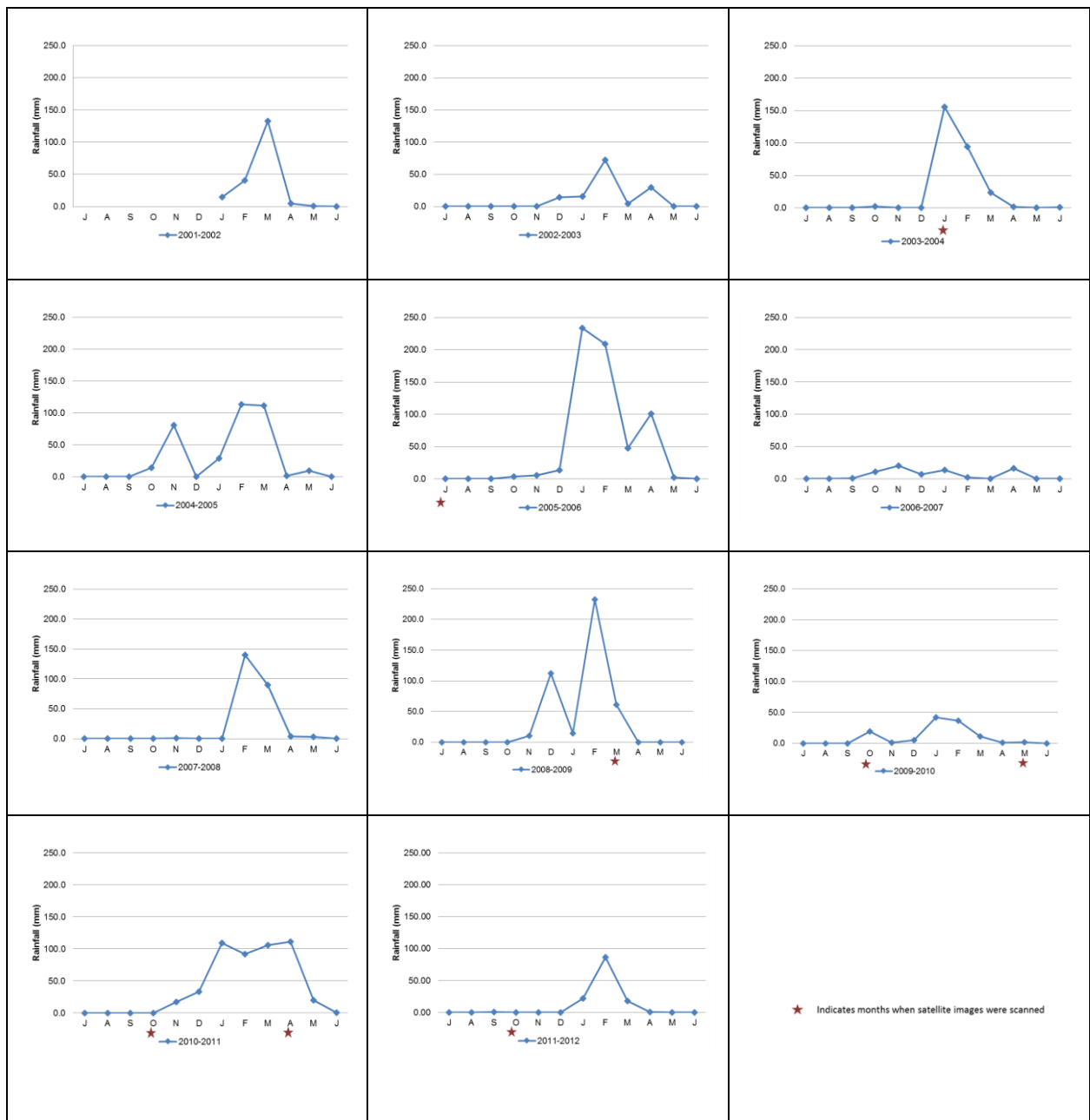


Figure 3.2 Navachab rainfall over the 10 years preceding the end of the study period

It was dry throughout October 2010 but early rains fell in November and December 2010. The scan date (1 October 2010) of the Image 6 coincides with the end of a five-month dry period and was therefore ideal for use as a dry season image with dry tailing conditions. Image 7 was acquired

during the wet season and followed two rain events on 20 April 2010 (39mm) and 21 April 2011 (10mm). The image was consequently classified as a wet season image with wet tailing conditions.

The rest of the 2010-11 rainy season was exceptionally wet with consistent monthly rainfall from November 2010 until late June 2011. The total rainfall for the season was 440mm. Image 8 was scanned on 31 October 2011, with the preceding four months being relatively dry apart from 0.76mm falling in September 2011. The image is therefore also considered to be a suitable dry season image with dry tailing conditions.

The eight high resolution Quickbird and GeoEye-1 images listed in were acquired and processed. Image preprocessing is explained in the next section.

3.2 IMAGE PREPROCESSING

Much of the image preprocessing was carried out by the supplier of the imagery (GeoData Design). This included radiometric correction, atmospheric correction and basic geometric correction. As explained in Section 2.4.2.1, radiometric correction is done to compensate for known characteristics of the sensor that affect the radiometric values of the pixels in the image. The radiometric corrections were performed to ensure that the relationships between the image bands are correct. Only basic atmospheric corrections were performed as, due to the remote location and arid conditions of the study area, atmospheric effects were assumed to be minimal and relatively stable.

Change detection relies on the selection of minimum and maximum thresholds that signify significant changes. The minimum threshold disregards small-magnitude changes including those that are the result of sensor noise or atmospheric differences. The maximum threshold removes changes registered due to very large differences such as the presence of clouds or cloud shadows (ERDAS 2013c). Sophisticated atmospheric corrections and cloud masking procedures were consequently not required in this study.

Basic geometric corrections were carried out by the supplier of the imagery. This involved the large scale orthorectification of the images to a map coordinate system based on the satellites' position and viewing angle at the time of acquisition (Dorfling 2012d, Pers com). All images were supplied in the UTM Zone 33 map projection and WGS84 datum with the band sequences: blue (Band 1), green (Band 2), red (Band 3) and NIR (Band 4). Some of the images were received in

different projections and had incorrect band sequences, but these errors were corrected using the appropriate software tools.

The resolution of the multispectral images acquired was considered inadequate for monitoring growth of small shrubs and trees. The value of improving the spatial resolution of multispectral images using pansharpener techniques was discussed in Section 2.4.3.

This section investigates suitable pansharpener and geometric correction methods to ensure that the resulting change detection maps are accurate.

3.2.1 Pansharpener

Eight pansharpener methods offered by ERDAS Imagine software were evaluated in this study. Refer to Section 2.4.3 for an overview of these techniques. Quantitative assessment methods were not considered in the evaluation as other studies (e.g. Alparone et al. 2004 and Zhang 2008) showed that there is no reliable measurement for quantifying the quality of pansharpener images. Instead the qualitative approach described by Wei, Yuan & Cai (1999) was adopted. This approach makes use of subjective scoring such as the mean opinion score (MOS).

MOS relies on the interpreter's own experiences and motivations. The authors compared the MOS to a more elaborate approach called the perceptual mean square error (PMSE) and found that the two methods correlated very well. The much simpler MOS was consequently used here. The purpose of the MOS is to identify the pansharpener method that produces the most accurate alignment of GCP's while still retaining spatial and spectral fidelity. Table 3.3 shows the MOS as described by Shi et al. (2005).

Table 3.3 Mean opinion score grades

Grade	Absolute measure	Relative measure
1	Excellent	The best in the group
2	Good	Better than the average level in a group
3	Fair	Average level in a group
4	Poor	Lower than the average level
5	Very poor	The lowest in a group

Source: Shi et al. (2005: 247)

The results of testing the various pansharpener methods were compared with the unsharpened multispectral (Figure 3.3a) and the panchromatic (Figure 3.3b) images.

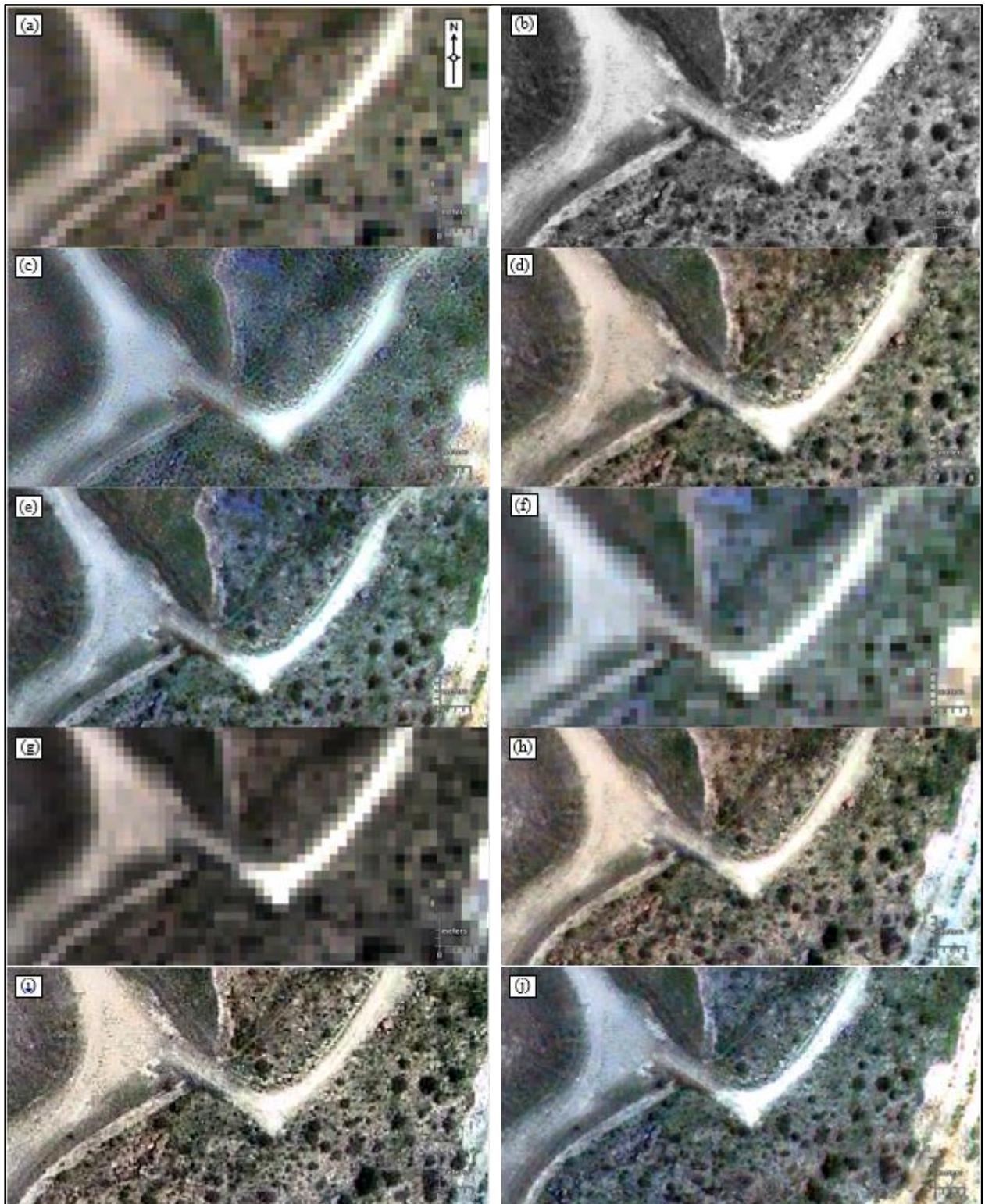


Figure 3.3 Comparison of (a) unsharpened multispectral image, (b) panchromatic image and (c) Ehlers fusion, (d) high pass filter, (e) modified intensity hue saturation, (f) Brovey transform, (g) multiplicative, (h) principle components analysis, (i) SRM and (j) wavelet pansharpening methods.

The images produced by Ehlers fusion (Figure 3.3c), Brovey transform (Figure 3.3f) and multiplicative pansharpener methods (Figure 3.3g) all show severe blurring so that individual pixels cannot be easily identified. Better results were obtained from HPF (Figure 3.3d), modified IHS (Figure 3.3e), PCA (Figure 3.3f), subtractive (Figure 3.3g) and wavelet (Figure 3.3h) pansharpener. The best pansharpener images were delivered by the SRM method, followed by HPF and modified IHS. The results of MOS process are shown in Table 3.4.

Table 3.4 Mean opinion score for eight pansharpener methods tested

Pansharpener method used	Relative measure scored	Grading
Subtractive resolution merge (SRM)	Excellent	1
High pass filter (HPF)	Good	2
Modified hue saturation intensity (HIS)	Good	2
Wavelet	Fair	3
Brovey	Poor	4
Ehlers fusion	Poor	4
Principal component analysis (PCA)	Poor	4
Multiplicative	Very poor	5

Based on the qualitative assessment of the various pansharpener methods it was concluded that SRM is the most suitable pansharpener method for this study. This finding is supported by Ashraf, Brabyn & Hicks (2012) who found that this method was superior for use with very high resolution images. Hence all the acquired images were pansharpener using this method. The georegistration process is recounted in the next section.

3.2.2 Georegistration of the images

The next preprocessing step involved georegistration of the various images. Because the study area is highly localised, no suitable DEM of the study area was available and fine-scale orthorectification was not an option (refer to Section 2.4.2.2 for a background on geometric corrections). Instead a simple image-to-map georegistration was attempted. Official topographic maps of Namibia were obtained in digital and hard copy format to be used as spatial reference. The maps covering the study area are 2115DC Usakos North, 2115DD Karibib, 2215BA Usakos South and 2215BB Marmorkuppen. It was clear that the maps were produced long before the Navachab mine existed as none of the pits, WRDs or TSFs appear on the maps.

The georegistration of the images using global positioning system (GPS) points was also considered. Seven GPS points (see) on TSF1 were surveyed by the Navachab Survey team using a Trimble R8 GNSS GPS rover and R7 GNSS base station. The seven points were allocated identification numbers MB1 to MB7.

Plotting the surveyed GPS points on the satellite images revealed large discrepancies between the GPS coordinates and the satellite image coordinates. The matter was referred to specialist surveyors Coetzer & Symons (2012, Pers com) as well as Dorfling (2012c, Pers com) who both concluded that the Karibib beacon, from where local surveying data is referenced, should be remeasured. The initial measuring of this beacon was done a long time ago and preliminary readings done by Coetzer indicated that the beacon coordinates were out by several metres in x, y and z coordinate directions.

This finding is of great consequence because the Karibib beacon coordinates are used as reference point for all surveying done in the area and the incorrect reference coordinates would result in all related surveyed points being incorrect as well. However, the survey team at Navachab mine has been using a unique Navachab grid and the inconsistencies with the coordinate system were never detected (or relevant) prior to this study.

For assessing whether the rehabilitation efforts at Navachab mine have been successful, relative spatial accuracy was considered more important than absolute accuracy. The decision was taken not to use the GPS coordinates based on the old Karibib beacon and to rather perform a relative image-to-image co-registration (see Section 2.4.2.2). Image 5 was selected as the reference image and all the other GeoEye-1 and Quickbird pansharpened images were georegistered to it by using the ERDAS AutoSync Workstation software. Autosync uses an automatic point matching algorithm to generate thousands of tie points, and produces a mathematical model to tie the images together. The resulting workflows significantly reduce or sometimes completely eliminate manual GCP collection (ERDAS Imagine 2013b).

The intended number of GCPs per image was set at 200 and the output geometric model chosen as polynomial. Other settings included 'avoid shadows' and 'exclude background area'. The best results were obtained when the 'use manual tie points for initial connection between images' option was selected. Image projection was chosen as 'same as reference image' and 'maximum polynomial order' was set to 3 with tolerance of 0.1 pixels. Thereafter 'continue approximation'

was implemented. Images were resampled at a nearest neighbour interpolation with a cell size of 0.5m by 0.5m. The options to ‘ignore statistics’, ‘clip to reference image boundary’ and ‘force square pixels on reprojection’ were also chosen.

The accuracy of the georegistration process was tested with the ERDAS AutoSync Swipe View function at three different locations on the output images at intervals of roughly one quarter of the image width. The steep, irregular slopes of TSF1 made georegistration difficult. The best results were obtained by first creating some manual GCPs and then running the automatic tie process. Furthermore, to eliminate the problem of AutoSync trying to match irrelevant areas outside the study’s scope, close-cut subsets were made of the area under investigation. The entire process was then rerun with all the image combinations.

The RSME and the SD remained very high, 9.46 and 5.31 pixels respectively, in spite of the visibly-correct overlapping of the images as viewed with the AutoSync Swipe function. The RSME of individual GCPs were checked to reduce possible errors, but error contribution of individual point was minimal. Where GCPs were adjusted to favour a smaller RMSE and SD, the visually alignment of images suffered. Preference was given to visual accuracy and overlap of points as indicated by the software swipe function as the relatively high RMSE was attributed to relief displacements, especially toward the edges of the images. These displacements were not significant in the main focus area (tailings) and consequently had a minimal effect on the change analysis results.

3.3 SUMMARY

This chapter overviewed the acquisition of the satellite images and the methods used to prepare it for analysis. An assessment of various pansharpener methods was done and the results confirmed that the subtractive pansharpener method best retains radiometric fidelity and provides the clearest on-screen image. The images were georegistered, but the nature of the data, the large difference between images and the very irregular topography, made it difficult to find automatic tie-points and to obtain an RMSE of less than 1. The georegistered images were used as inputs to the change detection process described in the next chapter.

CHAPTER 4 VEGETATION INDICES AND CHANGE DETECTION

Section 4.1 gives a short overview of some of the spectral properties of land cover classes typical to Navachab TSF1. The spectral differences between land cover classes and the differences in reflectivity of wet and dry substrates were discussed in Section 2.2. These differences are discussed further based on the observations made in the study area. In addition, differences between the wet and dry season images are also illustrated. Section 4.2 overviews the available vegetation indices and highlights their main advantages and disadvantages and reports on the index values measured from the imagery. These values were used to identify the most suitable vegetation index, which was then applied to the pansharpened images for producing a series of change detection maps. The perspective was that the vegetation indices that best separated land cover classes will be the most useful for change monitoring. The change detection results are discussed in Section 4.3.

4.1 SPECTRAL PROPERTIES OF LAND COVER CLASSES IN TSF1

Published spectral properties of water, soil and rock, and vegetation were discussed in Section 2.2. An understanding of the spectral properties of different land cover classes is important in order to interpret why certain vegetation indices perform better than others in different circumstances. Environmental monitoring staff are not necessarily trained remote sensing practitioners and the importance and relevance of spectral properties of land cover classes need to be discussed. This section compares these spectral profiles to spectral response patterns observed in the study area.

The land cover classes on TSF1 consist of a rain water pond, natural rock occurring around TSF1, soil (capping material), trees and shrubs. The rainwater pond area is a small depression on the TSF surface where water collects during the rainy season. The trees are mostly Acacia species that were planted on the TSF as part of the rehabilitation process, while the shrubs are pioneering species that naturally invade disturbed areas. The rock types consist mainly of weathered dolomitic marbles while the soils class represents the capping material that was used to cover the surface of the TSF. This material is also typically of dolomitic origin and is in abundance in the mining area.

To assess the radiometric fidelity of the images, spectral readings of each class were needed. Image 5 was chosen as the reference image for the spectral profiles because of the favourable weather conditions preceding the image. This image had water in the rain water pond from which the rain water spectral readings could be obtained. In addition the weather conditions were relatively dry for about six weeks prior to the image acquisition and therefore the soil and rocks on the TSF were

dry and the spectral readings were not influenced by moisture. Spectral readings from each class were obtained by using the spectral profile viewer function of the processing software.

False colour images with band sequence 4 (NIR), 3 (red) and 2 (green) were made of Image 5 (wet season) and Image 6 (dry season). These false colour images were then used to identify pixels within the respective land cover types. The false colour images provided a good indication of vegetated and non-vegetated pixels, as discussed in Section 2.5.

Ten samples were collected for each of the five land cover classes. The percentage reflectance values plotted for the respective bands are discussed in the next section.

4.1.1 TSF1 rainwater pond

The rain water pond is a very shallow (< 0.5m) pond where rainwater collects during the rainy season. At the time that Image 5 (22 May 2010) was captured, no plants or algae were growing in the pond and therefore the spectral signature is expected to be very similar to that of a shallow body of clear water.

Figure 4.1 compares the spectral signatures of water to those of soil and vegetation. Water normally show a steady decrease in reflectance from the green region to the NIR region with a small zone of higher reflectivity in the blue/green bandwidth. The distinguishing feature is the very low reflectance in the NIR region which is typical of the absorption of NIR wavelengths and beyond in this type of substrate (Lillesand, Kiefer & Chipman 2008).

Figure 4.1 and Figure 4.2 are photographs taken of the rain water pond during this period. Vegetation can be seen emerging from the areas around the pond, but within the pond itself no vegetation is visible. The chemical composition was analysed and found to be uncontaminated. The presence of tadpoles in Figure 4.3 also suggest that the water is safe for animal consumption.

When compared with the spectral response pattern obtained from the imagery (Figure 4.3), the rain water pond shows lower reflection in the blue region than in the red region followed by a sharp decrease in the NIR bandwidth. The higher reflectance in the red band was attributed to the shallow nature of the pond. The spectral variance between samples is likely due to varying depth over its extent.



Figure 4.1 Rainwater pond on old TSF



Figure 4.2 Close-up of water in pond

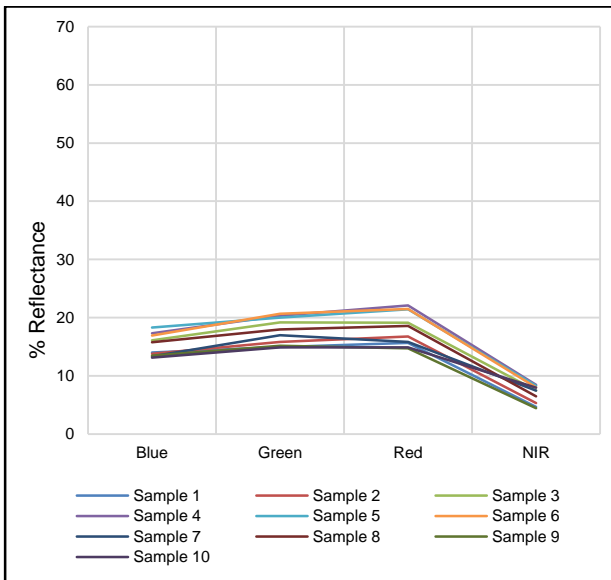


Figure 4.3 Spectral response pattern from the rain water pond as extracted from Image 5

The pond has been covered with topsoil during rehabilitation activities in 2005/6 and no tailings are visible any longer. Ideally the selected VI should therefore classify the pixels relating to the covered pond as soil rather than vegetation or tailings.

4.1.2 TSF1 soil and rock classes

The reflectance profiles of rock and soil as measured from Image 5 is shown in Figure 4.4. The reflectance of rock and soil is relatively high in the blue band but drops considerably in the green band. This is followed by a steep increase in the red band followed by a relatively low reflection in the NIR region.

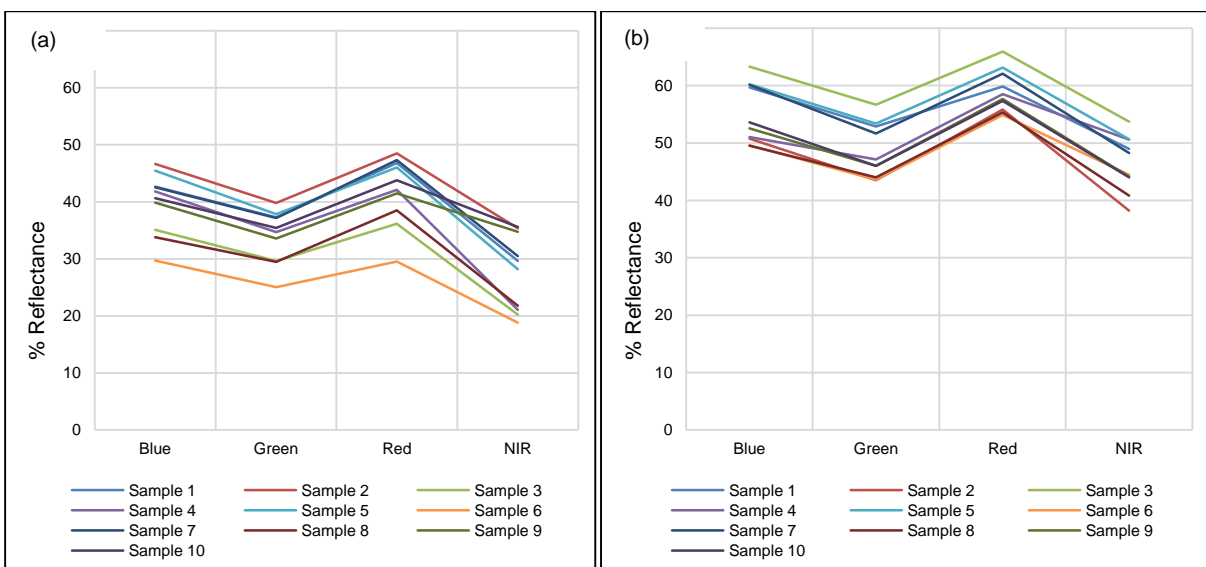


Figure 4.4 Spectral profiles of (a) rock and (b) soil as extracted from Image 5

This pattern is different when compared to the published profile of soil (Figure 2.6) which shows a steady increase in reflection from blue to NIR. Dolomite is the dominant mineral in Navachab soils and rocks. The dolomitic soils are light in colour and are expected to have a high reflectivity in the visible region of the electromagnetic spectrum. However, wet rock and soil usually have lower reflectance than dry substrates (Lillesand, Kiefer & Chipman 2008) and the decrease in reflectivity of wet soils is pronounced in finely textured soils with poor drainage like those on TSF1. Organic materials also cause an overall decrease in reflectance but the presence of live, photosynthetic plants would lead to an increase in reflectance in the NIR region.

The spectral response pattern of rock (Figure 4.4a) shows that reflectance is very similar across all four the bands with slightly less reflectance in Band 4 (NIR), while the overall reflectance of the soil (Figure 4.4b) is generally higher. The shape of the reflectance curves for rock and soil are very similar, with the least reflectance in Band 2 (green) followed by Band 4 (NIR). Most of the samples in Figure 4.4 were void of any living plants, but were clearly influenced by moisture as evidenced by the relatively low NIR reflectance. Two samples in Figure 4.4a (samples 9 and 10) and one sample in Figure 4.4b (sample 4) seem to include less moisture as the NIR is slightly higher. Another possible explanation for the slight increase in NIR reflection in these samples may be the presence of plant material.

Although all attempts were made to select pure samples, some pioneering shrubs and ground cover (Figure 4.5) may have contaminated some of the samples.



Figure 4.5 View of top of TSF during the 2010 rainy season indicating presence of pioneering ground cover species

The presence of plants in Image 5 made it very difficult to select soil and rock samples (i.e. 0.5 x 0.5m areas) that were totally void of vegetation. However, Image 5 was ideal for selecting samples relating to vegetation as discussed next.

4.1.3 TSF1 vegetation classes

Vegetation types in the area are typical of semi-arid savannah and dominated by various Acacia thorn trees. Moringa trees inhabit the hills around TSF1 and are also used in the rehabilitation process while trumpet thorn is an invader shrub found all over the mine. Various small and large pioneering shrub types grow on in the rehabilitated areas. Grasses on TSF1 consist mainly of annual species but dense grass stands only occur during the rainy season.

The spectral profiles of the vegetation samples taken from Image 5 are shown in Figure 4.6. These profile of trees in Figure 4.6a are very similar to published spectral signatures of vegetation (e.g. Figure 2.6) with a very low reflectivity in the blue band, an increase in the green band, a decrease in the red band and a sharp increase in the NIR band.

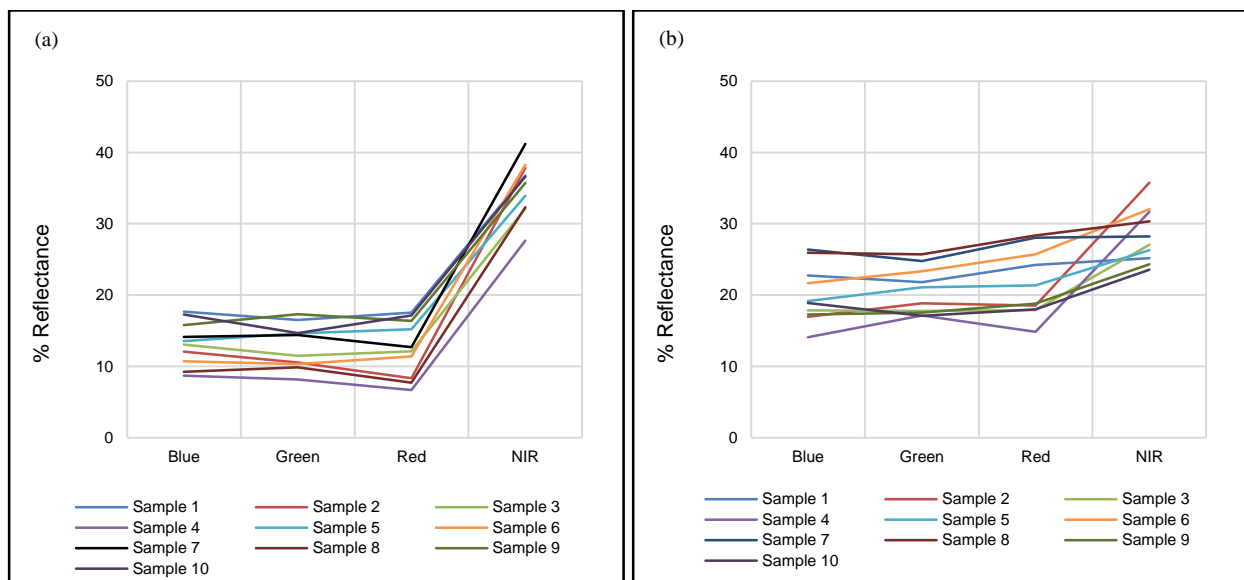


Figure 4.6 Spectral profiles of vegetation classes (a) trees and (b) shrub.

During a wet period the trees turn green and are actively photosynthesizing. The high levels of chlorophyll leads to a steep increase in the NIR band which makes vegetation appear bright red on the false colour images. The profile in Figure 4.6a is typical of vegetation (see Section 2.2.2) although the relatively lower green peak and higher reflectance in the red band is likely due to the influence of background soil reflectance as most of the trees on TSF1 do not have closed canopies.

The influence of background soil is more dramatic in Figure 4.6b due to the smaller and less dense canopies of shrubs.

The selection of a suitable vegetation index to highlight the differences between vegetation and soil background is discussed in the following section taking into account the unique properties of the TSF tailings, soil and vegetation cover.

4.2 VEGETATION INDEX SELECTION

Navachab soils used for the rehabilitation activities are very light in colour due to the very high marble content and were expected to have very similar properties to the dry tailings. The vegetation is not dense (low LAI) consisting of various grasses, pioneering species of shrub and some young Acacia trees. Although the pond has been covered by soil, a depression still remains and precipitation often collects there during the rainy season. An ideal index would separate the two vegetation classes (shrub and tree) from the bare areas (soil and rock). The vegetation and bare classes should also be well separated from the rainwater pond class. The spectral values that were extracted from Image 5 (see previous section) for each land cover class were used as basis for evaluating the different VI's. The values were used as input to each of the vegetation index formulae discussed in Section 2.6 and the results were then displayed on a graph. The values obtained for the various indices were then used to determine which index would most effectively differentiate the changes from tailings to soil, water and vegetation. In order to compare the VIs, the values were normalised to a common scale between 0 and 1 based on the minimum and maximum values for each VI using linear scaling.

The normalised values are listed in Table 4.1 and graphed in Figure 4.7.

Table 4.1 Normalised vegetation index values calculated from Image 5

Land cover class	DVI	SRI	NDVI	TVI	SSRI	EVI	SAVI	TSAVI	ARVI
Rain water pond	0.09	0.00	0.00	0.00	0.00	0.01	0.00	0.00	0.00
Natural rock	0.00	0.11	0.26	0.41	0.18	0.00	0.26	0.28	0.27
Trees	1.00	1.00	1.00	1.00	1.00	1.00	1.00	1.00	1.00
Shrub	0.57	0.39	0.63	0.75	0.50	0.37	0.63	0.66	0.61
Soil	0.05	0.17	0.36	0.51	0.25	0.08	0.35	0.38	0.35

Each VI's ability to separate classes were determined by subtracting the index values of the classes. Separability can also be visually assessed by comparing the profiles in Figure 4.7.

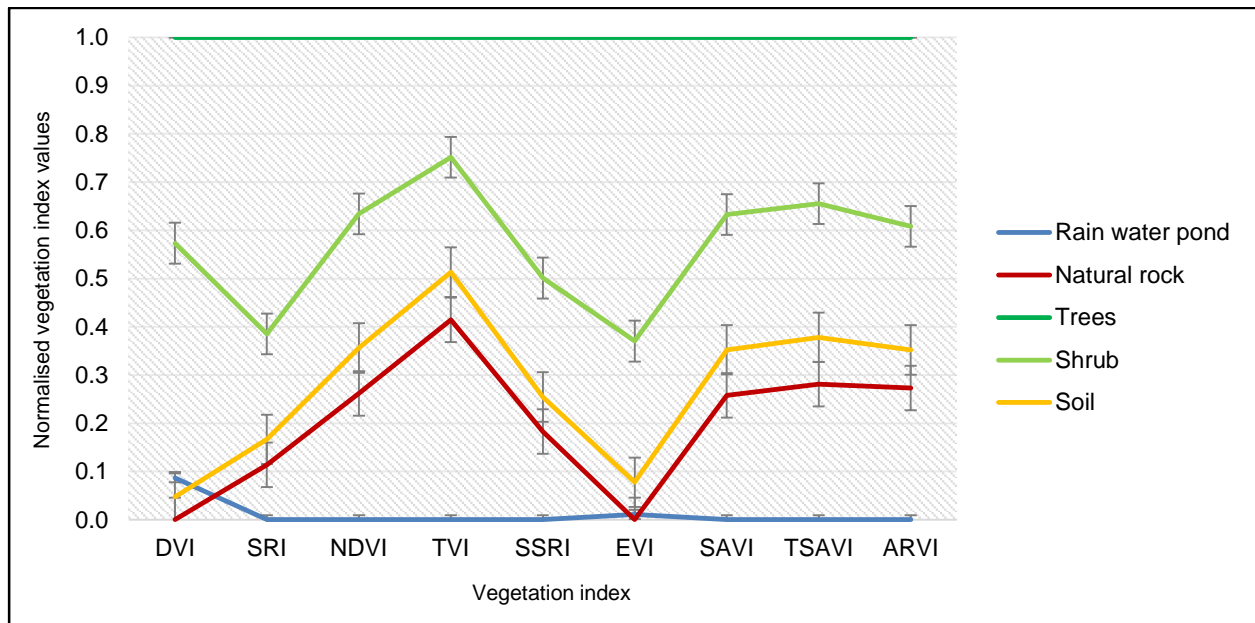


Figure 4.7 Normalised vegetation index values calculated from reflectance readings

None of the indices gave near perfect results, but overall the SRI, NDVI, TVI, SSRI, SAVI, TSAVI and ARVI all showed very similar trends with the correct expected sequence of bands where water has the lowest values followed by rock and soil and with the vegetation classes having the highest values. In contrast, water has higher values than rock and soil in the DVI and in EVI the values for water and rock are almost identical.

All the VI's grouped soil and rock close together and well separated from the vegetation classes. The DVI best separates shrub from soil (0.53 normalised difference) followed by EVI (0.29) and TVI, SAVI and TSAVI (0.28). These VIs are consequently expected to best distinguish between the vegetation and non-vegetation classes. Lower separability values between the shrub and soil class indicating that the relevant VI's are more sensitive to background soil reflectance. Furthermore, the shrub and the tree classes are least separated by TVI (0.25) followed by TSAVI (0.34) and NDVI and SAVI (0.37 each). The rain water pond is well distinguished from the rock class by most of the VI's but TVI once again shows the best separation (0.41) followed by TSAVI (0.28), ARVI (0.27) and NDVI and SAVI again performing similar (0.26 each).

Based on these findings most of the VI's showed similar results but the indices that will most likely show the best separation between the vegetation and non-vegetated classes are DVI, NDVI, SAVI and TSAVI (in that order). TVI was the most effective in separating water from rock classes. NDVI

performed very similar to SAVI, TSAVI and ARVI and therefore only NDVI was considered further. The DVI and EVI were found to be unsuitable due to the incorrect sequence of the reflectance curves. In conclusion, TVI and NDVI were found to have the most potential for rehabilitation change detection. To confirm this deduction, these indices are evaluated for change detection in the next section.

4.3 CHANGE DETECTION RESULTS

Change detection was done using ERDAS DeltaCue specialised change detection software. The software incorporates multiple change detection algorithms including magnitude-, Tasseled Cap-, primary colour-, single band- and band slope algorithms from which the primary colour algorithm was selected for required process work.

NDVI and TVI were used as input in the change detection process. The VI difference maps were generated by setting a minimum of 10% change between a baseline image and a recent image. Image 1 and Image 2 were used alternatingly as wet and dry baselines respectively. The resulting change maps were visually compared to Band 4, 3 and 2 (NIR, red and green) false colour images. The results are presented and discussed the following subsections.

4.3.1 Changes from wet and dry baselines to Image 3 (2009 wet season image)

Figure 4.8 compares the change detection results between Image 1 (the wet tailing baseline image from January 2004) and Image 3 (March 2009), while Figure 4.11 compares the change detection results between Image 2 (the dry tailing baseline image from July 2005) and Image 3 (March 2009). Image 3 was scanned after a relatively dry spell of seven days in an exceptionally wet rainy season.

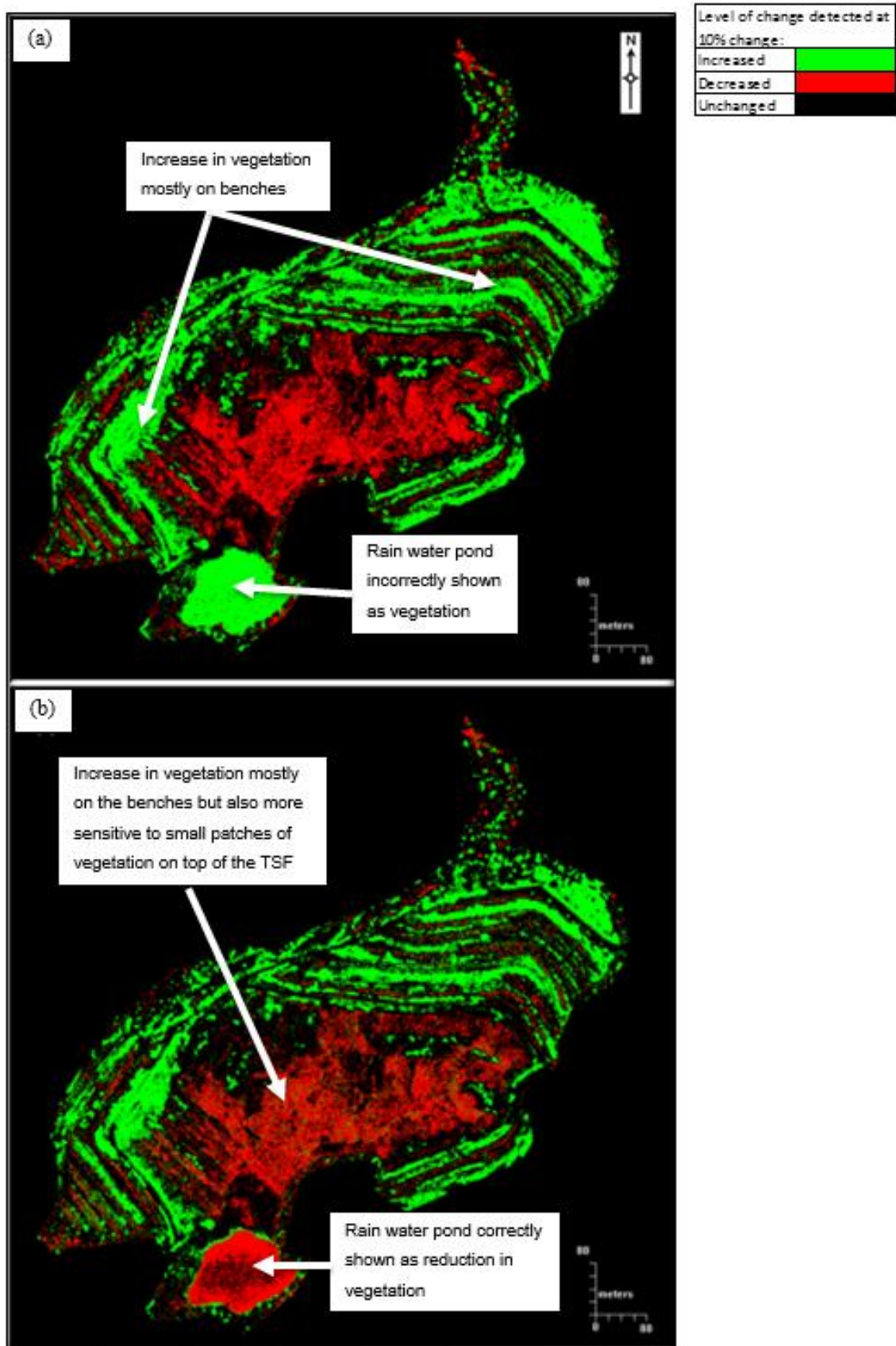


Figure 4.8 Increases and reductions in vegetation cover between Image 1 and Image 3 according to (a) NDVI and (b) TVI

The rainfall figures are listed in Table A.1 in Appendix A. Overall the NDVI logs consistent soil coverage (shown in black) very well but registers water in the rain-water pond as an increase in vegetation (green). When this result is compared with the false colour images in Figure 4.9, it is clear that the increase in NVDI values in the area of the pond is not due to an increase in vegetation but rather a failure of this vegetation index to adequately separate the vegetation and water classes.

In contrast, the change map based on the TVI (Figure 4.8b) compares well with what is seen on the false colour images (Figure 4.9). Small patches of vegetation on the top of the TSF and the pond are shown in red (reduction of vegetation) but the uncovered tailings around the pond and the small hill to the south are shown correctly in black (no change). The vegetation increases (green) in Figure 4.8b consists mostly of grasses on the benches.

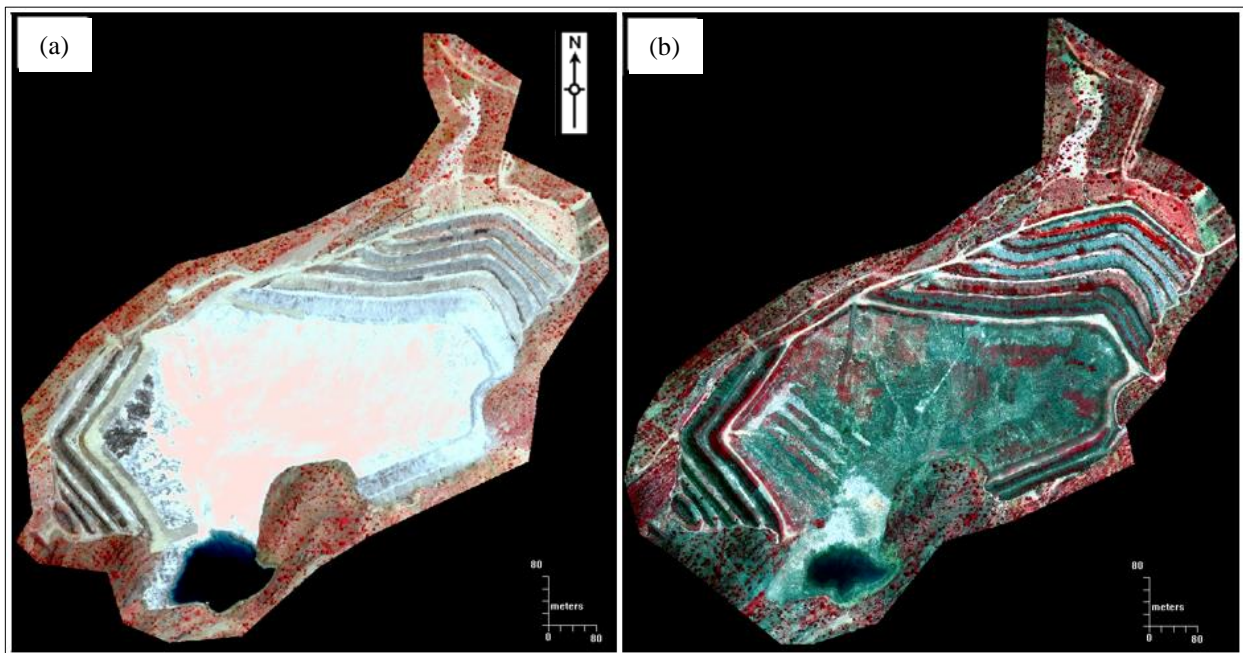


Figure 4.9 False colour images of (a) Image 1 (Quickbird January 2004) and (b) Image 3 (GeoEye-1 March 2009).

When the dry tailings image (Image 2) is used as baseline for the change analysis (Figure 4.10b) the results are slightly different. NDVI clearly distinguishes between dry tailings and cover material (shown in black) but slightly less vegetation increases (green) are logged. This is because the rehabilitation of vegetation on the benches had already started by July of 2005 when Image 2 was captured. The tailings on the wall along the north-western rim of the TSF are also logged as increase in vegetation (Fig4.11a).

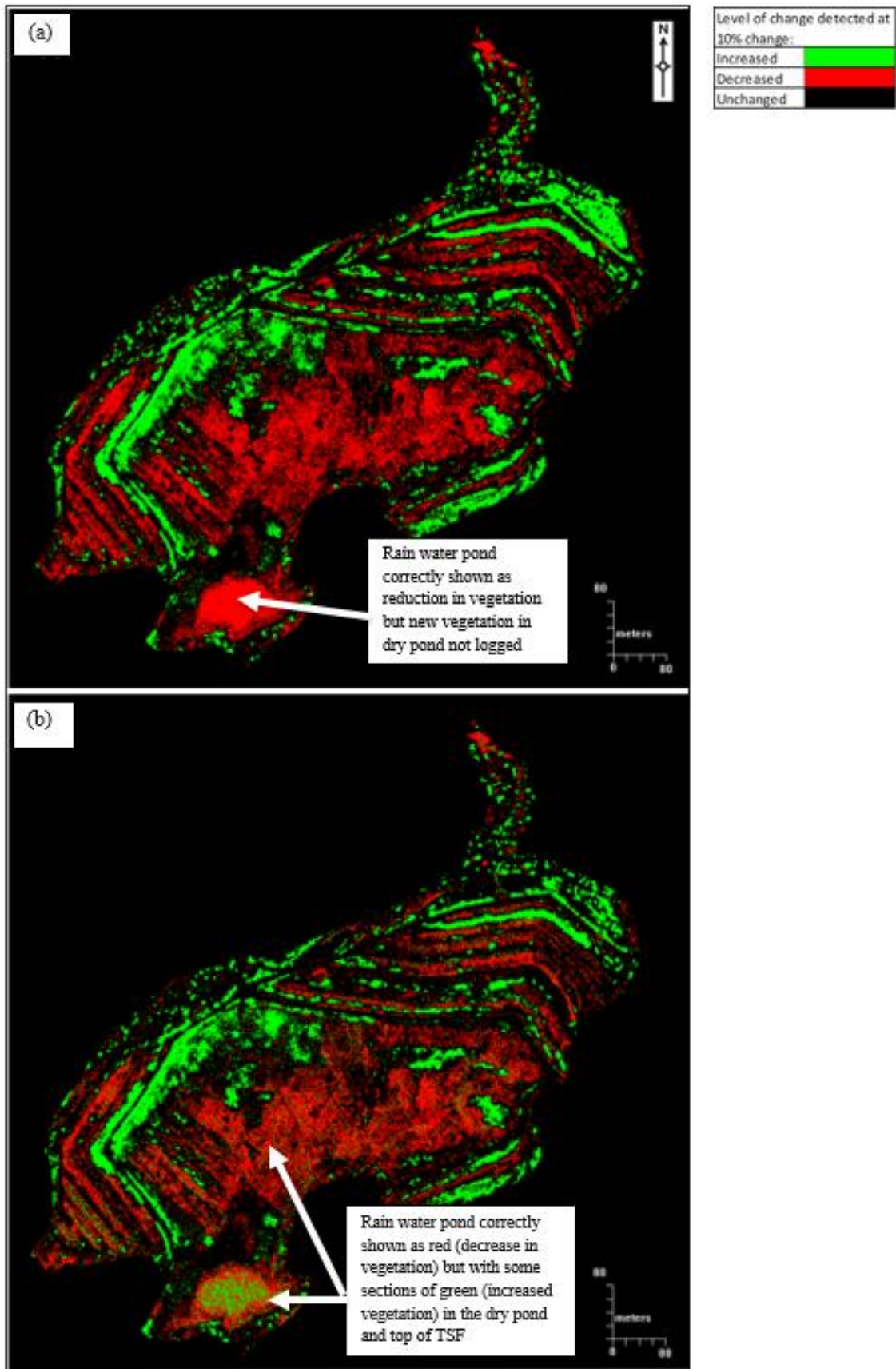


Figure 4.10 Increases and reductions in vegetation cover between Image 2 and Image 3 according to (a) NDVI and (b) TVI.

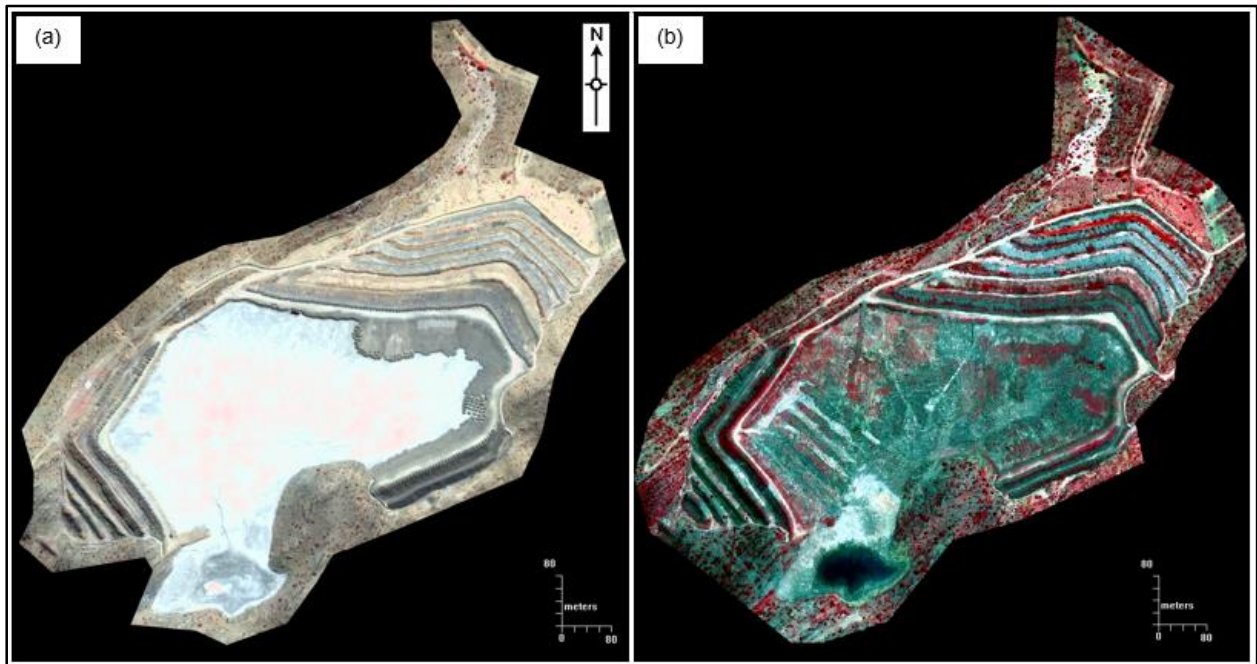


Figure 4.11 False colour images of (a) Image 2 (July 2005) and (b) Image 3 (March 2009).

TVI distinguishes very well between dry tailings and soil cover but shows the dry pond as changing to a mixture of soil and vegetation (Fig4.11b). This is accurate as in 2009 there was sparse vegetation growing in the pond area. Based on the visual comparisons between the NDVI and TVI classification results, TVI was more consistently accurate and therefore the more suitable indexing method for this study.

4.3.2 Changes from baselines to Image 4 (2009 dry season image)

Image 4 was acquired during a very dry period (October 2009) with only a small amount (1.3mm) of rain since the last good rains in March 2009 (Figure 3.2). The overall change seen in Figure B.1a&c is therefore that of a wet tailings baseline to a combination of dry soil and dry vegetation. From the wet baseline (Image 1), NDVI again incorrectly classifies the change from pond to dry soil as vegetation (Figure B.1a) when compared to the false colour images Figure B.2. The tailings on the wall along the north-western rim of the TSF are also classified as vegetation and the soil cover is not recognised, except for some small patches. TVI (Figure B.1c) better distinguishes between water and soil as more bare soil is classified compared to NDVI.

When Image 2 is used as a baseline, NDVI does not distinguish wet tailings and soil coverage well and very bare soil is detected (Figure B.1b). TVI is more sensitive to change from tailings to bare soil (shown in red) (Figure B1d) and identifies less change from tailings to vegetation (shown in green) when compared with the false colour images (Figure B.3).

4.3.3 Changes from baselines to Image 5 (2010 wet season image)

Even though Image 5 was acquired in the rainy season, the preceding six weeks were dry. From Figure B.4a it is clear that NDVI fails to distinguish between water and vegetation, although the other vegetated areas are accurately portrayed. The very dry conditions of Image 5 was not conducive to an increase in vegetation cover and therefore improvement in vegetation cover is marginal and only visible on the north-eastern and south-western benches on the false colour images (Figure B.5a&b). TVI results for vegetation (Figure B.4c) are very similar to those of the NDVI. The rain water pond is dry in Image 5 and here a significant difference is seen between the TVI and NDVI results. TVI indicates change in the rain water pond area as a decrease in vegetation (red) which is interpreted as 'soil' while the NDVI results show this drying up of the rainwater pond incorrectly as an increase in vegetation (green).

The changes in vegetation from Image 2 (dry baseline) using NDVI seem accurate and the dry pond is correctly shown as unchanged (Figure B.4b). The TVI results are very similar to those of NDVI, although less vegetation increases are highlighted (Figure B.4d). Actual vegetation can be seen in false colour images Figure B.6a&b.

From these results it is difficult to determine which index performed best, although TVI classified the changes in the rain-water pond area more accurately and is therefore more suitable for images that contain water bodies.

4.3.4 Changes from baselines to Image 6 (2010 dry season image)

October 2010, when Image 6 was acquired, was much dryer than January 2004 (Image 1) and most of the changes detected between these images are consequently classified as a reduction in vegetation cover (shown in red) when NDVI is used (Figure B.7a). The tailings that were covered in June 2010 are incorrectly classified as a reduction of vegetative cover. Only small patches of increases in vegetation are noticeable. Changes from water to soil are incorrectly classified as an increase in vegetation (compare with false colour images in Figure B.8a&b). TVI (Figure B.7c) overestimated increases in vegetation and the covering of the tailings is classified as a reduction in vegetation cover.

Most of Image 6 is classified as having experienced a reduction in vegetation cover when using NDVI and the dry baseline (Image 2) (Figure B.7b). This is attributed to NDVI's sensitivity to soil background (add refs) as much of the area was covered by dry or sparse vegetation during the

acquisition of Image 6 (compare Figure B.9a&b). TVI is known to be less sensitive to background soil and correctly classified most of the area as having experienced an increase in vegetation cover (Figure B.7d).

Compared to the previous results this set of results seem to be erroneous. The large variation in change was attributed to outlier values, highlighting that the pre-processing of imagery is of critical importance in change detection applications. The risk of such errors should be taken into consideration when applying image-to-image change detection algorithms.

4.3.5 Changes from baselines to Image 7 (2011 wet season image)

Image 7 is was taken during a wet period and the change detection results using Image 1 as baseline and NDVI (Figure B.10a) shows that the pond water was incorrectly classified as an increase in vegetation, although new vegetation growth seems to be reasonably accurate when compared to the false colour image pair (Figure B.11a&b). TVI slightly underestimated vegetation increases when Image 1 was used as baseline, but the pond water is correctly classified (Figure B.10c).

Using the Image 2 as a baseline, NDVI correctly classified the pond water as unchanged or reduced vegetation (Figure B.10b). Vegetation increases seems slightly overestimated when compared to the false-colour images (Figure B.12a&b) and photographic records. The TVI result (Figure B.10d) is almost identical to that of NDVI.

4.3.6 Changes from baselines to Image 8 (2011 dry season image)

From Image 1 (wet baseline) to the Image 8 the NDVI change detection result is almost completely green (Figure B.13a) indicating a 10% or more increase in vegetation throughout the area. Compared to the false colour image (Figure B.14a&b) this is an unrealistic increase. By contrast, the TVI change detection result (Figure B.13c) is mostly red apart from some specks of vegetation increases on the benches. If the changes detected include both soil coverage and dried-out vegetation, this signifies a very accurate representation.

Using Image 2 (dry) as baseline the NDVI change detection results in a decrease in vegetation (Figure B.13b). Very limited increases in vegetation are detected, which disagrees with the amount of vegetation seen on the false-colour images (Figure B.15a&b). A very similar (even more pronounced) reduction in vegetation was detected when TVI was used for the change analysis (Figure B13.d).

4.4 SUMMARY

Several VIs were considered for detecting changes at TSF1. Of these, NDVI, TVI and TSAVI were expected to perform better than EVI and SRI as the former group of indices were specifically developed for semi-arid conditions (refs). SAVI can be calibrated for semi-arid regions with low vegetation cover, while ARVI incorporates the blue band to correct for atmospheric scattering. The VIs were evaluated by comparing their spectral response curves for five land cover classes namely water, natural rock, soil, trees and shrub. DVI and EVI were found to be unsuitable as their reflectance curves were inconsistent. Overall, the land cover classes were best separated with TVI. NDVI performed very similar to SAVI, TSAVI and ARVI and only NDVI and TVI were considered for further evaluation.

TVI and NDVI were evaluated for change detection between the two baselines (Images 1 and 2) and all the successive images (Images 3 to 8). TVI outperformed NDVI when there was water present in the scenery, but with dry images the two indices performed very similar.

In the next chapter the study aims are revisited and the findings of the research are discussed.

CHAPTER 5 CONCLUSIONS AND RECOMMENDATIONS

The aim of this research was to investigate the effectiveness of remotely sensed change detection as a method to measure the success of the Navachab Gold Mine rehabilitation programme.

A literature review (Objective 1) on the suitable satellite sensors, image characteristics, and the various image-processing methods for vegetation indexing and change detection was carried out (see Chapter 2).

Information on Navachab Gold Mine's operational history was collected. Other information such as climatic data and satellite imagery was also acquired for the study period (2004 to 2011) (Objective 2). The satellite imagery was preprocessed (Objective 3) to ensure that all images were comparable. An overview of the data collection process and image preprocessing was provided in Chapter 3.

Several vegetation indices and change detection methods were evaluated in Chapter 4 (Objective 4). The change detection maps were assessed to identify the most suitable procedure to confirm the success of the Navachab Gold Mine's rehabilitation programme. A number of change detection maps were produced and evaluated (Objective 5). The next section evaluates the suitability of satellite remote sensing for mine rehabilitation monitoring.

5.1 EVALUATION OF SATELLITE REMOTE SENSING FOR MINE REHABILITATION MONITORING

The Navachab tailings are unique as it represent very fine milled rock from the ore body and are mostly calcisilicate and dolomitic marbles (Bell 2010, Pers com) whereas tailings from most other gold mines are predominantly granite based. The spectral properties of water were also important in this study because the pond on the TSF was often filled during rainy seasons.

Due to the low rainfall in the study area, the increases in vegetation cover was not dramatic enough to be captured by the year-on-year VIs, but were in most cases detected over five year periods. Change analyses based on dry season images provides better results as it mostly captured perennial (long-term) vegetation changes whereas much of the vegetation detected using the rainy season images were dominated by annual grasses. The results of the change analyses showed that remote sensing provides a potential method for assessing the effectiveness of the rehabilitation programme

at Navachab Gold Mine, but that care should be taken in the interpretation of the resulting change maps.

The most suitable images were those scanned shortly before the onset of the rainy season. For Navachab Gold Mine, this period is early October. Several pansharpener methods were evaluated and the best method proved to be SRM as it retains most of the radiometric fidelity and provided the most detail for on-screen GCP matching.

Change detection performed with NDVI and TVI delivered similar results for the images acquired during dry conditions, but according to the results NDVI was less successful where there was water present in the baseline image. The experimentation showed that both NDVI and TVI are suitable for use in rehabilitation monitoring in semi-arid regions (such as Karibib) provided only dry-season images are utilised for the change analyses. However, TVI generally performed better than NDVI.

The hypothesis that remotely sensed vegetation indices and image-to-image change detection can effectively be used for the monitoring of mine rehabilitation success is accepted, provided that the process and results are interpreted with proper understanding of the timing of image acquisition and the processing techniques followed. It is not advisable to do a single change detection from a tailings baseline to a vegetated image. Making use of multiple images improves understanding of the rehabilitation process and reduced the risks of applying simple image-to-image change analyses. Post-classification change detection carried out by a trained remote sensing practitioner with the necessary skills will likely deliver better results, particularly when fewer images are available.

A more detailed discussion follows in Section 5.2 where the problems encountered during the study and recommendations for further research are made.

5.2 PROBLEMS ENCOUNTERED AND SUGGESTIONS FOR FURTHER STUDY

A number of challenges were encountered in this research. Some of these challenges were very specific to monitoring TSF rehabilitation, mainly because the rehabilitation process consists of two consecutive changes. The first change takes place during the capping process when the tailings is covered with soil. The change detection tool rendered this change in red which indicates a 'reduction' in vegetation cover (i.e. a negative impact in terms of rehabilitation). However, in reality the capping process is a positive development and the change detection method evaluated

in this study was consequently unable to adequately represent this transition. The second step in the TSF rehabilitation process is when the covered TSF is vegetated. The change detection tool successfully rendered this transition as green, indicating an increase in vegetation cover. Simple VI-based change detection tools, such as the one used in this study, should therefore be used with caution as it can lead to incorrect interpretations.

Sources of error in the change analyses were mainly due to the images not being correctly georeferenced. Topographic maps of Namibia are very old and available only as hard copies and attempts to join the maps were unsuccessful as the contour lines and topographic features did not line up perfectly. Moreover, the appearance of the mining area has changed so much that very few features shown on the topographic maps still exist. The Karibib base beacon used as a surveying reference at Navachab was also found to be several metres off the target and the use of surveyed points as reference was consequently abandoned. Instead one image was used reference and all other images were registered to this image. The semi-automated registration process did not deliver adequate results and visual alignment to GCPs was subsequently used. However, the absolute accuracy of the georegistration process should be improved in future studies. A digital elevation model and accurate GPS points should be used to orthorectify the images. The existing GPS points taken at the inception of the study should be recalibrated in line with the new, revised coordinates for the Karibib beacon.

Baseline images with the same spatial resolution as the later GeoEye-1 images were not available. However, lower resolution Quickbird imagery was found to be adequate for the purposes of this study. This suggests that multi-temporal multi-sensor images can successfully be applied in monitoring rehabilitation areas as long as the spectral resolution is similar. Satellite sensors are continuously improving and higher resolution imagery has become available since the inspection of this study and even higher resolution imagery is likely to become available in the future. The challenge remains to find suitable historic baseline images and the best practise would be to choose the highest resolution sensor available at the time and to acquire images of mining sites on a regular basis.

5.3 RECOMMENDATIONS

Vegetation monitoring and change detection is not new, but the application thereof in mining rehabilitation monitoring is still not well established. Under normal circumstances rehabilitation involves mainly vegetating disturbed areas. With TSF rehabilitation the change detection should

be addressed in two separate but consecutive steps – first detection of change from tailings to soil and secondly the detection of change from soil cover to vegetation.

Mine rehabilitation areas are usually relatively small in size and non-contiguous. In this study very high-resolution imagery worked well and the spectral, spatial and temporal resolutions of GeoEye-1 imagery fulfilled the needs for vegetation indexing and change detection. It is recommended that this imagery be used for similar rehabilitation monitoring studies in the future. Newer sensors such as WorldView-2/3 have even higher spatial and spectral resolutions and will consequently also be suitable. Where archived GeoEye-1 or WorldView images are not available, Quickbird images can also be used as baselines. Although Quickbird imagery has a lower spatial resolution compared to more modern sensors, the spatial resolution is still high enough to be used for monitoring purposes.

The subsetting of the relevant areas before pansharpening and georegistration is recommended as it reduces processing times and increases the accuracy of the geo-referencing process as the data is not skewed by irrelevant points outside the area of interest.

The desktop study of the various pansharpening methods concluded that the methods that would best retain radiometric fidelity are PCA, Ehlers fusion and/or SRM. The visual assessment of the methods confirmed that HPF, modified HIS, SRM and wavelet pansharpening delivered the clearest on-screen results which aids visual matching of objects during georegistration. The SRM was chosen as the most suitable method of pansharpening and is recommended for similar studies.

In this study the pansharpened images were georegistered using ERDAS AutoSync Workstation and the accuracy of the georegistration process was evaluated with RMSE and SD values. The accuracy of the georegistration process was also visually assessed using the ERDAS Autosync Swipe View function at three different locations at intervals of roughly one quarter of the image width. The automatic registration process failed to find GCPs over the entire area and usually stopped after finding nine. The minimum number of GCP points that delivered accurate registration was found to be 100. In similar studies it is recommended to manually identify some tie points before running the automatic tie point matching process. The steep, irregular slopes of TSF1 complicated georegistration and the RSME and the SD remained high in spite of the visibly-correct overlapping of the images as viewed with the AutoSync Swipe function. The influence of individual GCPs on RSME was checked to reduce errors, but the error contribution of individual points was minimal. Attempts to reduce RSME and SD were abandoned in favour of visual

alignment of geographical features. In similar studies it is recommended that a suitable digital terrain model from the same period is obtained to orthorectify the images.

Mathematical calculations were carried out using the spectral readings obtained in ERDAS Imagine and substituting them into the various vegetation index formulae. The VI separation or closeness of classes was calculated by simply subtracting the index values of the classes. This approach was sufficient for the purposes of this study, but other more advanced separability measures (e.g. Jeffries-Matusita distance) are recommended for future studies.

5.4 PRACTICAL IMPLICATIONS FOR NAVACHAB GOLD MINE

In Chapter 1 the need for mining companies to prove compliance with government regulations and requirements in terms of mine closure was stated as the reason for undertaking this study. The AngloGold Ashanti (2009:7) closure and rehabilitation standard document prescribes development of a rehabilitation programme that will “assess the extent of impacts on land and to develop, implement, monitor, assess and refine rehabilitation methodologies in line with agreed closure objectives and/or environmental permit conditions” and refers to the description of rehabilitation by the Australian Government Department of Resources, Energy and Tourism (Australia 2006: 1-2) as “the process used to repair the impacts of mining on the environment” and one of the objectives of rehabilitation as “establishing appropriate sustainable ecosystems.”

The results of this study showed that VIs can be employed as a mechanism to monitor rehabilitation progress. Sustainable ecosystems will show a year-on-year improvement in the vegetation conditions and these improvements were illustrated with the use of false colour images. Vegetation indices and change detection maps were not always successful in illustrating the unique consecutive changes taking place during the rehabilitation of a TSF and a follow-up investigation needs to take this into account.

This study determined the best change detection method and vegetation index for the detection of vegetation changes at Navachab Gold Mine. Many suppliers of satellite imagery provide image preprocessing services, which reduces the need for an on-site remote sensing practitioner to produce the difference maps. Although a change detection map can never replace an ecological study, it reduces the need for employing full-time ecologists or the cost of appointing consultants to assess vegetation progress. The study demonstrated that remote sensing with high-resolution satellite imagery can successfully be incorporated into Environmental Impact Assessments (EIAs)

and Environmental Management System (EMS) as a mechanism to monitor the success of mine rehabilitation.

REFERENCES

- Agarwal S, Vailshery LS, Jaganmohan M & Nagendra H 2013. Mapping urban tree species using very high resolution satellite imagery: Comparing pixel-based and object-based approaches. *ISPRS International Journal of Geo-Information* 2: 220-236.
- Alparone L, Aiazzi B, Baronti S, Garzelli A & Nencini P 2004. A global quality measurement of pansharpened multispectral imagery. *IEEE Geoscience and Remote Sensing Letters* 1: 313-317.
- Al-Ruzouq R & Al Rawashdeh S 2014. Geomatics for rehabilitation of mining area in Mahis, Jordan. *Journal of Geographic Information System* 6:123-134.
- Amro I, Mateos J, Vega M, Molina R & Katsaggelos AK 2011. A survey of classical methods and new trends in pansharpening of multispectral images. *EURASIP Journal on Advances in Signal Processing* 79: 1-22.
- AngloGold Ashanti 2008. Namibia country report 2008 [online]. n.p., s.n. Available from: <http://moss/sites/ca/Country%20Reports/Forms/AllItems.aspx> [Accessed 27 May 2013].
- AngloGold Ashanti 2009. Management standard 06: Closure and rehabilitation version 01 [online]. n.p.: s.n. Available from: http://moss/sites/ev/Community%20and%20Environment%20Management%20Standards/Closure%20and%20Rehabilitation%20Management%20Standard%20Ver01_2009.pdf [Accessed 13 August 2012].
- Antwi EK, Krawczynski R & Wiegleb G 2008. Detecting the effect of disturbance on habitat diversity and land-cover change in a post-mining area using GIS. *Landscape and Urban Planning* 87: 22-32.
- Ashraf MS, Brabyn L & Hicks BJ 2012. Image data fusion for the remote sensing of freshwater environments. *Applied Geography* 32: 619-628.
- Australia (Commonwealth of) 2006. Leading practice sustainable development program for the mining industry: Mine rehabilitation [online]. S.I. Department of Industry, Tourism and Resources. Available from: http://www.ret.gov.au/resources/resources_programs/lpsdp_mining/handbooks/handbooks-English/Pages/English.aspx [Accessed 22 October 2012].
- Baldrige AM, Hook SJ, Grove SI & Rivera G 2009. The ASTER Spectral Library Version 2.0. *Remote Sensing of Environment* 113: 711-715.
- Baret F, Guyot G & Major DJ 1989. *TSAVI: A vegetation index which minimizes soil brightness effects on LAI or APAR estimation*. 12th Canadian symposium on remote sensing and IGARSS 1990 held 10-14 July 1989. Vancouver: PN.
- Baret F & Guyot G 1991. Potentials and limits of vegetation indices for LAI and APAR assessment. *Remote Sensing of Environment* 35: 161-173.
- Baumgardner MF, Silva LF, Biehl LL & Stoner ER 1985. Reflectance properties of soils. *Advances in Agronomy* 38: 1-44.

- Borstad G, Brown L, Martinez M, Hamaguchi B, Dickson J & Freberg M 2009. Airborne mapping of vegetation changes in reclaimed areas at Highland Valley between 2001 and 2008. Presented at the 33rd Annual Mine Reclamation Symposium held 14-17 September 2009. Cranbrook, s.n.
- Brown L, Borstad G, Martínez M, Kerr R, Willis P, Richards M & Witt P 2006. Temporal trends in reclamation assessed with airborne multispectral remote sensing. Paper presented at the 30th British Columbia Mine Reclamation Symposium held 19-22 June 2006. Smithers: s.n.
- Buschmann C, Langsdorf G & Lichtenthaler HK 2000. Imaging of blue, green, and red fluorescence emission of plants: an overview. *Photosynthetica* 38: 483-491.
- Castillejo-González IL, López-Granados, García-Ferrer A, Peña-Barragán JM, Jurado-Expósito M, De la Orden MS & González-Audicana M 2009. Object- and pixel-based analysis for mapping crops and their agro-environmental associated measures using QuickBird imagery. *Computers and Electronics in Agriculture* 68: 207-215.
- Chavez PS, Sides SC & Anderson JA 1991. Comparison of three different methods to merge multiresolution and multispectral data: Landsat TM and SPOT panchromatic. *Photogrammetric Engineering & Remote Sensing* 57: 295-303.
- Clarke RN, Swayze GA, Gallagher AJ, King TVV & Calvin WM 1993. The U.S. Geological Survey, Digital Spectral Library: Version 1: 0.2 to 3 microns. U.S. Geological Survey Open File Report 93-592, U.S. Geological Survey, Reston, VA. Available from: <http://speclab.cr.usgs.gov>. [Accessed 2 January 2014].
- Clarke RN, Swayze GA, Wise RA, Livo KE, Hoefen TM, Kokaly RF & Sutley SJ 2007. USGS digital spectral library splib06a: U.S. Geological Survey, Digital Data Series 231. U.S. Geological Survey, Denver, Colorado. Available from: <http://speclab.cr.usgs.gov/spectral.lib06> [Accessed 20 February 2015].
- Clements FE, Weaver JE & Hanson HC 1929. Plant competition: An analysis of community functions. Carnegie Institution of Washington, Publication no 398.
- Coetzer W & Symons G 2012. E-mail to W, Coetzer, and G, Symons on 12 April 2012 on the accuracy of the Karibib base station GPS points.
- Collins JB & Woodcock CE 1996. An assessment of several linear change detection techniques for mapping forest mortality using multitemporal Landsat TM data. *Remote Sensing of Environment* 56:66-77.
- Congalton RG 2005. *Thematic and positional accuracy assessment of digital remotely sensed data*. Proceedings of 7th Annual Forest Inventory and Analysis Symposium held 3-6 October 2005. Portland, n.p.
- Congalton RG & Green K 2009. Assessing the accuracy of remotely sensed data: principles and practices. Florida: CRC Press.
- Coppin PR & Bauer ME 1996. Change detection in forest ecosystems with remote sensing digital imagery. *Remote Sensing Reviews* 13: 207-234.

- Coppin P, Jonckheere I, Nackaerts K, Muys B & Lambin E 2004. Digital change detection methods in ecosystem monitoring: a review. *International Journal of Remote Sensing* 25: 1565-1596.
- Crist EP & Cicone RC 1984. A physically-based transformation of thematic mapper data: the TM Tasseled Cap. *IEEE Transaction of Geoscience and Remote Sensing* 22: 256-263.
- Deering DW, Rouse JW, Haas RH & Schell JA 1975. *Measuring forage production of grazing units from Landsat MSS data*. Proceedings of the Tenth International Symposium on Remote Sensing of Environment 2: 1169-1178. Ann Arbor: ca 1975.
- Dial G, Bowen H, Gerlach F, Grodecki J & Oleszczuk R 2003. IKONOS satellite, imagery, and products. *Remote Sensing of Environment* 88: 23-36.
- DiBiase D 2014. The nature of geographic information: spectral response patterns. The Pennsylvania State University, Pennsylvania. Available from: https://www.e-education.psu.edu/natureofgeoinfo/c8_p5.html [Accessed 20 February 2015].
- DigitalGlobe 2013. GeoEye-1 data sheet [online]. S.l.: s.n. Available from: <http://www.digitalglobe.com/resources/satellite-information> [Accessed 30 August 2013].
- ERDAS Imagine 2013a. ERDAS Field Guide [online]. S.l.: s.n. Intergraph Inc September 2013. Available from: http://www.hexagon-solutions.com.cn/Libraries/Misc_Docs/ERDAS_FieldGuide_PDF_Intergraph_brand.sflb.pdf [Accessed 10 November 2013].
- ERDAS Imagine 2013b. Imagine AutoSync theory [online]. S.l.: s.n. Intergraph Inc September 2013. Available from: file:///C:/Intergraph/ERDAS%20IMAGINE%202013/help/html/wwhelp/wwhimpl/common/html/wwhelp.htm#href=FieldGuide/Contents_Field_Guide.html&single=true [Accessed 10 November 2013].
- ERDAS Imagine 2013c. Imagine DeltaCue User Guide. Intergraph Inc September 2013. Available from: file:///C:/Intergraph/ERDAS%20IMAGINE%202013/help/html/wwhelp/wwhimpl/js/html/wwhelp.htm#href=delta_cue_UG/ChangeDetection.html [Accessed 15 March 2014].
- Ehlers M, Klonus S & Åstrand PJ 2008. *Quality assessment for multi-sensor multi-date image fusion*. 21st ISPRS Congress 3-11 July 2008. The International Archives of the Photogrammetry, Remote Sensing and Spatial Information Sciences Vol. XXXVII Part B4: 499-506. Beijing: 2008.
- Ehlers M, Klonus S, Jarmer T, Sofina N, Michel U, Rienartz P & Sirmacek B 2012. *CEST analysis: automated change detection from very-high-resolution remote sensing images*. 22nd ISPRS Congress 25 August – 1 September 2012. International Archives of the Photogrammetry, Remote Sensing and Spatial Information Sciences 39-B7: 317-322. Melbourne: International Society for Photogrammetry and Remote Sensing.
- ENVI Online Help 2012. *Vegetation indices* [online]. S.l.: s.n. Available from: <http://www.exelisvis.com/docs/VegetationIndices.html> [Accessed 25 September 2012].

- Fonseca L, Namikawa L, Castejon E, Carvalho L, Pinho C & Pagamisse A 2011. Image fusion for remote sensing applications. In Zheng Y (ed) *Image Fusion and Its Applications* Rijeka: Intech.
- Ford GE & Zanelli CI 1985. Analysis and quantification of errors in the geometric correction of satellite images. *Photogrammetric Engineering and Remote Sensing* 51: 1725-1734.
- Fricker P & Rohrbach A 2005. Pushbroom scanners provide highest resolution earth imaging information in multispectral bands. *Proceedings of IPSRS Hannover Workshop: High Resolution Earth Imaging for Geospatial Information* held 17-20 May 2005. Hannover: Information Processing System for Remote Sensing.
- GeoEye 2008. GeoEye-1 Fact Sheet [online]. S.l.: s.n. Available from: http://www.geoeye.com/CorpSite/assets/docs/brochures/GeoEye-1_Fact_Sheet.pdf [Accessed November 2008].
- GeoEye 2009. Imagery Sources [online]. S.l.: s.n. Available at <http://www.geoeye.com/CorpSite/products/imagery-sources/Default.aspx#geoeye1>. [Accessed 31 March 2009].
- Gibbons P & Freudenberger D 2006. An overview of methods used to assess vegetation condition at the scale of the site. *Ecological Management & Restoration* 7: S10-S17.
- Glenn-Lewin DC, Peet RK & Veblen TT 1992. *Plant succession: Theory and prediction*. London: Chapman & Hall.
- Green K, Kempka D & Lackey L 1994. Using remote sensing to detect and monitor land-cover and land-use change. *Photogrammetric Engineering and Remote Sensing* 60: 331-337.
- Gross JE, Goetz SJ & Cihlar J 2009. Application of remote sensing to parks and protected area monitoring: Introduction to special issue. *Remote Sensing of Environment* 113: 1343-1345.
- Hester DB, Cakir HK, Nelson SAC & Khorram S 2008. Per-pixel classification of high spatial resolution satellite imagery for urban land-cover mapping. *Photogrammetric Engineering & Remote Sensing* 74: 463-471.
- Horler DNH, Dockray M & Barber J 1982. The red edge of plant leaf reflectance. *International Journal of Remote Sensing* 4, 2: 273-288.
- Hoskin T no date. Parametric and nonparametric: Demystifying the terms [online]. Mayo Clinic Department of health sciences. Available from: <http://www.mayo.edu/mayo-edu-docs/center-for-translational-science-activities-documents/berd-5-6.pdf> [Accessed 19 September 2013]
- Huete A 1988. A soil-adjusted vegetation index (SAVI). *Remote Sensing of Environment* 25: 295-309.
- Huete A, Didan K, Miura T, Rodriguez EP, Gao X & Ferreira LG 2002. Overview of the radiometric and biophysical performance of the MODIS vegetation indices. *Remote Sensing of Environment* 83: 195-213.
- Huete AR, Jackson RD & Post DF 1985. Spectral response of a plant canopy with different soil backgrounds. *Remote Sensing of Environment* 17: 37-53.

- Huete AR & Liu HQ 1994. An error and sensitivity analysis of the atmospheric and soil-correcting variants of the NDVI for the MODIS-EOS. *IEEE Transactions in Geoscience and Remote Sensing* 32: 897-905.
- Hunt ER & Rock BN 1989. Detection of changes in leaf water content using near- and middle-infrared reflectances. *Remote Sensing of Environment* 30: 43-54.
- Jarlan L, Mangiarotti S, Mougin E, Mazzega P, Hiernaux P & Le Dantec V 2007. Assimilation of SPOT/vegetation NDVI data into sahelian vegetation dynamics model. *Remote Sensing of the Environment* 112: 1381 – 1394.
- Jenerette DG, Scott RL & Huete A 2010. Functional differences between summer and winter season rain assessed with MODIS-derived phenology in a semi-arid region. *Journal of Vegetation Science* 21: 16-30.
- Jensen JR 2005. *Introductory digital image processing: A remote sensing perspective*. 3rd ed. Upper Saddle River: Pearson Prentice Hall.
- Jensen JR 2007. *Remote sensing of the environment: An earth resource perspective*. 2nd ed. Upper Saddle River: Pearson Prentice Hall.
- Kauth RJ & Thomas GS 1976. *The tasseled cap: a graphic description of the spectral-temporal development of agricultural crops as seen by Landsat*. Symposium on Machine Processing of Remotely Sensed Data held 29 June to 1 July 1976. West Lafayette, Indiana.
- Kennedy RE, Townsend PA, Gross JE, Cohen PB, Wang YQ & Adams P 2009. Remote sensing change detection tools for natural resource managers: Understanding concepts and trade-offs in the design of landscape monitoring projects. *Remote Sensing of Environment* 13: 1382-1396.
- Kerr JT & Ostrovsky M 2003. From space to species: ecological applications for remote sensing. *TRENDS in Ecology and Evolution* 18, 6: 299-305.
- Khorram S, Koch FH, Van der Wiele CF & Nelson SAC 2012. *Remote sensing*. New York: Springer Verlag.
- Klonus S & Ehlers M 2009. Performance of evaluation methods in image fusion. 12th International Conference on Information Fusion. Seattle Washington 6-9 July 2009.
- Kohm K 2004. OrbView-3 spatial characterization. JACIE – High Spatial Resolution Commercial Imagery Workshop 2004.
- Koruyan K, Deliormanli AH, Karaca Z, Momayez M, Lu H & Yalçin E 2012. Remote sensing in management of mining land and proximate habitat. *The Journal of the Southern African Institute of Mining and Metallurgy* 112: 669-672.
- Leblon B 1997. Soil and vegetation optical properties [online]. S.l.: s.n. The remote sensing core curriculum: Volume 4 applications in remote sensing. Available from: http://www.uriit.ru/japan/Our_Resources/Books/RSTutor/Volume4/leblon/frame9.html [Accessed 10 June 2013].

- Li R & Li J 2004. Satellite remote sensing technology for lake water clarity monitoring: an overview. *Environmental Informatics Archives* 2: 893-901.
- Li Z, Li X, Wang Y, Ma A & Wang J 2004. Land-use analysis in Yulin prefecture, north-western China using remote sensing and GIS. *International Journal of Remote Sensing* 25: 5691-5703.
- Liew SC 2001. Principles of remote sensing [online]. Centre for remote imaging, sensing and processing. Singapore. Available from: <http://www.crisp.nus.edu.sg/~research/tutorial/image.htm> [Accessed: 7 January 2014].
- Lillesand TM, Kiefer RW & Chipman JW 2008. *Remote sensing and image interpretation*. Hoboken: John Wiley & Sons, Inc.
- Lobser SE & Cohen WB 2007. MODIS tasselled cap: land cover characteristics expressed through transformed MODIS data. *International Journal of Remote Sensing* 28: 5079-5101.
- Lösel G 2009. *Earth observation solutions from RapidEye for agricultural needs* [online]. S.l.: s.n. Available from: <http://www.fieldfact.com/LinkClick.aspx?fileticket=VSSWiiCU%2Brs%3D&tabid=601&mid=1297> [Accessed 8 January 2013].
- Lu D, Mausel P, Brondizio E & Moran E 2004. Change detection techniques. *International Journal of Remote Sensing* 25: 2365.
- Lunetta RS, Congalton RG, Fenstermaker LK, Jensen JR, McGwire KC & Tinney LR 1991. *Photogrammetric Engineering & Remote Sensing* 57: 677-687.
- Lyzenga DR 1978. Passive remote sensing techniques for mapping water depth and bottom features. *Applied Optics* 17: 379-383.
- Martínez M, Brown LN, Borstad GA, Dickson J & Martell P 2012. Multispectral mapping of vegetation changes in reclaimed areas at Highland Valley between 2001 and 2011. Paper presented at the 36th Annual British Columbia Mine Reclamation Symposium held 17-20 September 2012. Kamloops: s.n.
- Matiwane N 2009b. Memorandum: Gecko spectral analysis report. AngloGold Ashanti (Pty) Ltd.
- Mather PM 2006. *Computer processing of remotely-sensed images: An introduction*. 3rd ed. West Sussex: John Wiley & Sons, Ltd.
- McCoy RM 2005. *Field methods in remote sensing*. New York: The Guilford Press.
- Mehner H, Cutler M, Fairbairn D & Thompson G 2004. Remote sensing of upland vegetation: The potential of high spatial resolution satellite sensors. *Global Ecology and Biogeography* 13: 359-369.
- Mouton J 2001. *How to succeed in your master's and doctoral studies: A South African guide and resource book*. Pretoria: Van Schaik Publishers.

- Musande V, Kumar A, Kale K & Roy PS 2012. Temporal indices data for specific crop discrimination using fuzzy based noise classifier. *International Archives of the Photogrammetry, Remote Sensing and Spatial Information Sciences held 25 August – 1 September 2012* Volume XXXIX-B8, 2012. XXII ISPRS Congress. Melbourne, Australia.
- Myint SW, Gober P, Brazel A, Grossman-Clarke S & Weng Q 2011. Per-pixel vs. object-based classification of urban land cover extraction using high spatial resolution imagery. *Remote Sensing of the Environment* 115: 1145-1161.
- Namibia (Republic of) 2012. Environmental impact assessment regulations: Act on Environmental management act, Act 7 of 2007. *Government Gazette of Namibia* Volume 4878, 6 February, No 30 2012.
- National Aeronautics and Space Administration Climate Science Investigations (CSI) [online]. <http://www.ces.fau.edu/nasa/module-2/radiation-sun.php> [Accessed 22 November 2015].
- National Aeronautics and Space Administration Earth Observatory [online]. http://earthobservatory.nasa.gov/Features/MeasuringVegetation/measuring_vegetation_2.php [Accessed November 2008].
- Nichol J & Wong MS 2007. Remote sensing of urban vegetation life form by spectral mixture analysis of high-resolution IKONOS satellite images. *International Journal of Remote Sensing* 28: 985-1000.
- Nishio JN 2000. Why are higher plants green? Evolution of the higher plant photosynthetic pigment complement. *Plant, Cell and Environment* 23: 539-548.
- Ollinger SV 2010. Sources of variability in canopy reflectance and the convergent properties of plants. *New Phytologist* 189: 375-394.
- Otterman J & Fraser RS 1979. Adjacency effects on imaging by surface reflection and atmospheric scattering: cross radiance to zenith. *Applied Optics* 18: 2852-2860.
- Paniagua L, Bachmann M, Fischer C, Kooistra L & Müller A 2009. Monitoring mining rehabilitation development according to methods derived from imaging spectroscopy: Case study in the Sotiel-Migollas mine complex, southern Spain. Paper delivered at the 6th EARSel SIG IS workshop held from 16-19 March 2009. Tel-Aviv: n.p.
- Podger NE, Colwell WB & Taylor MH 2011. GeoEye-1 radiance at aperture and planetary reflectance (online). https://apollomapping.com/wp-content/user_uploads/2011/09/GeoEye1_Radiance_at_Aperture.pdf [Accessed 12 September 2014].
- Prithvish N & Kudrat M 1998. *Digital Remote Sensing*. New Delhi: Concept Publishing Company.
- Qi J, Moran MS, Cabot F & Dedieu G 1995. Normalization of sun/view angle effects using spectral albedo-based vegetation indices. *Remote Sensing of the Environment* 52: 207-217.
- Randall J 2004. Ecosystem function analysis: A tool for monitoring mine-site rehabilitation success. *MESA Journal* 25: 24-27.

- Radke RJ, Al-Kofahi O & Roysam AS, B 2005. Image change detection algorithms: a systematic survey. *IEEE Transactions on Image Processing* 14: 294-307.
- Richards DM, Borstad G & Martínez M 2004. Using multispectral remote sensing to monitor reclamation at Highland Valley Copper. Paper presented at the 28th British Columbia Mine Reclamation Symposium held from 2004. Cranbrook: n.p.
- Richards DM, Martínez M & Borstad GA 2003. The use of multispectral remote sensing to map reclaimed areas at Highland Valley Copper. Paper presented at the 105th Canadian Institute of Mining, Metallurgy and Petroleum Annual General Meeting held from 4-7 May 2003. Montreal: n.p.
- Röder A, Udelhoven T, Hill J, Del Barrio G & Tsiourlis G 2008. Trend analysis of Landsat TM and -ETM+ imagery to monitor grazing impact in a rangeland ecosystem in Northern Greece. *Remote Sensing of Environment* 112: 2863-2875.
- Satellite Imaging Corporation 2013. Orthorectification [online]. S.l.: s.n. Available from: <http://www.satimagingcorp.com/svc/orthorectification.html> [Accessed 19 September 2013].
- Satellite Imaging Corporation 2013. RapidEye satellite sensor [online]. S.l.: s.n. Available from: <http://www.satimagingcorp.com/satellite-sensors/rapideye.html>. [Accessed 7 January 2014].
- Seager S, Turner EL, Schafer J & Ford EB 2005. Vegetation's red edge: A possible spectroscopic biosignature of extraterrestrial plants. *Astrobiology* 5: 372-390.
- Science education through earth Observation for high schools website 2014. Introduction to remote sensing. S.l.: s.n. Available from: <http://www.seos-project.eu/modules/remotesensing/remotesensing-c01-p05.html> [Accessed 16 September 2014].
- Shank M 2008. Using remote sensing to map vegetation density on a reclaimed surface mine. Paper presented at the Incorporating Geospatial Technologies into SMCRI Business Processes. Atlanta, Georgia.
- Sheng L, Huang J & Tang X 2011. A tasseled cap transformation for CBERS-02B CCD data. *Journal of Zhejiang University Science B (Biomedicine & Biotechnology)* 12: 780-786.
- Sheskin DJ 2004. *Handbook of parametric and nonparametric statistical procedures*. 3^{de} ed. Florida: Chapman & Hall/CRC Press.
- Shi W, Zhu C, Tian Y & Nichol J 2005. *Wavelet-based image fusion and quality assessment*. *International Journal of Applied Earth Observation and Geoinformation* 6: 241-251.
- Silleos NG, Alexandridis TK, Gitas IZ & Perakis K 2006. Vegetation indices: Advances made in biomass estimation and vegetation monitoring in the last 30 years. *Geocarto International* 21: 21-28.
- Sims DA & Gamon JA 2003. Estimation of vegetation water content and photosynthetic tissue area from spectral reflectance: a comparison of indices based on liquid water and chlorophyll absorption features. *Remote Sensing of Environment* 84: 526-537.

- Singh A 1989. Digital change detection techniques using remotely-sensed data. *International Journal of Remote Sensing* 10: 989-1003.
- Stenberg P, Rautiainen M, Manninen T, Voipio P & Smolander H 2004. Reduced simple ratio better than NDVI for estimating LAI in Finnish Pine and Spruce Stands [online]. *Silva Fennica* 38: 3-14. <http://www.metla.fi/silvafennica/full/sf38/sf381003.pdf> [Accessed 7 June 2013].
- Stoner ER & Baumgardner MF 1981. Characteristic variations in reflectance of surface soils. *Soil Science Society of America Journal* 45: 1161-1165.
- Straker J, Blazecka M, Sharman K, Woelk S, Boorman S & Kuschminder J 2004. Use of remote sensing in reclamation assessment at Teck Cominco's Bullmoose mine site. Mine Reclamation Symposium Proceedings. British Columbia Technical & Research Committee on Reclamation.
- Streck NA, Rundquist D & Connot J 2003. Spectral signature of selected soils. *Revista Brasileira de Agrometeorologia* 11: 181-184.
- Švab A & Oštir K 2006. High-resolution image fusion: Methods to preserve spectral and spatial resolution. *Journal of the American Society for Photogrammetry and Remote Sensing* 72: 565-572.
- The Commonwealth Scientific and Industrial Research Organisation (CSIRO) 2011. Clayton: s.n. Fact sheet: Using remote sensing for environmental monitoring and mapping. Available from: <http://www.csiro.au/Organisation-Structure/Divisions/Mathematics-Informatics-and-Statistics/EMMRemoteSensing/Remote-sensing-of-local-variation.aspx> . [Accessed 25 March 2009].
- Thenkabail PS, Smith RB & De Pauw E 2000. Hyperspectral vegetation indices and their relationships with agricultural crop characteristics. *Remote Sensing of Environment* 71:158-182.
- Thompson SA & Thompson GG 2004. Adequacy of rehabilitation monitoring practices in the Western Australian mining industry. *Ecological management & restoration* 5: 30-33.
- Tongway DJ & Hindley NL 2003. Indicators of ecosystem rehabilitation success: Stage two – verification of EFA Indicators [online]. Canberra: CSIRO Sustainable Ecosystems. Available from: <http://www.cse.csiro.au/publications/2003/IndicatorsOfMinesiteRehabilitationSuccessStage2-100703.pdf>. [Accessed 23 October 2012].
- Tongway DJ & Hindley NL 2005. Landscape function analysis: Procedures for monitoring and assessing landscapes with special reference to mine sites and rangelands. Canberra: CSIRO Sustainable Ecosystems.
- Tucker CJ 1979. Red and photographic infrared linear combinations for monitoring vegetation. *Remote Sensing of the Environment* 10: 127-150.
- Turner W, Spector S, Gardiner N, Fladeland M, Sterling E & Steininger M 2003. Remote sensing for biodiversity science and conservation [online]. *Trends in Ecology and Evolution* 18: 306-314.

- University of Oregon Solar Radiation Monitoring Laboratory 2013. Solar position calculator [online]. Eugene, Oregon. Available from: <http://solardat.uoregon.edu/SolarPositionCalculator.html> [Accessed 14 September 2014].
- Ustin SL, Roberts DA, Gamon JA, Asner GP & Green RO 2004. Using imaging spectroscopy to study ecosystem processes and properties. *BioScience* 54, 6: 523-534.
- Vakalopoulou M & Argialas D 2012. Evaluation of change detection methods in remote sensing, and development of relevant open source algorithms in the Orfeo Toolbox platform. EARSel Symposium Proceedings: Advances in Geosciences 21-24 May 2012. Mykonos Island: European Association of Remote Sensing Laboratories.
- Vijayaraj V 2004. A quantitative analysis of pansharpened images. Master's thesis. Mississippi: Mississippi State University, Department of Electrical & Computer Engineering.
- Walker RW & Del Moral R 2003. *Primary succession and ecosystem rehabilitation*. Cambridge: The Press Syndicate of the University of Cambridge.
- Walsh SJ, McCleary AL, Mena CF, Shao Y, Tuttle JP, González A & Atkinson R 2008. Quickbird and Hyperion data analysis of an invasive plant species in the Galapagos Islands of Ecuador: Implications for control and land-use management. *Remote Sensing of the Environment* 112: 1927-1941.
- Witharana C & Civco DL 2012. Evaluating remote sensing image fusion algorithms for use in humanitarian crisis management.
- Whiteside TG, Boggs GS & Maier SW 2011. Comparing object-based and pixel-based classifications for mapping savannas. *International Journal of Applied Earth Observation and Geoinformation* 13: 884-893.
- Wei ZG, Yuan JH & Cai YL 1999. A picture quality evaluation method based on human perception. *Acta Electron* 27: 79-82.
- Wiegleb G & Felinks B 2001. Primary succession in post-mining landscapes of Lower Lusatia – change or necessity. *Ecological Engineering* 17: 199-217.
- Wulder MA, Butson CR and White JC 2007. Cross-sensor change detection over a forested landscape: Options to enable continuity of medium spatial resolution measures. *Remote Sensing of Environment* 112: 796-809.
- Wulder MA White JC Coops NC & Butson CR 2008. Multi-temporal analysis of high spatial resolution imagery for disturbance monitoring. *Remote Sensing of Environment* 112: 2729-2740.
- Zhang Y 2004. Understanding image fusion. *Photogrammetric Engineering & Remote Sensing* 70: 657-661.
- Zhang Y 2008. Methods for image fusion quality assessment – a review, comparison and analysis. *The International Archives of Photogrammetry, Remote Sensing and Spatial Information Sciences* 37: 1101-1109.
- Zhang C & Guo X 2008. Monitoring northern mixed prairie health using broadband satellite imagery. *International Journal of Remote Sensing* 29: 2257-2271.

Zhang Y & Mishra RK 2012. A review and comparison of commercially available pan-sharpening techniques for high resolution satellite imagery fusion. *IEEE IGARSS 2012*

Zhou J, Civco DL & Silander JA 2010. A wavelet transform method to merge Landsat TM and SPOT panchromatic data. *International Journal of Remote Sensing* 19: 743-757.

PERSONAL COMMUNICATIONS

- Badenhorst F 2009. Operations Manager, Navachab Gold Mine. Karibib. Interview on 26 March 2009 about historical progression of activities at Navachab Gold Mine.
- Bell GR 2010. Mineral Resource Manager, Navachab Gold Mine, Karibib. Discussion about ore types represented in tailings of TSF1.
- Carr-Hyde G 2009. E-mail G, Carr-Hyde (greg@datadesign.co.za) on 23 January 2009 about various options of satellite imagery available for the study area.
- Dorfling J 2008. Email to J, Dorfling (jaurez@datadesign.co.za) 28 November 2008 on GeoEye-1 specifications. Dorfling J 2012b. E-mail to J, Dorfling (jaurez@datadesign.co.za) 3 February 2012b on DEM creation and ERDAS LPS workflow. Dorfling J 2012c. E-mail to J, Dorfling (jaurez@datadesign.co.za) 6 April 2012 on GCP accuracy of GeoEye-1 images.
- Dorfling J 2012a. Technical Director GEO Data Design (Pty) Ltd., Cape Town. Telephonic discussion on 3 February 2012 regarding RSME and SD values.
- Dorfling J 2010. Technical Director GEO Data Design (Pty) Ltd., Karibib. Personal conversation on 17 April 2010 on the influence of pansharpening on vegetation indexes and change detection.
- Dorfling J 2012d. Technical Director Geo Data Design (Pty) Ltd., Cape Town. Telephonic discussion on 22 June 2012 on corrections done by suppliers on imagery.
- Fourie 2014. E-mail to A, Fourie (Andre.Fourie@navachab.com.na) 10 September 2014 about GPS equipment used and Namibian mapping system.
- Matiwane N 2009a. E-mail to N, Matiwane (nmatiwane@anglogoldashanti.com) 9 October 2009 on spectral analysis of Navachab substrates.
- Mazus H 2012a. GIS Specialist: Geo Data Design (Pty) Ltd. Cape Town. Telephonic conversation on LPS and DEM creation.
- Mazus H 2012b. GIS Specialist: Geo Data Design (Pty) Ltd. Cape Town. Telephonic conversation and e-mail on problems experienced with Autosync.
- Van Niekerk A 2009. Director: Centre for Geographical Analysis, Stellenbosch University. Email on 13 May 2009 about geo-correction of satellite images.
- Van Niekerk A 2010. Director: Centre for Geographical Analysis, Stellenbosch University. Email on 9 October 2010 about merits of various methods of pansharpening.

Table A.2 Navachab daily rainfall, 2010

Day \ Month	Jan	Feb	Mar	Apr	May	Jun	Jul	Aug	Sep	Oct	Nov	Dec
1	0.51	0.00	4.83	0.00	0.00	0.00	0.00	0.00	0.00	0.00**	0.00	0.00
2	0.00	0.00	1.52	0.00	1.27	0.00	0.00	0.00	0.00	0.00	0.00	0.00
3	0.00	0.00	0.00	1.02	0.00	0.00	0.00	0.00	0.00	0.00	0.00	0.00
4	0.00	0.00	0.00	0.00	0.00	0.00	0.00	0.00	0.00	0.00	0.00	0.00
5	0.00	0.00	0.00	0.00	0.00	0.00	0.00	0.00	0.00	0.00	0.00	0.00
6	6.10	0.00	0.00	0.00	0.00	0.00	0.00	0.00	0.00	0.00	0.00	0.00
7	0.00	3.30	0.00	0.00	0.00	0.00	0.00	0.00	0.00	0.00	0.00	0.00
8	0.00	1.02	0.00	0.00	0.00	0.00	0.00	0.00	0.00	0.00	0.00	0.00
9	0.00	0.00	0.00	0.00	0.00	0.00	0.00	0.00	0.00	0.00	0.00	0.00
10	0.00	0.00	0.00	0.00	0.00	0.00	0.00	0.00	0.00	0.00	0.00	0.00
11	0.00	0.00	0.00	0.00	0.00	0.00	0.00	0.00	0.00	0.00	0.00	0.76
12	0.76	5.08	0.51	0.00	0.00	0.00	0.00	0.00	0.00	0.00	0.00	0.00
13	22.61	0.25	0.00	0.00	0.00	0.00	0.00	0.00	0.00	0.00	0.00	0.00
14	1.78	0.51	0.00	0.00	0.00	0.00	0.00	0.00	0.00	0.00	1.27	0.00
15	0.00	0.00	0.00	0.00	0.25	0.00	0.00	0.00	0.00	0.00	4.83	0.00
16	6.10	0.00	0.00	0.00	0.00	0.00	0.00	0.00	0.00	0.00	0.00	0.00
17	1.78	0.00	0.00	0.00	0.00	0.00	0.00	0.00	0.00	0.00	10.92	0.00
18	0.00	0.00	0.00	0.00	0.00	0.00	0.00	0.00	0.00	0.00	0.00	0.00
19	0.00	0.00	0.00	0.00	0.00	0.00	0.00	0.00	0.00	0.00	0.00	0.00
20	0.00	0.00	0.00	0.00	0.00	0.00	0.00	0.00	0.00	0.00	0.00	0.00
21	2.29	0.76	0.00	0.00	0.00	0.00	0.00	0.00	0.00	0.00	0.00	0.00
22	0.00	0.00	0.00	0.00	0.00*	0.00	0.00	0.00	0.00	0.00	0.00	0.00
23	0.00	0.00	0.00	0.00	0.00	0.00	0.00	0.00	0.00	0.00	0.00	0.00
24	0.00	0.00	0.00	0.00	0.00	0.00	0.00	0.00	0.00	0.00	0.00	0.00
25	0.00	0.00	0.00	0.00	0.00	0.00	0.00	0.00	0.00	0.00	0.00	0.00
26	0.00	0.00	0.00	0.00	0.00	0.00	0.00	0.00	0.00	0.00	0.00	0.00
27	0.00	25.15	0.00	0.00	0.00	0.00	0.00	0.00	0.00	0.00	0.00	2.54
28	0.00	0.25	0.00	0.00	0.00	0.00	0.00	0.00	0.00	0.00	0.00	2.29
29	0.00		0.00	0.00	0.00	0.00	0.00	0.00	0.00	0.00	0.00	0.00
30	0.00		3.81	0.00	0.00	0.00	0.00	0.00	0.00	0.00	0.00	14.48
31	0.00		0.25		0.00		0.00	0.00		0.00		13.21
* First annual image scan date												
** Second annual image scan date												

Table A.3 Navachab daily rainfall, 2011

Day \ Month	Jan	Feb	Mar	Apr	May	Jun	Jul	Aug	Sep	Oct	Nov	Dec
1	0.00	0.00	0.00	1.27	0.00	0.00	0.00	0.00	0.00	0.00	0.00	0.00
2	0.51	0.00	0.00	0.00	6.86	0.00	0.00	0.00	0.00	0.00	0.00	0.00
3	8.13	19.56	0.00	0.00	6.10	0.00	0.00	0.00	0.00	0.00	0.00	0.00
4	25.15	4.32	20.83	0.00	0.51	0.00	0.00	0.00	0.00	0.00	0.00	0.00
5	5.33	17.02	0.25	0.00	3.30	0.00	0.00	0.00	0.00	0.00	0.00	0.00
6	0.00	3.30	3.05	0.00	3.30	0.25	0.00	0.00	0.00	0.00	0.00	0.00
7	0.00	1.02	0.00	0.00	0.00	0.00	0.00	0.00	0.00	0.00	0.00	0.00
8	0.00	9.40	0.00	32.51	0.00	0.00	0.00	0.00	0.00	0.00	0.00	0.00
9	0.00	2.03	0.00	0.00	0.00	0.00	0.00	0.00	0.00	0.00	0.00	0.00
10	0.00	0.00	0.00	0.00	0.00	0.00	0.00	0.00	0.00	0.00	0.00	0.00
11	0.00	0.00	27.43	0.00	0.00	0.00	0.00	0.00	0.00	0.00	0.00	0.00
12	0.00	18.80	4.06	1.52	0.00	0.00	0.00	0.00	0.00	0.00	0.00	0.00
13	0.00	6.60	1.52	0.00	0.00	0.00	0.00	0.00	0.00	0.00	0.00	0.00
14	0.00	3.56	0.00	11.68	0.00	0.00	0.00	0.00	0.00	0.00	0.00	0.00
15	0.00	0.00	3.81	1.02	0.00	0.00	0.00	0.00	0.00	0.00	0.00	0.00
16	0.00	0.00	0.51	0.00	0.00	0.00	0.00	0.00	0.00	0.00	0.00	0.00
17	0.76	0.00	9.14	0.00	0.00	0.00	0.00	0.00	0.00	0.00	0.00	0.00
18	19.30	0.00	0.76	10.67	0.00	0.00	0.00	0.00	0.00	0.00	0.00	0.00
19	24.13	0.00	0.00	0.25	0.00	0.00	0.00	0.00	0.00	0.00	0.00	0.00
20	0.25	0.00	0.25	39.12	0.00	0.00	0.00	0.00	0.00	0.00	0.00	0.00
21	3.30	0.00	8.38	10.41	0.00	0.00	0.00	0.00	0.00	0.00	0.00	0.00
22	0.00	4.83	1.52	0.51 *	0.00	0.00	0.00	0.00	0.00	0.00	0.00	0.00
23	0.00	1.27	0.25	0.00	0.00	0.00	0.00	0.00	0.00	0.00	0.00	0.00
24	0.00	0.00	0.00	0.00	0.00	0.00	0.00	0.00	0.00	0.00	0.00	0.00
25	1.02	0.00	0.51	0.00	0.00	0.00	0.00	0.00	0.76	0.00	0.00	0.00
26	1.78	0.51	12.19	0.00	0.00	0.00	0.00	0.00	0.00	0.00	0.00	0.00
27	0.25	0.00	3.30	0.00	0.00	0.00	0.00	0.00	0.00	0.00	0.00	0.00
28	0.00	0.00	0.00	0.00	0.00	0.00	0.00	0.00	0.00	0.00	0.00	0.00
29	19.30		8.13	0.00	0.00	0.00	0.00	0.00	0.00	0.00	0.00	0.00
30	0.00		0.00	2.29	0.00	0.00	0.00	0.00		0.00	0.00	0.00
31	0.00		0.00		0.00		0.00	0.00		0.00 **		0.00
	* First annual image scan date											
	** Second annual image scan date											

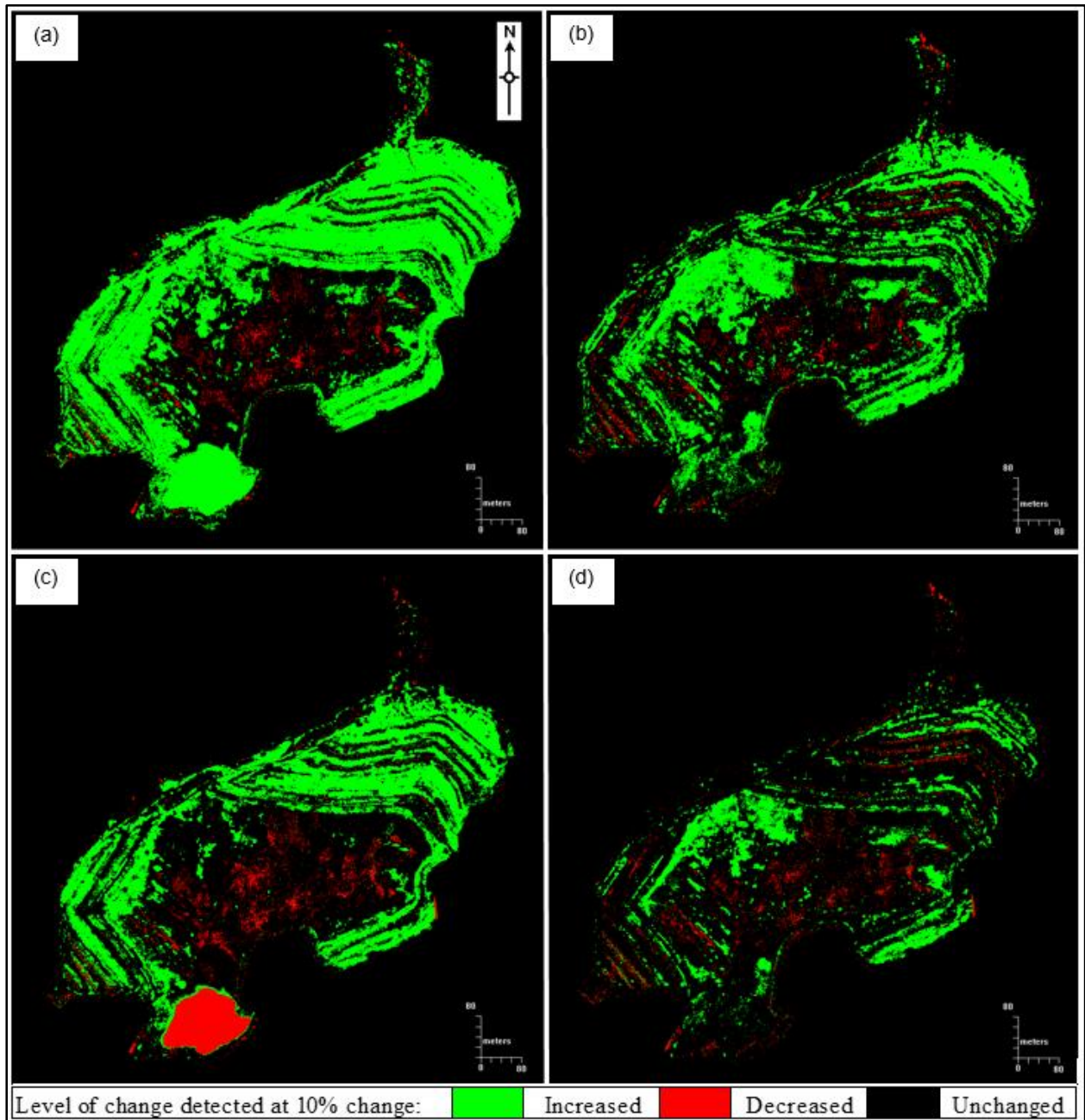
APPENDIX B CHANGE DETECTION RESULTS

Figure B.1 Change detection results between Quickbird January 2004 and GeoEye-1 October 2009 images (a) NDVI and (c) TVI RI versus results between Quickbird July 2005 and GeoEye-1 October 2009 images (b) NDVI, and (d) TVI

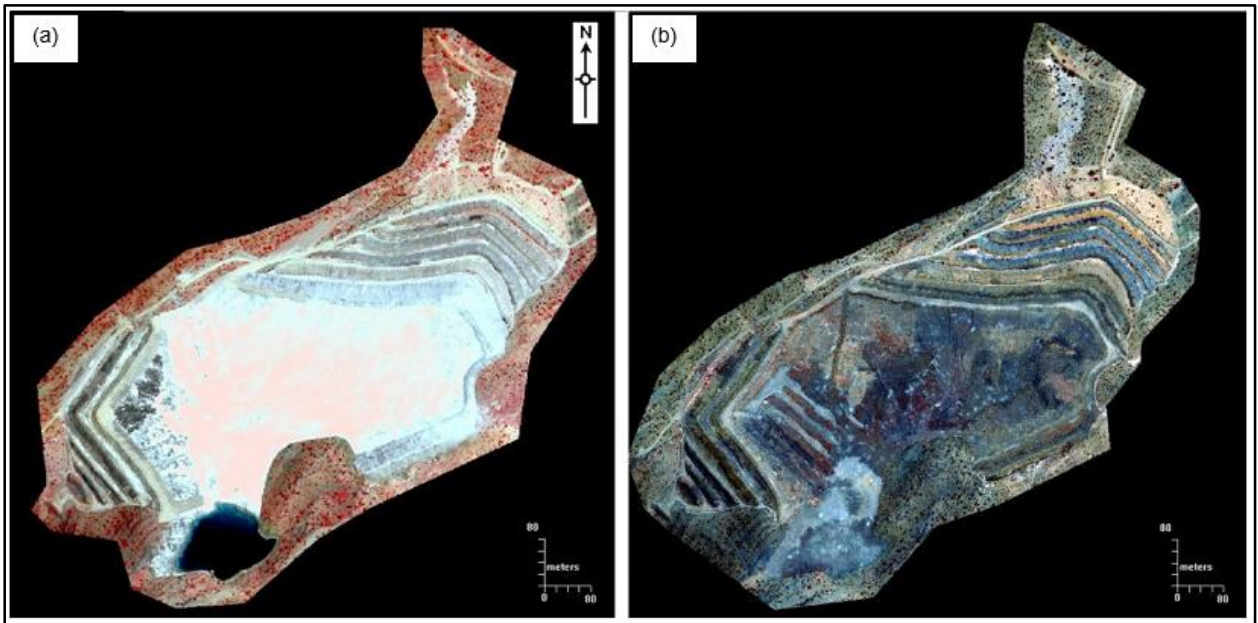


Figure B.2 False colour images of Quickbird January 2004 (a) and GeoEye-1 October 2009 (b)

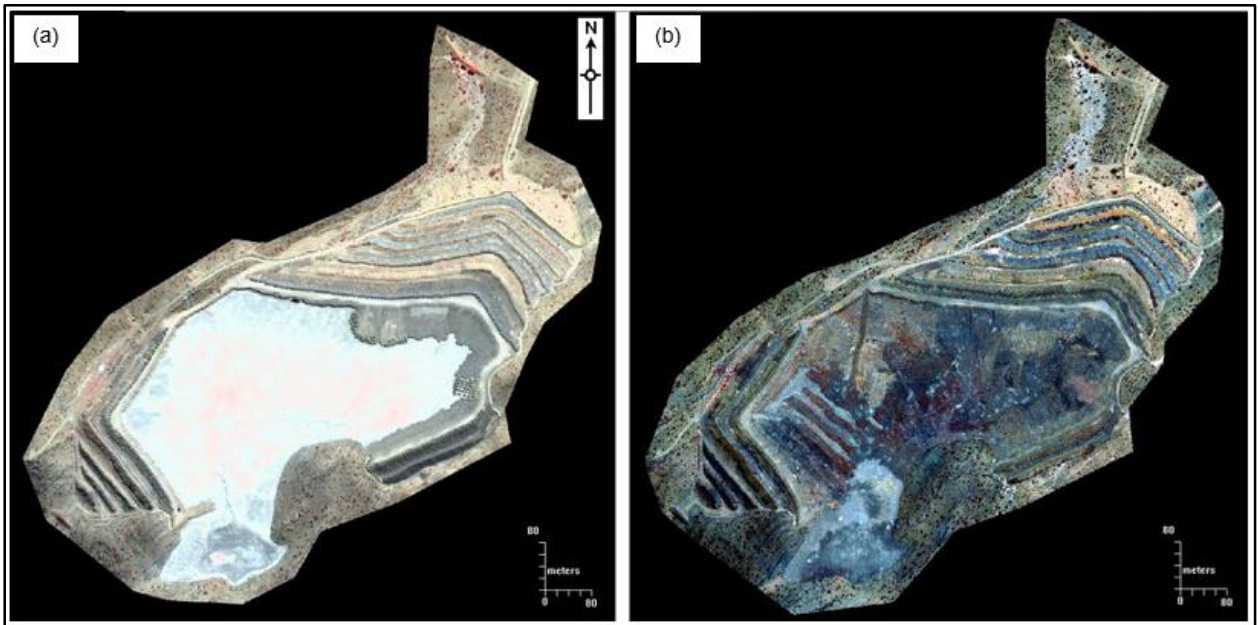


Figure B.3 False colour images of Quickbird July 2005 (a) and GeoEye-1 October 2009 (b)

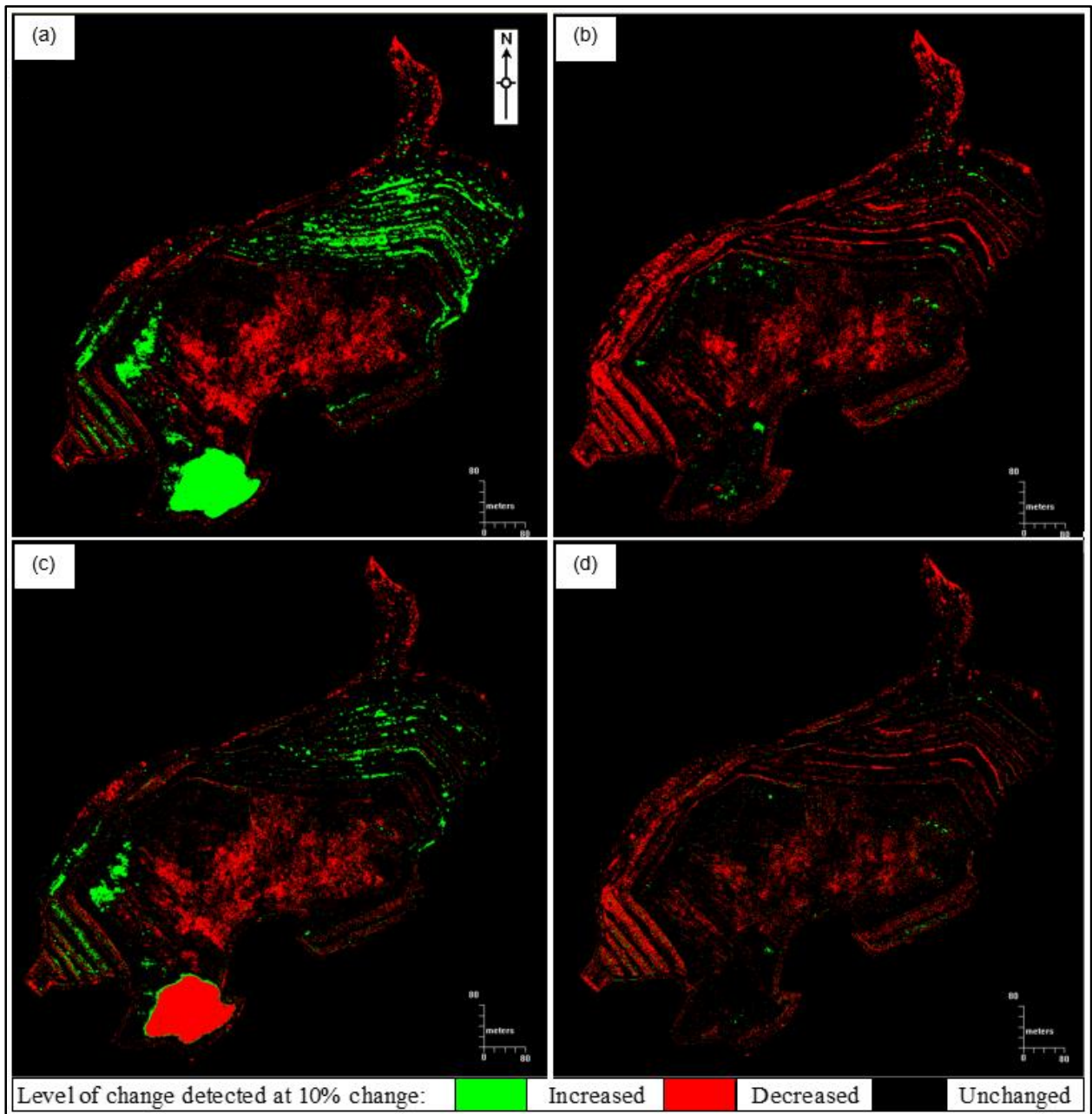


Figure B.4 Change detection results between Quickbird January 2004 and GeoEye-1 May 2010 images (a) NDVI and (c) TVI versus results between Quickbird July 2005 and GeoEye-1 May 2010 images (b) NDVI and (d) TVI.

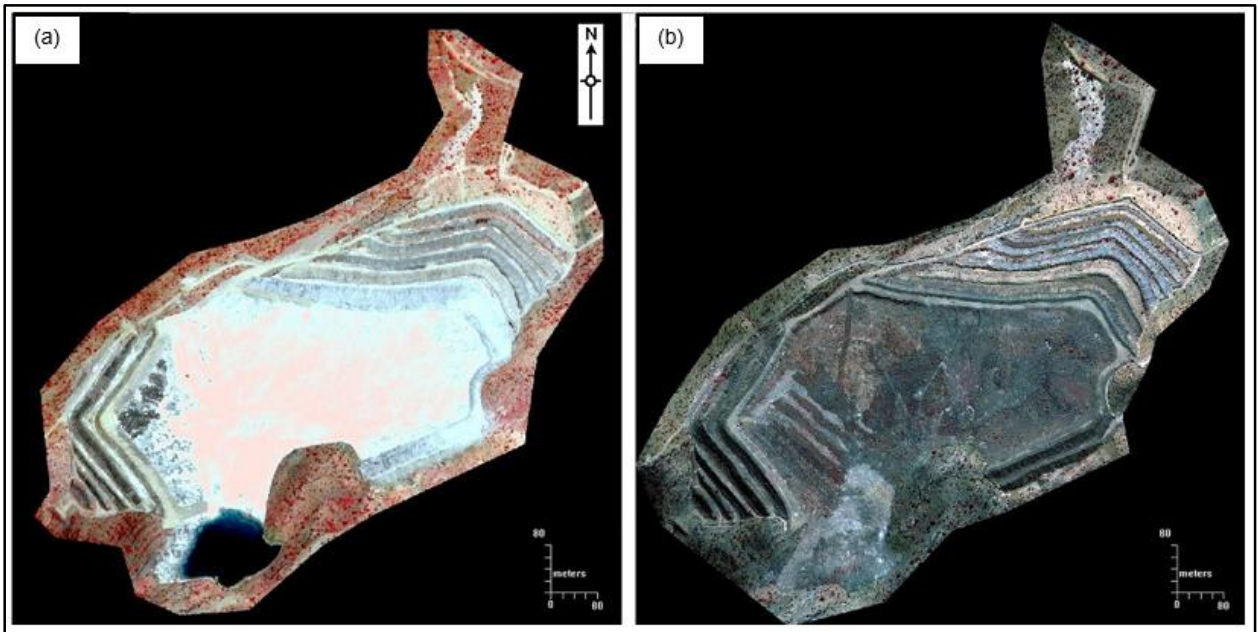


Figure B.5 False colour images of Quickbird January 2004 (a) and GeoEye-1 May 2010 (b)

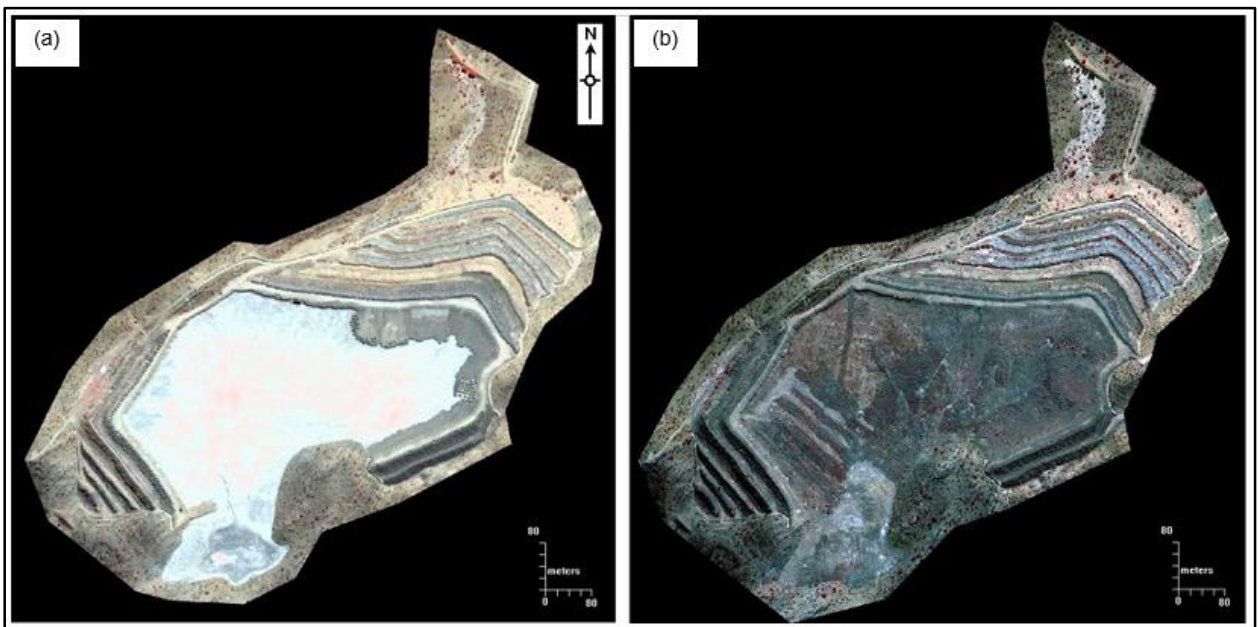


Figure B.6 False colour images of Quickbird July 2005 (a) and GeoEye-1 May 2010 (b)

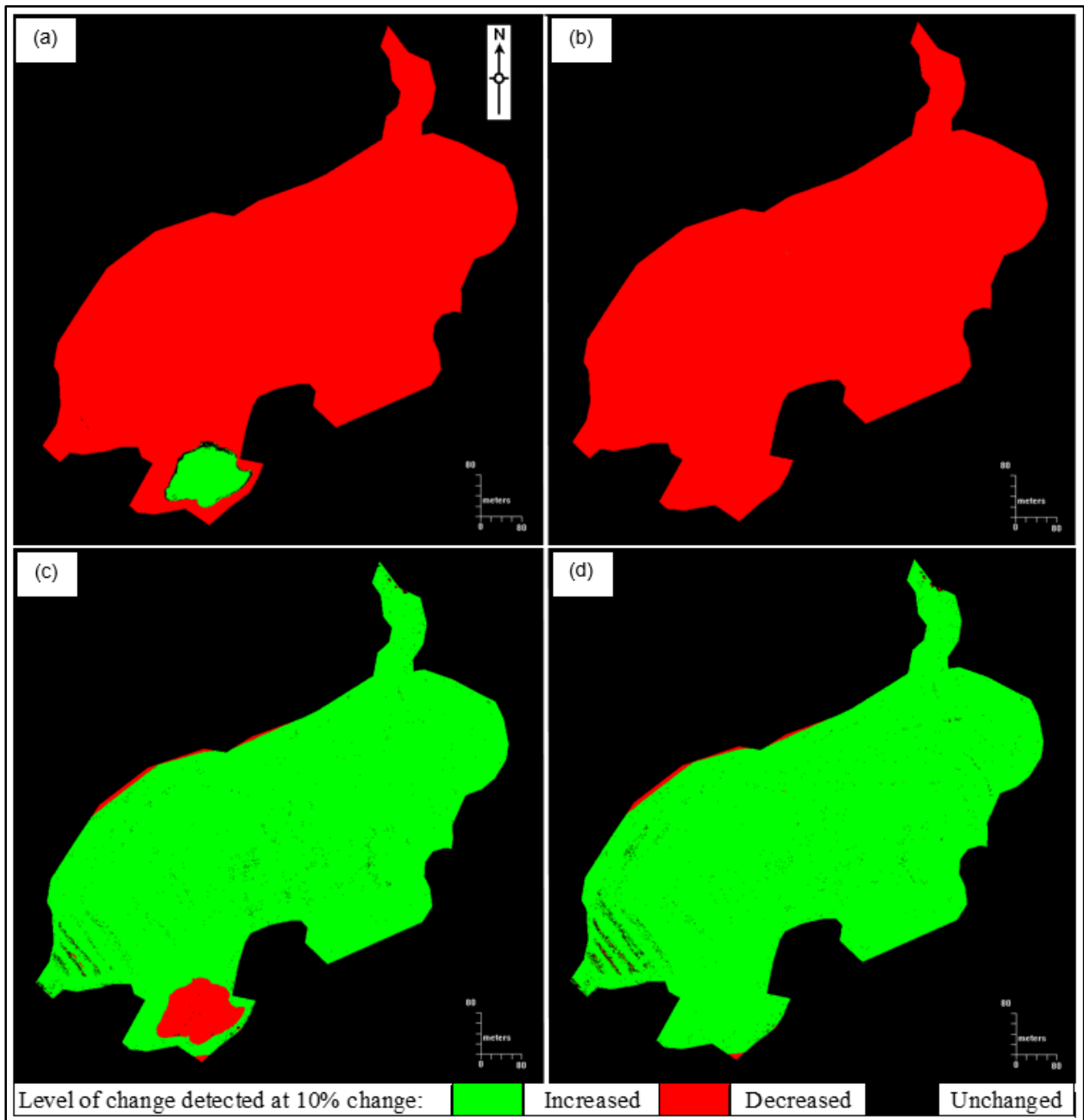


Figure B.7 Change detection results between Quickbird January 2004 and GeoEye-1 October 2010 images (a) NDVI and (c) TVI versus results between Quickbird July 2005 and GeoEye-1 October 2010 images (b) NDVI and (d) TVI.

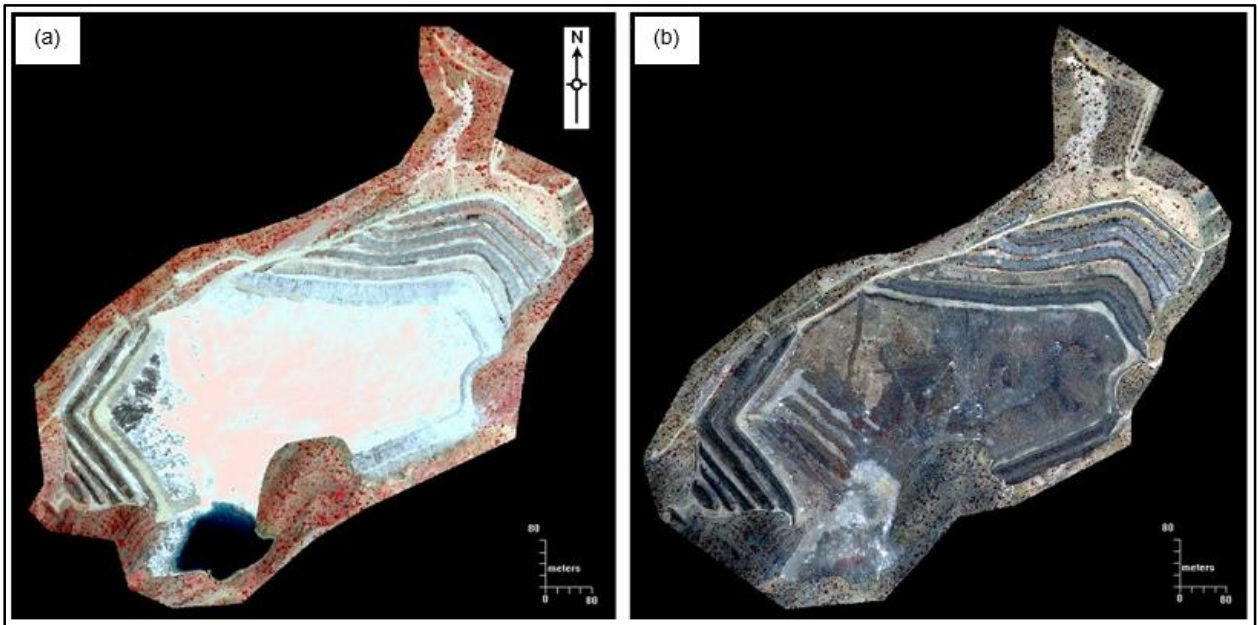


Figure B.8 False colour images of Quickbird January 2004 (a) and GeoEye-1 October 2010 (b)

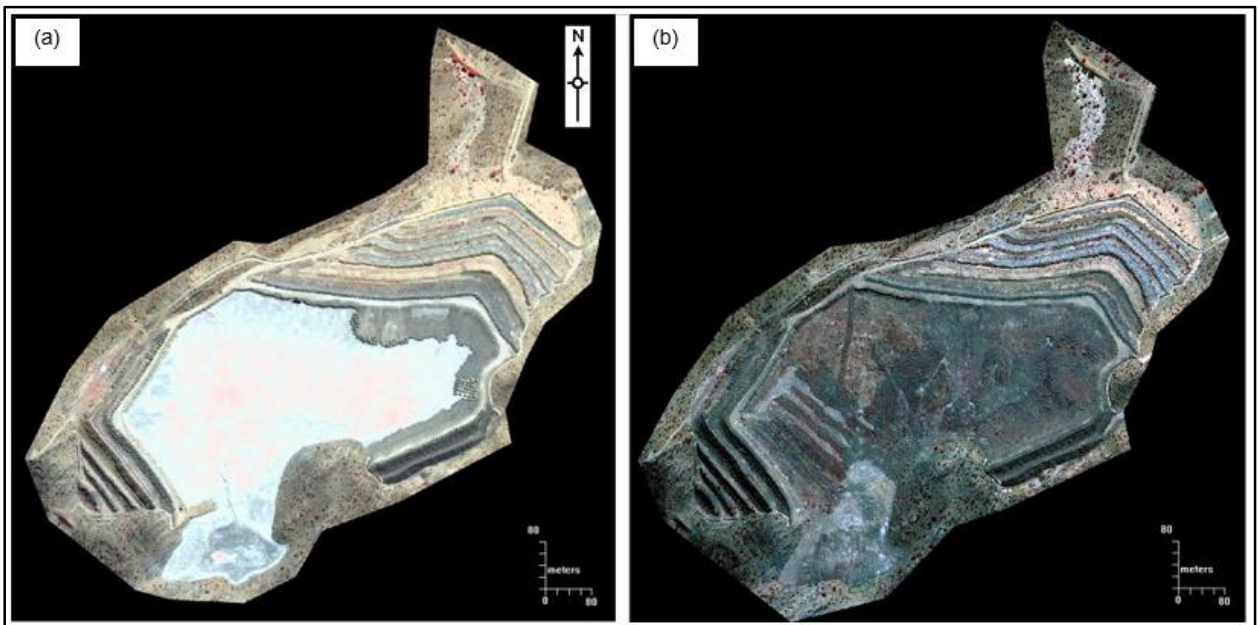


Figure B.9 False colour images of Quickbird July 2005 (a) and GeoEye-1 October 2010 (b)

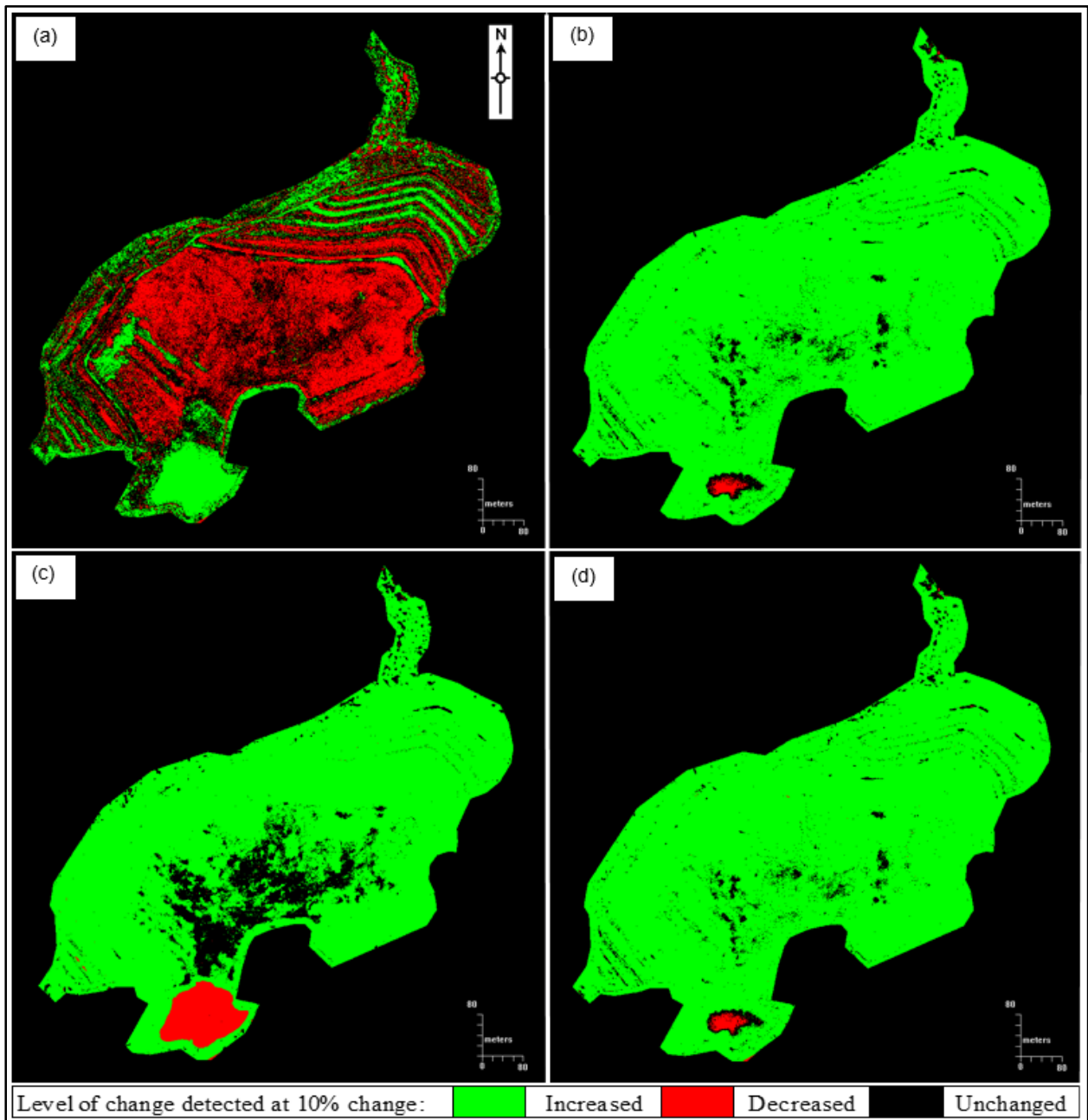


Figure B.10 Change detection results between Quickbird January 2004 and GeoEye-1 April 2011 images (a) NDVI and (c) TVI versus results between Quickbird July 2005 and GeoEye-1 April 2011 images (b) NDVI and (d) TVI.

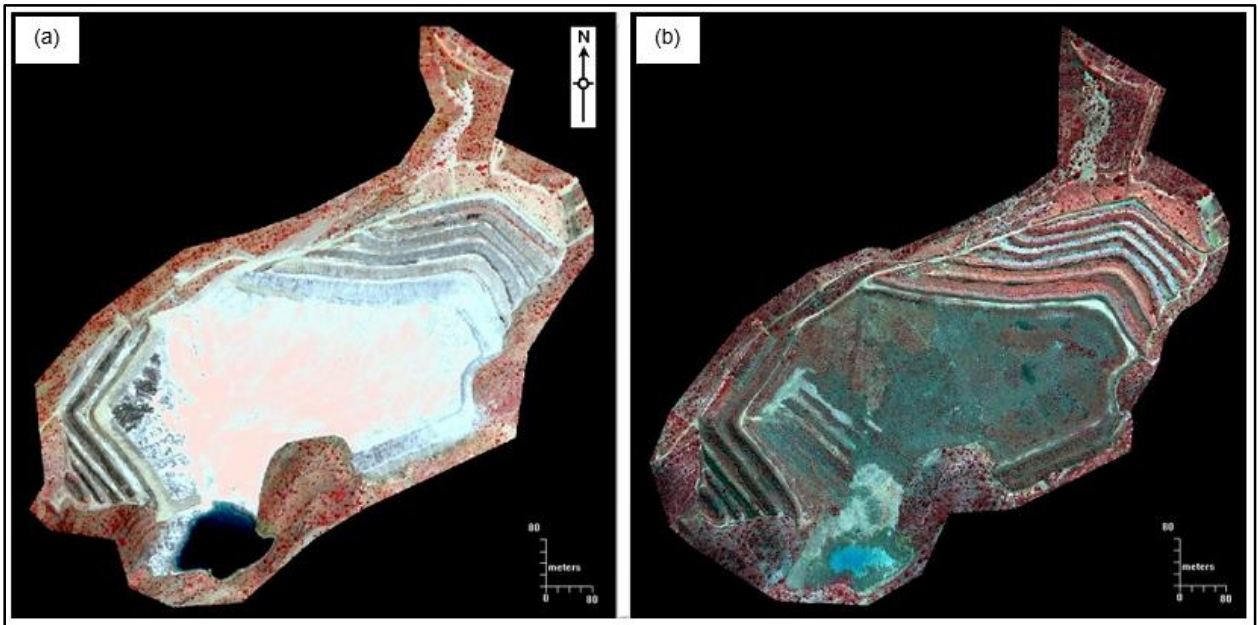


Figure B.11 False colour images of Quickbird January 2004 (a) and GeoEye-1 April 2011 (b)

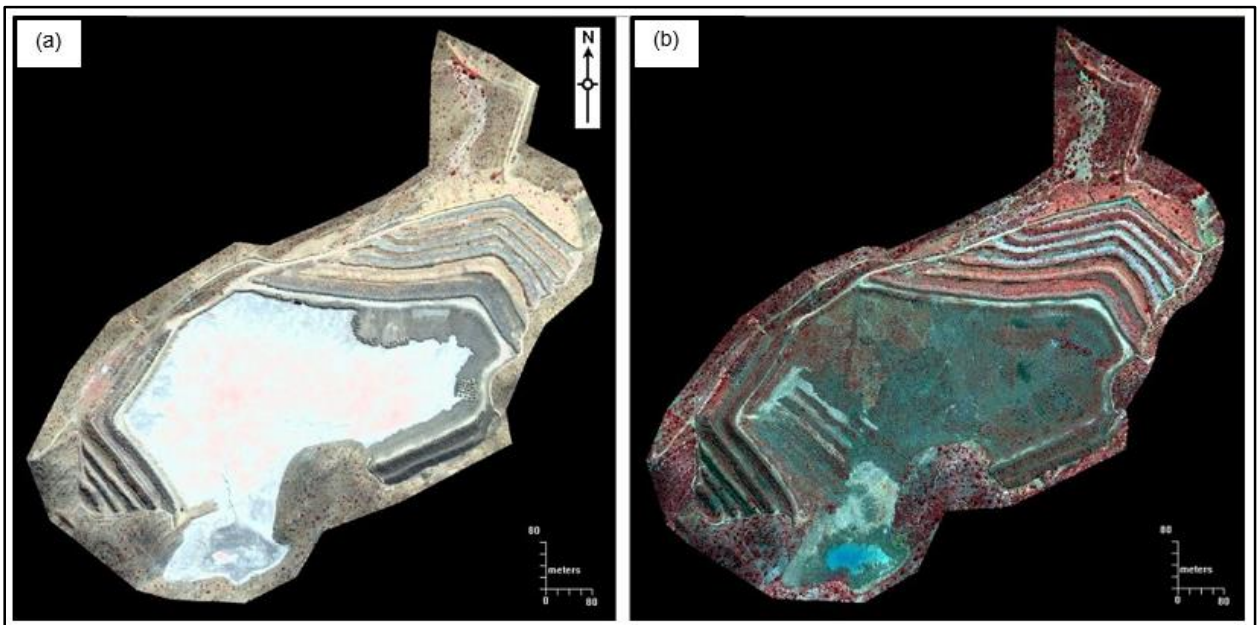


Figure B.12 False colour images of Quickbird July 2005 (a) and GeoEye-1 April 2011 (b)

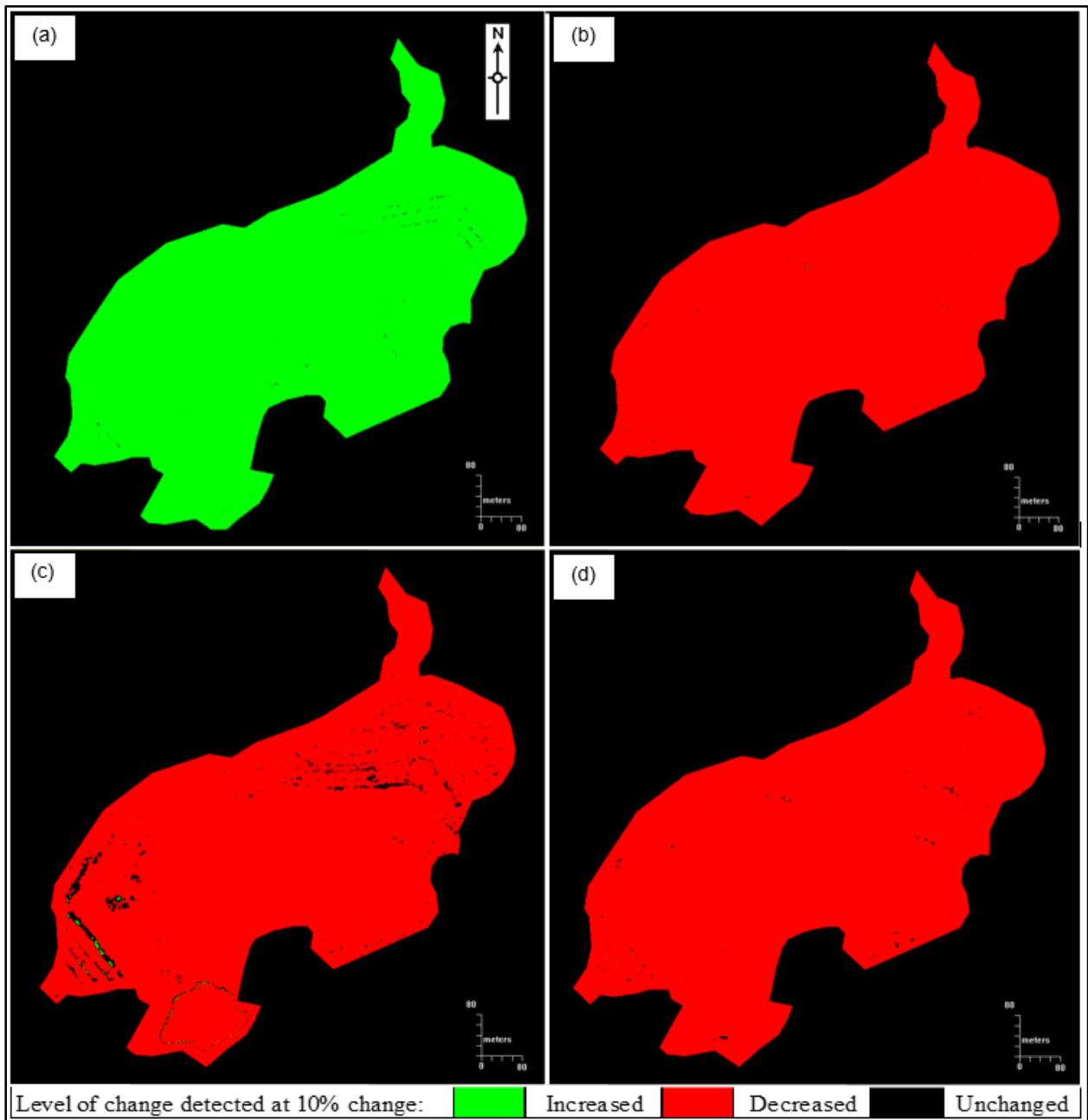


Figure B.13 Change detection results between Quickbird January 2004 and GeoEye-1 October 2011 images (a) NDVI and (c) TVI versus results between Quickbird July 2005 and GeoEye-1 October 2011 images (b) NDVI and (d) TVI.

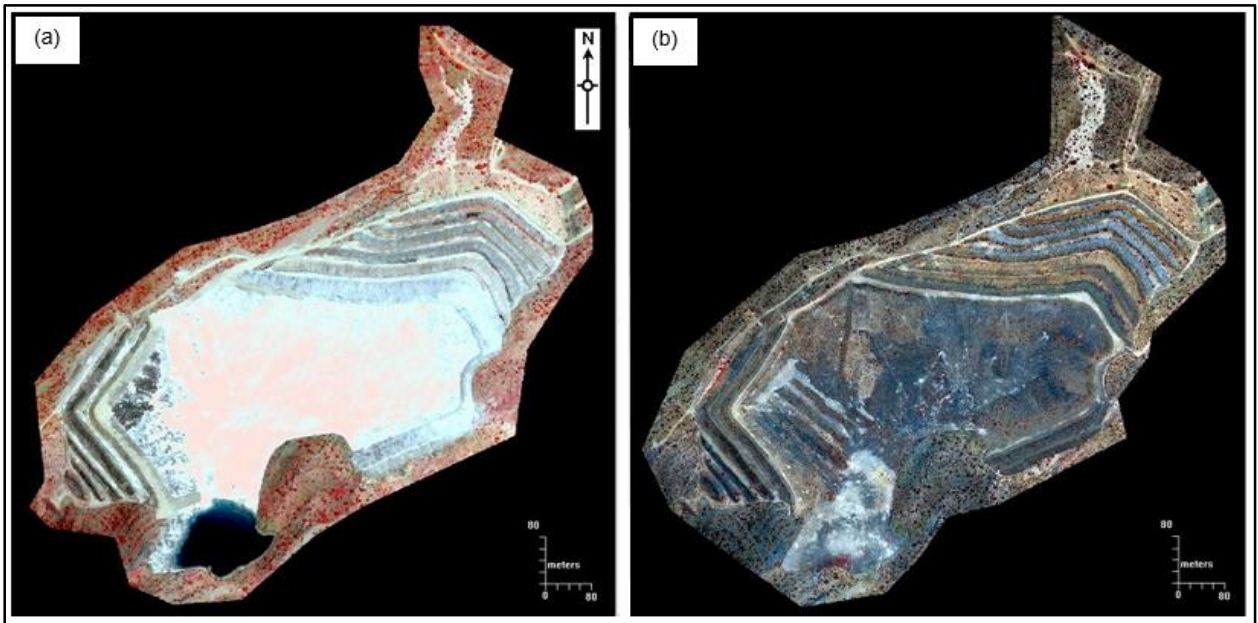


Figure B.14 False colour images of Quickbird January 2004 (a) and GeoEye-1 October 2011 (b)

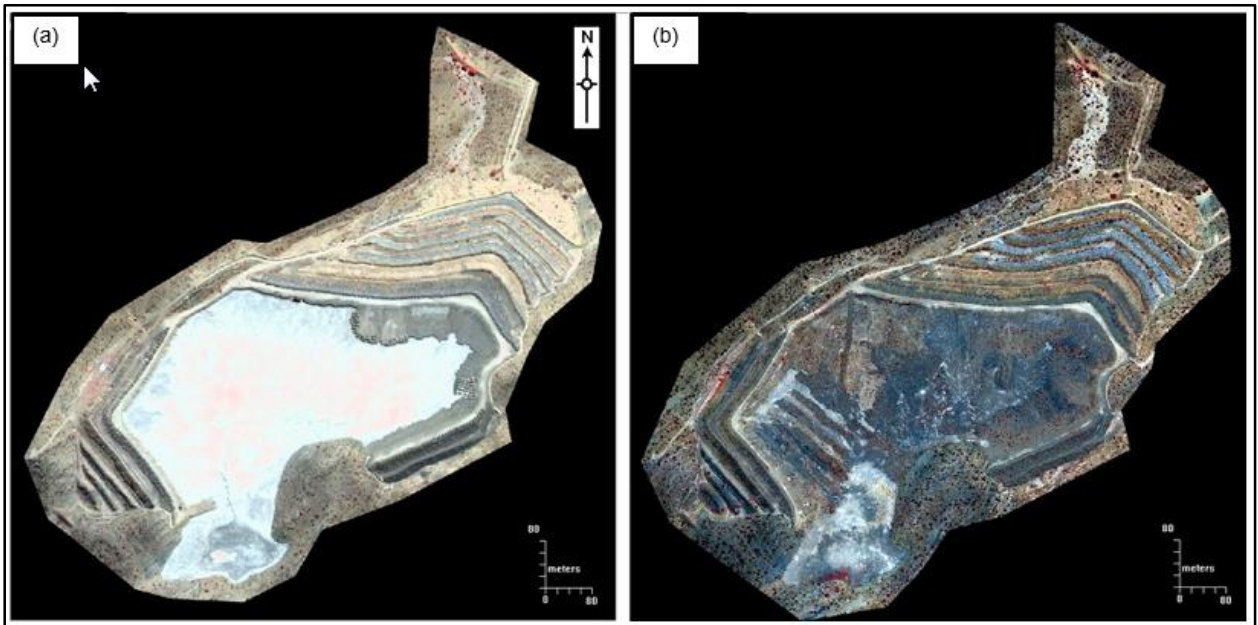


Figure B.15 False colour images of Quickbird July 2005 (a) and GeoEye-1 October 2011 (b)